

## Developing ruthenium-based complexes as redox labels for electrochemical biosensors

**Author:**

Lee, Yeng Ying

**Publication Date:**

2013

**DOI:**

<https://doi.org/10.26190/unsworks/16703>

**License:**

<https://creativecommons.org/licenses/by-nc-nd/3.0/au/>

Link to license to see what you are allowed to do with this resource.

Downloaded from <http://hdl.handle.net/1959.4/53367> in <https://unsworks.unsw.edu.au> on 2024-04-30

# **Developing Ruthenium-Based Complexes as Redox Labels for Electrochemical Biosensors**

by

Yeng Ying Lee

A thesis submitted in fulfilment  
of the requirement for admission to the degree of  
Master of Science



School of Chemistry

Faculty of Science

September 2013

## Acknowledgement

I want to first express my gratitude to my supervisors Professor Barbara Messerle and Professor Justin Gooding. I thank Justin wholeheartedly for the offer and scholarship for this project, without which I would not be here today. Both of them provided me with guidance and support, plus the occasional sage advice, which could only come from seasoned scientists. I highly appreciate the positivity and tolerance exuded by my supervisors even though things were at times a little trying.

This work could not be done by one person alone – I had much help from both Barbara's and Justin's group members who taught me much of what I wrote in this thesis. I also see in many of these people the attitudes and qualities I admire. Early on, Dr Guozhen Liu and the now Dr Naomi Khor showed me the ropes in the electrochemistry lab while the ever proficient Dr Khuong Vuong gave me useful hints for the synthesis of ligands and complexes. As the electrochemistry side of work progressed, I cleared up my queries on the techniques, instrumentation and software with Dr Callie Fairman, Dr Josh Peterson, Dr Tom Ellis and Dr Leo Lai. Whenever I bumped into problems with synthesis, Dr Gavin Edwards was always ready to lend me a hand.

After a long struggle with the synthesis side of work (over which I can only claim an extremely minor victory), Dr Nadim Darwish assisted me with the strategies over the immobilisation of the redox label and the ensuing electrochemical experiments. Nadim's wicked sense of humour definitely warrants a mention here, as well. Stephen Parker and Dr Alex Soeriyadi spent time characterising the surfaces and more time going over the data with me, for which I am really grateful. Nadim and Abbas Barfidokht were instrumental in the last set of experiments which involved antibodies that needed delicate handling. I want to express my appreciation to Abbas for his warm attitude, generosity and patience. Also, I want to thank Roya Tavallaie and Liz Murago for their help in data processing.

I would like to acknowledge the help and encouragement given by Dr Simone Ciampi, Dr Alicia Gui, Dr Bin Guan, Moinul, Roya, Liz, Maryam and Pauline from Justin's group at various points in time. Apart from the people from the groups, I would

like to thank Dr Donald Thomas and Dr Douglas Lawes (Doug) at the NMR facility, Lewis Adler at the Bioanalytical Mass Spectrometry Facility, Ian Aldred at the chemistry store, Grant Platt at the glass blowing workshop and James from the workshop for being helpful. Special thanks to Dr Nick Roberts, Doug and Giulia who proofread parts of my thesis. Also, I would like to extend my thanks to Ken McGuffin who was my first point of contact with the school, which led to this degree.

To this bunch of lovely people whom I hanged out with, whether it was inside or outside of the lab: Dr Michael Page, Andrey, Carol, Chin, Giulia, Khuong, Marina, Mark, Matt, Oanh, Sandy, Doug, Dr Carolina Surinach, Xevi, Foni, Mareike and Dr Rasmus Linser – thanks very much for your help, friendships, banter, refreshing insights and for simply being fantastic. And to Chris and John Mac who put me up when I got back to Australia. To my family and friends in my homeland, I send my eternal gratitude to you for your unconditional love, friendships and support even though we are oceans apart.

Yeng Ying Lee  
September 2013

## Abstract

Ferrocene-based redox labels have been used extensively for biosensing applications. However, the oxidised form of ferrocene, the ferricenium ion, is shown to decompose in solutions containing chloride salts or other strongly nucleophilic reagents. This thesis describes the synthesis and electrochemical studies on ruthenium-based complexes bearing 2,2'-bipyridine (bpy) and  $\beta$ -diketonato ligands in order to develop ruthenium-based redox labels for sensing applications.

Two series of ruthenium complexes,  $[\text{Ru}(\text{bpy})_2(\beta\text{-diketonato})](\text{PF}_6)$  (Series I) and  $\text{Ru}(\beta\text{-diketonato})_2(\text{bpy})$  (Series II) complexes were prepared. The complexes in Series I were prepared by displacing the Cl ligand in  $\text{Ru}(\text{bpy})_2\text{Cl}_2 \cdot 2\text{H}_2\text{O}$  with respective  $\beta$ -diketonato ligand while the complexes in Series II were synthesised by three major routes: Route 1: *via*  $\text{Ru}(\beta\text{-diketonato})_2(\text{MeCN})_2$ , Route 2: *via*  $\text{Ru}(\text{bpy})(\text{Cl})_4$  and Route 3: *via*  $\text{Ru}(\beta\text{-diketonato})_2(\text{diene})$  (MeCN = acetonitrile, diene = 1,5-cyclooctadiene (COD) or norbornadiene (NBD)). The complexes of both Series I and II were studied electrochemically to examine the effects of ligand substituents on the half-wave potentials ( $E_{1/2}$ ) of the complexes and showed that the use of  $\beta$ -diketonato ligands allowed the fine-tuning of  $E_{1/2}$  of these complexes. The electron-withdrawing and electron-donating groups on the  $\beta$ -diketonato ligands shifted the  $E_{1/2}$  in the anodic and the cathodic directions, respectively. In addition, the positioning of these groups on the  $\beta$ -diketonato ligands relative to the ruthenium centre also affected the extent of change in  $E_{1/2}$ . The  $E_{1/2}$  values of the complexes in Series I and II correlated well with Hammett constant, electrochemical ligand parameter and UV-Vis data.

Of the complexes studied, the  $E_{1/2}$  of  $\text{Ru}(\text{acac})_2(\text{bpy})$  and  $\text{Ru}(\text{dbm})_2(\text{bpy})$  fell in the desired range of -0.3 V to +0.5 V (*vs* Ag/AgCl) (acac = 2,4-pentanedionato, dbm = dibenzoylmethanato). To enable immobilisation of redox label onto gold electrodes and attachment of bioreceptor onto redox label, the bpy ligand was functionalised with primary amine groups (bpy-NH<sub>2</sub>). Redox label  $\text{Ru}(\text{acac})_2(\text{bpy-NH}_2)$  was prepared *via* Route 1 and immobilised on gold electrodes modified by 6-mercaptohexanoic acid (MHA) and thioctic acid (TA). The redox-label bound surfaces were characterised by cyclic voltammetry and X-ray photoelectron spectroscopy. The redox label was shown to be far more stable than the ferrocene-based label when subjected to repetitive redox

cycling in chloride-containing buffer. To evaluate the performance of the redox label, a sensing surface was constructed by immobilising *N*-glycosylated VHLTP (GPP) onto the redox label on MHA-modified gold electrode for the detection of Hb1Ac monoclonal antibody. The voltammetry response of the redox label upon the binding of Hb1Ac antibody to GPP was studied by square wave voltammetry, where it was shown that the signal was not affected by the buffer the antibody was in. The current of the redox label was attenuated when the sensing surface was incubated in the antibody solution: the longer the incubation time, the larger the decrease in current due to the binding of more antibodies to the peptides. This indicates that the redox label,  $\text{Ru}(\text{acac})_2(\text{bpy-NH}_2)$  has the potential to be applied in sensing applications.

Sections of this thesis which have been presented at the following scientific conferences and symposiums:

**Developing Ruthenium-Based Redox Labels for Electrochemical Biosensors**

Yeng Ying Lee, Barbara A. Messerle and J. Justin Gooding

*ACES: Electromaterials Symposium 2011*, University of Wollongong Innovation Campus, Wollongong, Australia, February 2011; poster presentation.

**Developing Ruthenium-Based Redox Labels for Electrochemical Biosensors**

Yeng Ying Lee, Barbara Messerle and Justin Gooding

*19<sup>th</sup> Reactive Organometallics Symposium*, The Australian National University, Canberra, Australia, June 2011; oral presentation.

**Developing Ruthenium-Based Redox Labels for Electrochemical Biosensors**

Yeng Ying Lee, J. Justin Gooding and Barbara A. Messerle

*Inaugural One-day Student Symposium in Inorganic Chemistry*, The University of Sydney, Sydney, Australia, June 2011; poster presentation.

**Developing Ruthenium-Based Redox Labels for Electrochemical Biosensors**

Yeng Ying Lee, Nadim A. Darwish, J. Justin Gooding, Barbara A. Messerle

*The 63<sup>rd</sup> Annual Meeting of the International Society of Electrochemistry*, Prague, Czech Republic, August 2012; poster presentation.

## Table of Contents

Title Page		i
Acknowledgements		ii
Abstract		iv
Table of Contents		vii
List of Abbreviations		xii
List of Figures		xiv
List of Schemes		xviii
List of Tables		xix
Chapter 1	Redox Labels in Electrochemical Affinity Biosensors	1
1.1	What is a Biosensor?	2
1.2	Transduction Principles in Electrochemical Biosensors	5
1.3	Design and Construction of Electrochemical Affinity Biosensors	7
1.4	Labelling in an Electrochemical Affinity Biosensor	8
1.5	Classes of Redox Labels	11
1.5.1	Metal-based Redox Labels	13
1.5.2	The Instability of Ferricenium Ion in Biological Samples	13
1.6	Redox Labels of Transition-metal Complexes	15
1.6.1	Redox Mediators Based on Transition-metal Complexes	15
1.6.2	Ruthenium Complexes as Redox Labels	17
1.7	Surface-bound Redox Labels: Advantage in Stability and Conformation on Sensing Surface	19
1.8	SAMs on Gold Electrodes	20
1.9	Surface-bound Redox Labels in Affinity Biosensors	22
1.10	Thesis Aims: Preparation of a Series of Ruthenium Complexes as Redox Labels for Biosensing Applications	25
1.11	Thesis Chapter Overview	26
1.12	References	27
Chapter 2	Synthesis, Instrumentation and Experimental Procedures	31
2.1	General Considerations	32
2.2	Chemicals, Reagents, Solvents	32
2.3	Instrumentation and Techniques	36
2.3.1	Electrochemical Instrumentation	36

2.3.2	Cyclic Voltammetry	36
2.3.3	Square Wave Voltammetry	39
2.3.4	Nuclear Magnetic Resonance Spectroscopy	40
2.3.5	Mass Spectrometry	40
2.3.6	UV-Vis Spectroscopy	40
2.3.7	X-ray Photoelectron Spectroscopy	41
2.3.8	pH meter	41
2.3.9	Other Characterisation Techniques	42
2.4	Electrochemical Studies	42
2.4.1	Preparation of Glassy Carbon Electrodes and Calculation of the Electrochemical Surface Area	42
2.4.2	Preparation of Gold Electrodes and Calculation of the Electrochemical Surface Area	42
2.4.3	Modification of Gold Electrodes with Self-assembled	43
2.4.4	Monolayers	44
2.4.5	Covalent Attachment of Ru(acac) <sub>2</sub> (bpy-NH <sub>2</sub> ) onto Gold Electrodes Modified with SAM	44
2.4.6	Determination of Surface Coverage of Ru(acac) <sub>2</sub> (bpy-NH <sub>2</sub> ) on Gold Electrodes	45
2.4.7	Attachment of Peptide GPP on Redox Label	45
2.5	Determination of Hb1Ac	45
	References	
Chapter 3	Synthesis and Electronic Tuning of $\beta$ -diketonate Ligands on Heteroleptic Ruthenium <sup>2+</sup> ( $\beta$ -diketonato) <sub>x</sub> (bpy) <sub>y</sub> Complexes (x and y = 1 or 2)	46
3.1	Ruthenium Complexes as Redox Labels	47
3.2	Metal Complexes and Their Half-Wave Potentials ( $E_{1/2}$ )	47
3.2.1	Ruthenium	48
3.2.2	Ligands	49
3.2.2.1	2,2'-Bipyridine (bpy)	50
3.2.2.2	Acetylacetonate (acac)	50
3.3	Approaches to Immobilising Redox Labels on Electrode Surface	52

3.4	Objectives	52
3.5	Experimental Section	53
3.5.1	Chemicals	53
3.5.2	Experimental Techniques	53
3.5.3	Synthesis	53
	Series I: Ruthenium Mono( $\beta$ -diketonato) complexes, [Ru(bpy) <sub>2</sub> ( $\beta$ -diketonato)](PF <sub>6</sub> )	53
	Series II: Ruthenium Bis( $\beta$ -diketonato) complexes, Ru(bpy)( $\beta$ -diketonato) <sub>2</sub>	56
	I. Preparation of Ru( $\beta$ -diketonato) <sub>3</sub> Complexes ( <b>11 – 14</b> )	56
	II. Preparation of Ru( $\beta$ -diketonato) <sub>2</sub> (acetonitrile) <sub>2</sub> Complexes ( <b>10, 15 – 17</b> )	58
	III. Preparation of Ru(bpy)( $\beta$ -diketonato) <sub>2</sub> Complexes ( <b>8, 18, 19 – 21</b> )	59 62
	IV. Preparation of Ru(diene)( $\beta$ -diketonato) <sub>2</sub> Complexes ( <b>22 – 28</b> )	62
3.6	Results and Discussion	64
3.6.1	Synthesis of Series I: Ruthenium Mono( $\beta$ -diketonato) Complexes, [Ru(bpy) <sub>2</sub> ( $\beta$ -diketonato)](PF <sub>6</sub> )	64
3.6.2	Routes to Prepare Series II: Ruthenium Bis( $\beta$ -diketonato) Complexes, Ru(bpy) <sub>2</sub> ( $\beta$ -diketonato)	65
3.6.2.1	Route 1: Ru( $\beta$ -diketonato) <sub>2</sub> (MeCN) <sub>2</sub>	66
	I. Preparation of Ru( $\beta$ -diketonato) <sub>3</sub> Complexes ( <b>9 and 11</b> )	66
	II a. Substituted Ru( $\beta$ -diketonato) <sub>3</sub> Complexes ( <b>12 – 14</b> ) by Direct Modification of Ru(acac) <sub>3</sub>	68
	II b. Proton NMR of Ru( $\beta$ -diketonato) <sub>3</sub> complexes ( <b>9, 11- 14</b> )	69
	II c. Preparation of <i>cis</i> -Ru( $\beta$ -diketonato) <sub>2</sub> (MeCN) <sub>2</sub> complexes ( <b>10, 15 – 17</b> )	70
	III: Preparation of Ru( $\beta$ -diketonato) <sub>2</sub> (bpy) Complexes ( <b>8, 18 and 19</b> ) <i>via</i> Ru( $\beta$ -diketonato) <sub>2</sub> (MeCN) <sub>2</sub> complexes	70
3.6.2.2	Route 2: Preparation of Ru( $\beta$ -diketonato) <sub>2</sub> (bpy) Complexes ( <b>8, 20 and 21</b> ) <i>via</i> Ru(bpy)(Cl) <sub>4</sub>	71
3.6.2.3	Route 3: Preparation of Ru( $\beta$ -diketonato) <sub>2</sub> (bpy) Complexes ( <b>8</b> )	73

	and <b>19</b> ) via Ru(diene)( $\beta$ -diketonato) <sub>2</sub> complexes	
3.7	Summary on the Synthesis of Ruthenium Complexes	75
3.8	Tuning of the Half-wave Potentials ( $E_{1/2}$ )	76
	Series I. Ruthenium Mono( $\beta$ -diketonato) Complexes, [Ru(bpy) <sub>2</sub> ( $\beta$ -diketonato)](PF <sub>6</sub> )	76
	Series II. Ruthenium Bis( $\beta$ -diketonato) Complexes, Ru( $\beta$ -diketonato) <sub>2</sub> (bpy)	78
3.8.1	Summary of the Half-wave potentials of Series I and II	79
3.9	Diffusion Coefficient, $D_0$	80
3.10	Relationships between the Nature of Ligands and $E_{1/2}$	81
3.11	Correlation between UV-Vis Absorbance and $E_{1/2}$	85
3.12	Summary	88
3.13	References	89
Chapter 4	Evaluation of a Ruthenium-based Redox Label on a Sensing Surface	93
		94
4.1	The Monitoring of Blood Glucose Level	94
4.2	Voltammetry Responses Generated by Redox Label upon Target Binding	96
4.2.1	Surface-bound Redox Labels	98
4.3	Objectives	99
4.4	Experimental Section	99
4.4.1	Chemicals	99
4.4.2	Experimental Techniques	99
4.4.3	Synthesis	101
4.4.4	Construction of Sensing Surface	102
4.4.5	Determination of Hb1Ac antibody	102
4.5	Results and Discussion	102
4.5.1	Synthesis of Ru(acac) <sub>2</sub> (bpy-NH <sub>2</sub> )	103
4.5.2	Redox Label, Ru(acac) <sub>2</sub> (bpy-NH <sub>2</sub> ) on SAM-modified Gold Surfaces	105
4.5.3	XPS Characterisation of Modified Gold Surfaces	106
	I. MHA- and TA-modified Gold Surfaces	105

	II. Activation of MHA- and TA-modified Surfaces	106
	III. Attachment of Redox Label onto MHA- and TA-modified Surfaces	107
	IV. Attachment of Peptide GPP onto MHA-modified Gold Surfaces	109
4.5.4	Electrochemical Studies on Modified Gold Electrodes	113
4.5.4.1	Redox Label Physisorbed onto Modified Gold Electrodes	115
4.5.4.2	Stability of Redox Label	116
4.5.5	Detection of Hb1Ac Antibody	119
4.5.5.1	Peptide GPP on Redox Label	119
4.5.5.2	Detection of Hb1Ac Antibody by Square-Wave Voltammetry	120
4.6	Summary	122
4.7	References	123
Chapter 5	Concluding Remarks and Future Work	125
5.1	Summary	126
5.2	Future Perspective	127
5.3	Conclusion	130
5.4	References	131

## List of Abbreviations

Acac	Acetylacetonate/2,4-pentanedionato
AcacH	2,4-pentanedione
At %	Atomic percentage
Au	Gold (electrode or surface)
bpy	2,2'-bipyridyl
bpy-NH <sub>2</sub>	4,4'-bis(aminomethyl)-2,2'-bipyridyl
C <sub>6</sub> D <sub>6</sub>	Deuterated benzene
CDCl <sub>3</sub>	Deuterated chloroform
COD	1,5-cyclooctadiene
Cp	Cyclopentadienyl
CV	Cyclic voltammetry
dbm	dibenzylmethanato
DCM	Dichloromethane
DMF	Dimethylformamide
dmhd	2,6-dimethyl-3,5-heptanedione
DMSO- <i>d</i> <sub>6</sub>	Deuterated dimethylsulfoxide
E	Potential
eacac	3-ethyl-2,4-pentanedione
EDC	1-(3-Dimethylaminopropyl)-3-ethylcarbodiimide hydrochloride
equiv.	Equivalents
EtOAc	Ethyl acetate
EtOH	Ethanol
eV	Electron volt
Fc/ FeCp <sub>2</sub>	Ferrocene
fwhm	Full width at half maximum
GC	Glassy carbon
GPP	<i>N</i> -glycosylated VHLTP
h	Hour
hfac	1,1,1,5,5,5-hexafluoro-2,4-pentanedione
<i>I</i> / <i>i</i>	Current
<i>j</i>	Current density
L	ligand

macac	3-methyl-2,4-pentanedione
mbpd	3-(4-methoxybenzyl)-2,4-pentanedione
MES	2-( <i>N</i> -morpholino)ethanesulfonic acid
MeCN	Acetonitrile
MHA	6-mercaptohexanoic acid
MLCT	Metal ligand charge transfer
NBD	Norbornadiene
nbpd	3-(4-nitrobenzyl)-2,4-pentanedione
NBu <sub>4</sub> PF <sub>6</sub>	Tetrabutylammonium hexafluorophosphate
NHS	<i>N</i> -hydrosuccinimide
$\nu$	Scan rate
PBS	Phosphate buffer saline
SAM(s)	Self-assembled monolayers
SWV	Square wave voltammetry
TA	Thioctic acid
tfac	1,1,1-trifluoro-2,4-pentanedione
tmhd	2,2,6,6-tetramethyl-3,5-heptanedione
UV	Ultra-violet
XPS	X-ray photoelectron spectroscopy

## List of Figures

Figure 1.1	Schematic of the components in a biosensor.	3
Figure 1.2	H <sub>2</sub> O <sub>2</sub> produced by GOx-catalysed consumption of glucose is oxidised to give electrons that diffuses to the electrode to give a current corresponding to the level of glucose in sample.	4
Figure 1.3	A peptide-based copper ion sensor. Inset: (a) before accumulation of copper ions; (b) after accumulation of copper ions.	4
Figure 1.4	Electrochemical detection of DNA strand with labelled oligonucleotide.	10
Figure 1.5	Selected examples of redox labels: (a) organic redox labels; (b) metal-based labels modified with linker groups.	12
Figure 1.6	(a) Osmium(4,4-dimethyl-2,2-bipyridyl) <sub>2</sub> chloride cross-linked to poly(1-vinylimidazole). (b) Structure of [Ru(LL) <sub>2</sub> (X) <sub>2</sub> ] and their potentials.	17
Figure 1.7	Cyclometalated (top) and non-cyclometalated (bottom) ruthenium complexes, along with their E <sub>1/2</sub> .	18
Figure 1.8	Structure of Ru(acac) <sub>2</sub> (R-bqdi) complexes and their E <sub>1/2</sub> .	18
Figure 1.9	Ruthenium and osmium complexes bearing two bpy ligands and one substituted β-diketonato/hydroxamic acid with linker groups to conjugate with nucleosides.	19
Figure 1.10	Structures of organosulfur compounds capable of forming SAMs.	21
Figure 1.11	Potential shift and decrease in current density when the target analyte, human immunodeficiency virus type I protease, HIV1-PR, is bound to the ferrocene-peptide conjugate.	23
Figure 1.12	Schematic of a fabricated immunosensor which displays a current attenuation upon binding of a target analyte, anti-biotin IgG: (a) Prior to incubation with the anti-biotin IgG; (b) after incubation with the anti-biotin IgG. A displacement assay in which free biotin displaces anti-biotin IgG to cause a current increase: (c) SWV of the sensing surface after exposure to biotin in increasing time interval; (d) calibration plot showing the increase in relative current (before and after exposure to free biotin) against the concentration of biotin.	24

Figure 1.13	Structures of (a) and (b) ruthenium complexes bearing $\beta$ -diketonato and bpy ligands; (c) bpy-NH <sub>2</sub> .	25
Figure 2.1	(a) Potential-time pulses in cyclic voltammetry. (b) A cyclic voltammogram of a reversible redox process: $i_{pa}$ and $i_{pc}$ are the anodic and cathodic peak current respectively; $E_{pa}$ and $E_{pc}$ are the anodic and cathodic peak potential respectively.	37
Figure 2.2	(a) Potential waveform in SWV. $\Delta E_{sw}$ is the pulse amplitude, $\Delta E$ the step height and $\frac{1}{\text{frequency}}$ the square wave period. Currents, $i_f$ and $i_r$ , are collected at the end of each pulse. (b) A SWV voltammogram (black line), the net current of which is the sum of currents from $i_f$ and $i_r$ .	39
Figure 2.3	A cyclic voltammogram of a clean gold electrode in 0.5 M H <sub>2</sub> SO <sub>4</sub> , $v = 0.1 \text{ V s}^{-1}$ .	43
Figure 3.1	Structure of bpy.	50
Figure 3.2	Keto/enol tautomerism of acacH, resulting in the more stable delocalised enol isomer.	51
Figure 3.3	Six-membered chelate ring in M(acac) <sub>3</sub> .	51
Figure 3.4	Phase-transfer equilibria in the reaction of Ru(acac) <sub>3</sub> .	67
Figure 3.5	Bromination on metal( $\beta$ -diketonates).	68
Figure 3.6	Positions of substituents on $\beta$ -diketonates.	77
Figure 3.7	Cyclic voltammograms of complexes <b>1 – 5</b> .	78
Figure 3.8	$E_{1/2}$ vs the sum of the Hammett constants ( $\Sigma\sigma_{pmp}$ ) of Ru( $\beta$ -diketonato) <sub>2</sub> (bpy) ( <b>8, 18-21</b> ) and Ru( $\beta$ -diketonato) <sub>3</sub> ( <b>9, 10-14</b> ) complexes.	83
Figure 3.9	$\Sigma E_{(L)}$ vs $E_{pc}$ of selected complexes.	85
Figure 3.10	UV-Vis absorbance spectra for complexes in Series I.	87
Figure 3.11	UV-Vis absorbance spectra for complexes in Series II.	88
Figure 4.1	(a) MHA- and (b) TA-modified gold electrodes.	97
Figure 4.2	Structures of (a) bpy and (b) bpy-NH <sub>2</sub> .	97
Figure 4.3	The sensing surface showing an immobilised redox label on MHA and the covalent binding of GPP onto redox label by carbodiimide	98

	coupling.	
Figure 4.4	Wide scans for (a) MHA- and (b) TA-modified gold surfaces with redox label <b>30</b> attached.	105
Figure 4.5	S 2p narrow scans for (a) MHA- and (b) TA-modified gold surfaces.	106
Figure 4.6	C 1s narrow scans for (a) MHA- and (b) TA-modified gold surfaces.	106
Figure 4.7	N 1s narrow scans for MHA-modified gold surface: (a) activated and (b) not activated; TA-modified gold surface: (c) activated and (d) not activated.	107
Figure 4.8	N 1s narrow scan for modified gold surface with <b>30</b> attached: (a) MHA-modified; (b) TA-modified.	108
Figure 4.9	Ru 3d <sub>5/2</sub> narrow scan for MHA-modified gold surface: (a) activated surface incubated with <b>30</b> ; (b) non-activated surface incubated with <b>30</b> .	109
Figure 4.10	C 1s narrow scan for modified gold surface: (a) MHA; (b) activated MHA; (c) MHA with <b>30</b> attached; (d) MHA with <b>30</b> and peptide.	110
Figure 4.11	N 1s narrow scan for modified gold surface incubated with: (a) GPP and (b) EDC/NHS activated GPP.	110
Figure 4.12	(a) Assumption model of four coupling efficiencies: 0%, 25%, 50% and 100%; (b) Table 1: % peptide bound to redox label based on the number of nitrogens present at different binding energies; Graph 1: A calibration of % peptide bound vs % coupling efficiency and Table 2: Estimation of % peptide bound on redox label.	112
Figure 4.13	(a) Plot of current density vs potential for MHA- and TA-modified gold electrode in phosphate buffer, pH 7, $\nu = 0.1 \text{ V s}^{-1}$ . (b) Linear plots of current vs scan rate for MHA- and TA-modified electrodes.	113
Figure 4.14	CVs of <b>30</b> on (a) MHA- and (b) TA-modified gold electrodes, without and without EDC/NHS activation, in phosphate buffer, pH 7, $\nu = 0.05 \text{ V s}^{-1}$ .	116

Figure 4.15	pH vs potential for (a) MHA- and (b) TA-modified gold electrodes in phosphate buffers of pHs 5 – 9, $v = 0.05 \text{ V s}^{-1}$ .	117
Figure 4.16	Current decrease of Fc on thiol compared to <b>30</b> bound to MHA and TA on gold electrodes.	118
Figure 4.17	Surface 3 – MHA-bound redox label and Surface 4 – GPP-bound redox label covalently attached on MHA-modified gold surface.	120
Figure 4.18	(a) A SWV showing that the signal of Surface 4 was equilibrated after 15 mins in PBS, recorded at 200 Hz. (b) Repeated scans ( $\times 10$ ) after Surface 4 was incubated in Hb1Ac antibody solution for 5 h, recorded at 210 Hz.	121
Figure 4.19	(a) SWV of Surface 4 when exposed to Hb1Ac antibodies in PBS at varying incubation time, recorded at 130 Hz. (b) Area under peak and peak potential of Surface 4 after exposing to Hb1Ac antibodies at varying incubation time.	122
Figure 5.1	An example of a sensing surface constructed with a mixed layer of a diluent, insulator oligoethyleneglycol (OEG), and a redox-active adlayer, ferrocene (FDMA) on molecular wire, for the detection of biotin in a displacement assay.	128
Figure 5.2	An example of a branched electrode approach to detecting tumour markers, carcino-embryonic antigen (CEA) by anti-CEA conjugated to methylene blue (MB) and $\alpha$ -fetoprotein (AFP) by anti-AFP conjugated to Prussian blue (PB) by differential pulse voltammetry (DPV); MB and PB are organic redox labels, the currents of which were reduced upon binding of CEA and AFP.	129
Figure 5.3	Partial structures of multipod anchoring groups suitable on gold and indium tin oxide surfaces, M represents a redox label.	130

## List of Schemes

Scheme 1.1	Steps 1 – 4 detailing the progressive decomposition of ferricenium ion, $\text{FeCp}_2^+$ , by L, where L is either a solvent molecule, a neutral nucleophilic agent or a mononegative anion.	14
Scheme 1.2	Adsorption of thiols on gold surfaces.	21
Scheme 3.1	Preparation of $\text{Ru}(\text{bpy})_2(\beta\text{-diketonato})$ complexes.	65
Scheme 3.2	Routes to $\text{Ru}(\beta\text{-diketonato})_2(\text{bpy})$ complexes.	66
Scheme 3.3	Synthesis of $\text{Ru}(\beta\text{-diketonato})_2(\text{bpy})$ complexes <i>via</i> Route 1.	71
Scheme 3.4	Synthesis of $\text{Ru}(\beta\text{-diketonato})_2(\text{bpy})$ <i>via</i> Route 2.	72
Scheme 3.5	Attempted syntheses <i>via</i> Route 2 to prepare $\text{Ru}(\beta\text{-diketonato})_2(\text{bpy})$ .	73
Scheme 3.6	$\text{Ru}(\beta\text{-diketonato})_2(\text{COD})$ complexes prepared from Route 3.	74
Scheme 4.1	Synthesis of ligand, 4,4'-bis(aminomethyl)-2,2'-bipyridine ( $\text{bpy-NH}_2$ ).	103
Scheme 4.2	Schematic on the attachment of redox label <b>30</b> on MHA-modified gold electrode (Surface 1 – 4).	104
Scheme 4.3	“Square” scheme of a redox cycle on SAM.	114

## List of Tables

Table 2.1	Chemicals used in this thesis.	32
Table 3.1	$E_{1/2}$ of $[\text{Ru}(\text{bpy})_{3-n}(\text{acac})_n]^{x+}$ complexes.	49
Table 3.2	$^1\text{H}$ NMR data for $\text{Ru}(\beta\text{-diketonato})_3$ complexes in $\text{C}_6\text{D}_6$ .	69
Table 3.3	Ruthenium complexes synthesised in Series II.	76
Table 3.4	Electrochemical data of $\text{Ru}(\text{bpy})_2(\beta\text{-diketonato})$ complexes.	76
Table 3.5	$E_{1/2}$ for selected complexes from precursors and complexes of Series II.	79
Table 3.6	Diffusion coefficients for ruthenium complexes in Series I and II in MeCN.	80
Table 3.7	Sums of the Hammett constants, $\Sigma\sigma_{\text{pmp}}$ , for the ruthenium complexes.	82
Table 3.8	Data of $\Sigma E_{(\text{L})}$ of selected complexes and their $E_{\text{pc}}$ (vs NHE)	84
Table 3.9	Absorption maxima, $\lambda_{\text{max}}$ , and molar extinction coefficient, $\epsilon$ in Series I.	86
Table 3.10	Absorption maxima, $\lambda_{\text{max}}$ , and molar extinction coefficient, $\epsilon$ in Series II.	88
Table 4.1	$E_{1/2(\text{solution})}$ and $E_{1/2(\text{surface-bound})}$ of <b>30</b> .	113

# *Chapter 1*

## *Redox Labels in Electrochemical Affinity Biosensors*

## 1.1 What is a Biosensor?

A biosensor is an analytical device which uses a biorecognition element in a detection event and transforms this into a quantifiable and processable signal. The earliest example of a biosensor is a glucose enzyme electrode designed by Clark and Lyons for blood glucose level monitoring.<sup>1-4</sup> The scope of detection has since expanded enormously to encompass targets such as antibody,<sup>4,5</sup> antigen,<sup>6</sup> DNA,<sup>7-10</sup> metal ions,<sup>5,11,12</sup> pesticides and gases,<sup>5,13</sup> which greatly showcases the versatility and applications of biosensors in the fields of medical diagnostics,<sup>12,14,15</sup> quality control,<sup>12</sup> public safety and environmental monitoring.<sup>13,16</sup> In everyday usage, the term “biosensor” refers to an analytical device which requires no additional separation step or sample processing, which distinguishes it from conventional analytical techniques, such as high performance liquid chromatography and flow injection analysis.<sup>2,5,13</sup> While some biosensors may not have the level of accuracy or sensitivity comparable to those of conventional techniques, they are highly useful in routine testing and screening of samples.<sup>13</sup>

A biosensor as defined by IUPAC is a self-contained integrated device constructed with a biorecognition element retained in direct spatial contact with a transduction element capable of providing quantitative or semi-quantitative analytical information.<sup>3,13,17</sup> A biosensor is characterised by the following five features: 1) target analyte; 2) transduction mode; 3) biorecognition principle; 4) application; and 5) the technology and material for its fabrication.<sup>18</sup> The three major components of a biosensor are bioreceptor, transducer and electronics (Figure 1.1). Broadly speaking, biosensors are classified by their transduction mode into several major types: optical, electrochemical, thermal and piezoelectric.<sup>2,13,19</sup> Alongside this, they can be differentiated into catalytic and affinity subtypes based on their biorecognition principle.<sup>19</sup>

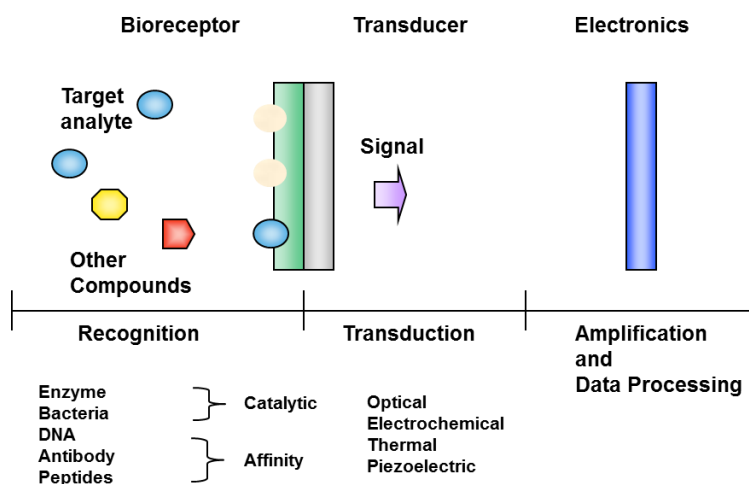


**Figure 1.1** Schematic of the components in a biosensor.

A bioreceptor is a bioactive substance, e.g., enzyme, bacteria, antibody, DNA, or peptide, with which analytes will interact.<sup>3</sup> The bioactive substances can be target- or class-specific, the interaction catalytic or affinity in nature.<sup>13</sup> The reaction of a target analyte catalysed by a bioreceptor in a catalytic biosensor gives a product which corresponds quantitatively to its presence in a sample.<sup>2</sup> A classic example of a catalytic biosensor is the glucose biosensor in which glucose oxidase (GOx) catalyses the oxidation of glucose to produce gluconic acid and hydrogen peroxide ( $\text{H}_2\text{O}_2$ ) (Figure 1.2).<sup>20</sup> The electrons released by the oxidation of  $\text{H}_2\text{O}_2$  then diffuses to the electrode to give the current which corresponds to the amount of glucose present.<sup>15</sup>

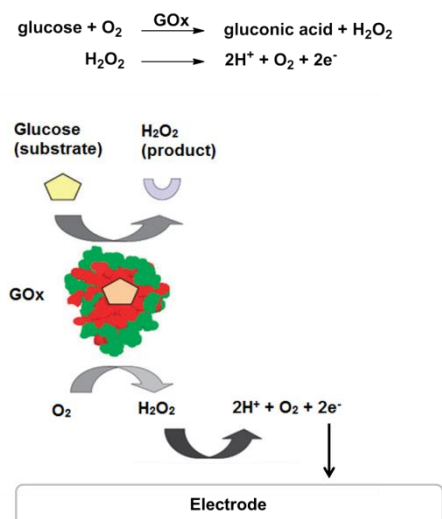


**Figure 1.2** H<sub>2</sub>O<sub>2</sub> produced by GOx-catalysed consumption of glucose is oxidised to give electrons that diffuse to the electrode to give a current corresponding to the level of glucose in sample.<sup>17</sup>

An affinity biosensor works by the selective and specific complexation of a target analyte to its bioreceptor.<sup>4</sup> For example, by exploiting the specificity and selectivity exhibited by peptide sequences towards metal ions, peptide-based metal ion sensors have been developed for the detection of metal ions.<sup>21-23</sup>

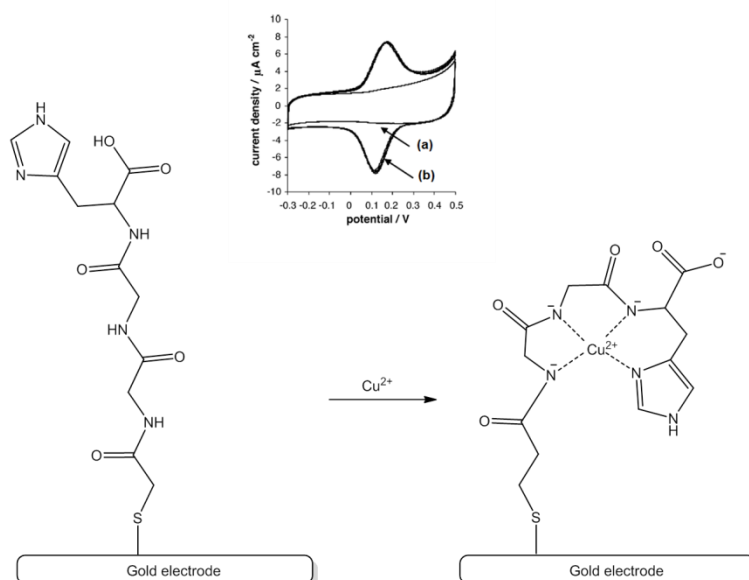


**Figure 1.3** A peptide-based copper ion sensor. Inset: (a) before accumulation of copper ions; (b) after accumulation of copper ions.<sup>22</sup>

Transducers are responsible for converting changes elicited by biorecognition events at the bioactive interface into electronic signals for data amplification and processing. Transduction elements can be optical, electrochemical, thermal or piezoelectric, with the former two employed in the majority of biosensors.<sup>2</sup> Electrochemical transducers have an advantage over optical transducer owing to their compatibility with miniaturisation.<sup>2,3</sup>

The combination of electrochemical transducers and the specificity of biorecognition systems in producing simple, economical and robust devices have established them as the dominating class of biosensors in commercial applications.<sup>19,24</sup> The high compatibility exhibited by electrochemical transducers with microfabrication and micromachining technology provides ideal access to miniaturised biosensors.<sup>24,25</sup> These miniaturised devices offer the advantages of portability: data collection on-site can proceed with minimal sample preparation and more meaningful data is obtained to account for spatio-temporal variations from collection points.<sup>13</sup> In addition, they require less handling of sample, resulting in cleaner and less hazardous analyses.<sup>25</sup> Other advantages brought about by miniaturisation include enhanced diffusion mixing efficiency, improved heat transport, decrease in by-products formation and shorter reaction time.<sup>25</sup>

## **1.2 Transduction Principles in Electrochemical Biosensors**

The three primary transduction principles in electrochemical biosensors are conductometry, potentiometry and amperometry.<sup>1,2</sup> To a lesser extent, impedimetry, which yields information on impedance – conductance, resistance or capacitance – and field-effect, which measures a current resulted from change in surface potential at a gate electrode have also been used.<sup>1,2,6</sup> Materials including carbon, gold, platinum and silicon are preferred as transducers due to their excellent conductivity, chemical stability and crystalline structures that are low in residual currents and high in signal-to-noise ratios.<sup>1,18</sup>

Conductometric biosensors relate fluctuations in conductivity between a pair of electrodes or reference nodes to biological or chemical changes, e.g., changes in the

concentration of charged species in a solution, which occur when target analytes are present.<sup>1</sup> Their application is however made unfavourable by ionic components in samples: corrections are needed for various levels of ionic background that might be present and minute conductivity changes in samples of high ionic strength are difficult to monitor.<sup>15</sup>

Potentiometric biosensors measure changes in potential caused by selective binding of charges on the sensing electrode, i.e., potential difference, to provide information on ion activity, when there is no significant current flowing between the sensing electrode and a reference electrode.<sup>1,2</sup> The potential difference is proportional to the logarithm of the ion activity, gas fugacity or concentration, as governed by the Nernst equation.<sup>1,2</sup> The majority of devices in this class are pH electrodes, ion-selective electrodes, and gas-selective electrodes.<sup>2,15</sup>

An amperometric biosensor measures current which results from the electrochemical oxidation or reduction of an electroactive species, typically by 1) holding a constant potential – amperometry; or 2) controlled variations of potential – voltammetry, with respect to a reference electrode.<sup>1,2</sup> The response has a linear concentration dependence which relays information on the bulk concentration of an electroactive species, or its production or consumption rate within the adjacent biocatalytic layer, depending on the design and application of the system.<sup>2,19</sup> Only a negligible charging current results when a fixed potential is applied during amperometric measurement, hence the limit of detection is not adversely affected by this background signal.<sup>17</sup>

Of available amperometric techniques, cyclic voltammetry (CV) is one of the most employed forms, where a current is measured by varying a potential to give information on half-wave potential ( $E_{1/2}$ ) and electrochemical reaction rates of analyte solutions.<sup>1</sup> Scan rate,  $v$ , which determines the duration of a scan, during which a chemical reaction occurs, can be changed to yield correspondingly varied results.<sup>1</sup> Square-wave voltammetry (SWV) is another popular technique from which better sensitivity can be obtained.<sup>26</sup> The sensitivity is enhanced by net current output which

discounts the background charging current and the repeated cycles of oxidation and reduction of the same analyte species.

Amperometric biosensors are more widely adopted compared to conductometric and potentiometric biosensors because of their faster response time, higher sensitivity, lower cost and suitability for single use.<sup>1,19</sup> Disposable biosensors which can be mass produced inexpensively minimise risks of inaccurate data collection associated with carry over, contamination, drift or loss of bioreceptor activity encountered in reusable biosensors.<sup>24</sup> An important consumer product based on amperometric transduction principle is the blood glucose meter, a catalytic biosensor.<sup>20</sup> These devices can be used by untrained personnel because their operation is simple and data read-outs quick and easy to understand.

### **1.3 Design and Construction of Electrochemical Affinity Biosensors**

An affinity biosensor bases its operation on the interaction between an analyte with macromolecules or organised molecular assemblies that are either sourced from their original biological environment or engineered.<sup>2</sup> In-depth understanding on the interactions between target compounds and bioreceptors and the capability to modify such interactions have led to the production of biosensors highly selective towards their target analytes.<sup>1,13</sup> Although non-specific interactions by other compounds in sample matrices often interfere with the intended detection and may foul the electrode surface, the use of polymeric thin films which resist adsorption of proteins and adhesion of bacteria<sup>27</sup> and pre-treatment steps have been shown to minimise matrix effects at biorecognition interfaces.<sup>1,13</sup> The main objective is to limit the interference–transducer interactions while at the same time maximise the analyte–transducer interactions to give optimal sensitivity or selectivity for a sensing device.<sup>28</sup> Other aspects to consider when applying biosensors in real samples are the stability during storage and operation of a biosensor and the appropriateness of the dynamic range of the device for the anticipated analyte concentration.<sup>13</sup>

A biosensor is evaluated by its selectivity, sensitivity, response time, limit of detection (LOD), linear and dynamic ranges.<sup>13,17</sup> The response from a biosensor should

be accurate, precise, reproducible and linear over the concentration range of interest, without dilution and concentration.<sup>1</sup> The reliability of the responses depends on both selectivity and reproducibility of the device: it is selective if the response can be directly related to the analyte concentration without contribution from interfering components within the sample matrix; it is reproducible if a series of results obtained over a time period has minimal drift from the actual result.<sup>2</sup>

Often, the performance and applicability of a biosensor hinges on the immobilisation of bioreceptors and biocompatible materials on transducers, in that the coupling of bioreceptors and transducers affects functions and stability of bioreceptors and the extent of reduction of electrode fouling offered by biocompatible materials.<sup>2,18,19</sup> Immobilisation of bioreceptors onto transducers is most commonly done *via* physical adsorption, cross-linking, entrapment, covalent bond, or a combination of all of these techniques.<sup>2,19,29,30</sup> Materials reported include permeable membranes, conductive and non-conductive polymers, self-assembled monolayers (SAMs), activated surfaces with bifunctional groups or spacers, e.g., glutaraldehyde, carbodiimide and silanes, and bulk modification, e.g., carbon pastes or carbon-polymer composites.<sup>2,18,30,31</sup> For the purpose of diffusion control, mechanical protection, surface density, and most importantly, elimination of interferences, biocompatible materials namely polymer membranes, hydrogels, polyethylene glycol, phospholipid copolymers and hydrophobic coatings of silanes have been used before or after immobilisation of bioreceptors to modify transducers.<sup>15,18</sup> As expected, an increase in binding sites over a larger surface area leads to increased binding events and sensitivity.<sup>6</sup>

#### 1.4 Labelling in an Electrochemical Affinity Biosensor

Electrochemical affinity biosensors have two modes of detection: label-free (direct) or labelled (indirect).<sup>6,15,19</sup> A label-free biosensor, which requires no chemical modification on both the bioreceptor and the analyte, obtains data by direct measurement of changes in physical phenomenon upon the binding of analytes. An affinity biosensor can be made label-free by incorporating an electroactive species into a construct such as sol-gel, hydrogel or polymer, or by depositing conducting polymer, i.e., chemically modified electrode to create an electroactive electrode surface.<sup>6,32-35</sup> The

binding of analyte to a bioreceptor attached onto an electroactive construct will directly affect the electrochemical properties of the electroactive interface, thus enabling detection. Alternatively, label-free detection can be achieved through pulsed techniques which record current transients or impedance spectroscopy which senses changes in surface density and conformational changes upon the presence of analytes.<sup>6</sup> A major drawback of label-free approaches is that the detections depend on the perturbations that result from binding, which at times can be non-selective due to non-specific binding.<sup>15,32</sup>

A label is a reporter molecule which renders a binding event detectable. Unless the analyte is intrinsically electroactive (e.g., the detection of electroactive copper ion in peptide-based metal ion sensor, see Figure 1.3), a redox label must be used to relay the detection event into an electrical signal. A biosensor can be labelled with an enzyme which produces an electroactive species or a redox molecule which enables changes during a binding event to be determined electrochemically.<sup>6,15,19</sup>

Enzymes with high catalytic rate constants, e.g., catalase, alkaline phosphatase, glucose oxidase, horseradish peroxidase,  $\beta$ -galactosidase, and glucose-6-phosphate have been used as labels in immunosensors, but their use can be limited by variations in temperature or inhibited by extraneous substances in sample matrix and non-specific binding interactions.<sup>15,36</sup> The use of such labels is further complicated by washing and separation steps to remove unbound labelled antigens before the introduction of substrates to yield electroactive products.<sup>5,15</sup> Nonetheless, these sensors can be made reagentless if the access of bound and unbound labels to electrodes can be properly segregated by size or charge without further treatment.<sup>15,36</sup>

The use of redox labels in electrochemical sensing can be traced back to artificial redox mediators which were adopted as electron acceptors in catalytic biosensors.<sup>37</sup> According to Marcus theory, the spatial separation between a redox centre buried in an enzyme and its transducer hinders efficient heterogeneous electron transfer, therefore the resultant current cannot accurately reflect analyte concentration.<sup>29,33,38</sup> Such slow transfer rates have also been attributed to electrode fouling.<sup>39</sup> In some cases, high overpotentials are needed to oxidise products of reactions, e.g.,  $H_2O_2$  (see Figure

1.2), such that oxidisable components in the sample interfere with the intended detection of target analytes.<sup>15</sup> One solution to counteract these problems is through the use of artificial redox mediators capable of rapid homogeneous electron exchange with the enzyme and heterogeneous electron exchange with the transducer to establish an electrical contact between the enzyme and transducer.<sup>29,33,39,40</sup>

By extension, biomolecules can be tagged with redox labels to enable electrochemical detection. A redox label is a bifunctional molecule: firstly, it allows interaction between a target analyte and bioreceptor linked to it and secondly, it reports a binding event through electrochemical changes it experiences during the event. Initial efforts by Heinemann *et al.*<sup>41</sup> demonstrated that the electrochemistry of an electroactive label, mercuric acetate, conjugated to estriol, was perturbed upon binding to estriol antibodies. Around the same time, Weber and Purdy noted that ferrocene carbonyl conjugated morphine did not interfere with the binding of morphine to its antibody.<sup>42</sup> This shows that the presence of redox label can have minimal impact upon target binding to biorecognition elements.

While nucleic acids are inherently electroactive, they can benefit from the use of redox labels. Sensitivity and/or specificity in DNA sensing are improved by electrochemical responses produced by redox labels which are distinguishable from the ones from natural DNA (Figure 1.4).<sup>43-47</sup> Metallonucleosides can be obtained by covalent attachment to, or intercalation in oligonucleotides at the termini or within the DNA sequence, either by complexing a chelate-containing oligonucleotide to a metal complex or by conjugating a functionalised oligonucleotide to a suitably activated metal complex.<sup>46-50</sup> Multiple redox-labelled oligonucleotides, known as a “multicolour” approach, can be employed in parallel to allow detection of specific sequences.<sup>46</sup>

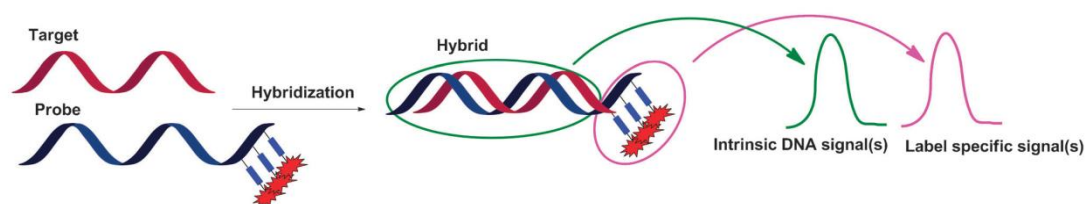


**Figure 1.4** Electrochemical detection of DNA strand with labelled oligonucleotide.<sup>46</sup>

To reiterate, the advantages offered by redox labels are the lowering of operating potential of an electrode, the window of which minimises interferences of electroactive substances, and an improved linearity range, sensitivity and selectivity.<sup>9,15,19</sup> Compared to enzyme labels, redox labels provide a more direct route in biosensing in that bioreceptors can be made electroactive by labelling it with a redox label, thereby alleviating the need for an associated enzymatic reaction to give an electroactive product.<sup>15</sup> Most of all, biorecognition elements modified with redox labels allow the detection of non-electroactive target analytes.<sup>51</sup>

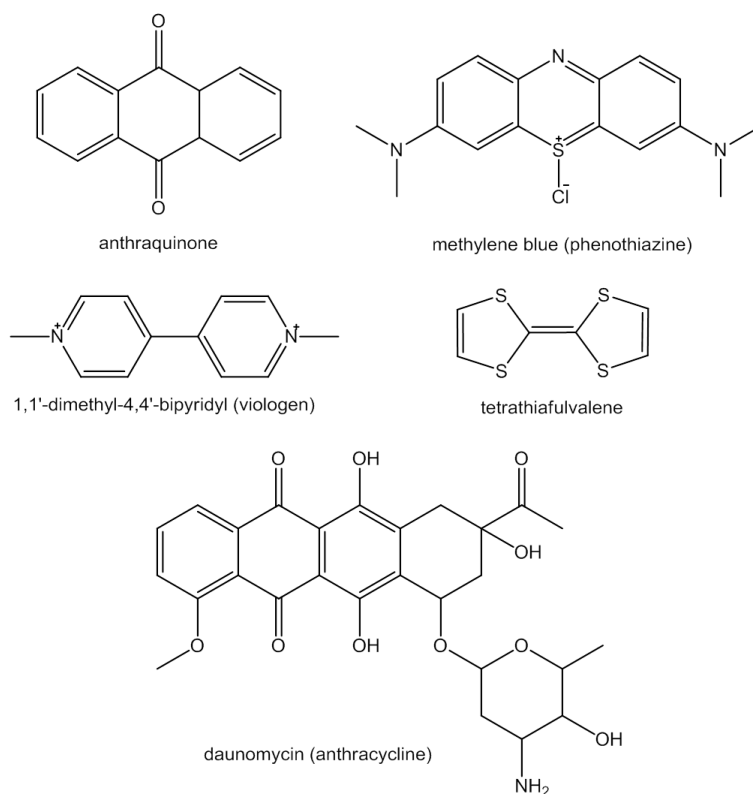
## 1.5 Classes of Redox Labels

Redox labels come in different structures, properties and a diverse range of  $E_{1/2}$ . They undergo cyclisations of oxidation and reduction during detection, hence the reversibility of these compounds in both oxidised and reduced forms directly affect their performance in electron transfer. Interaction with target biomolecules will alter electron-transfer properties of the redox labels, the changes of which are manifested in the form of potential shift and/or current fluctuation to indicate their presence.<sup>52</sup>

Similar to redox mediators, redox labels are categorised into two major groups: organic compounds and metal-based compounds.<sup>45</sup> In recent times, nanoobjects, e.g., nanocrystals, quantum dots and carbon nanotubes loaded with redox-active compounds have also been employed as redox labels but they are not within the scope of this discussion.<sup>7,8</sup>

The major types of organic redox labels include anthracyclines, quinones/hydroquinones, phenoxazines, phenothiazines, quinoxaline, tetrathiafulvalene and viologens, all of which share the common feature of  $\pi$  bonds for efficient electron transfer.<sup>3,12,39,45,53</sup> Apart from examples where metal ions are directly ligated to the biorecognition elements (e.g., antibodies),<sup>54</sup> metal-based redox labels are typically metal chelates containing heterocyclic nitrogenous bidentate ligands, e.g., 2,2'-bipyridyl (bpy) or 1,10-phenanthroline (phen), metalloporphyrins, osmium complexes and organometallics such as ferrocene and its derivatives.<sup>45,53,55-57</sup>

(a)



(b)

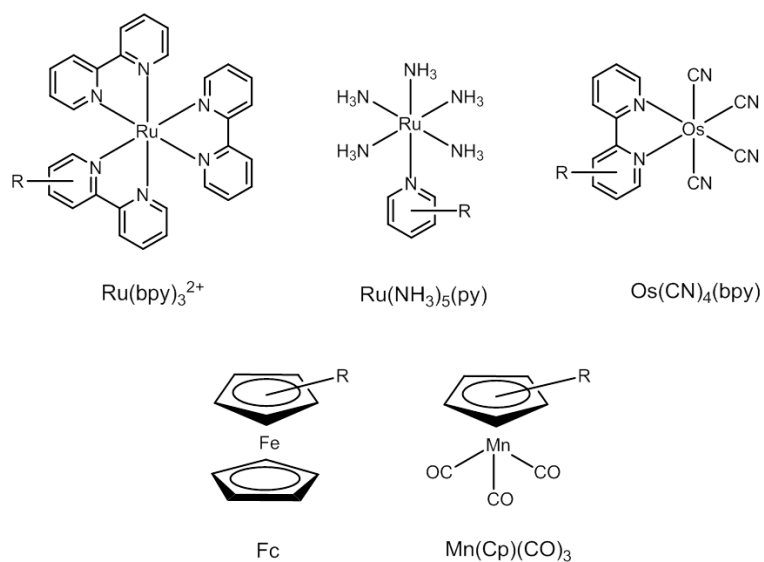


**Figure 1.5** Selected examples of redox labels: (a) organic redox labels; (b) metal-based redox labels modified with linker groups.

Metal-based redox labels are generally modified with linker groups (depicted as R groups in Figure 1.5b), e.g., ethynyl bridge,<sup>45</sup> carboxylic acid,<sup>52,58</sup> amino group,<sup>55,59</sup> methyl imidate,<sup>56</sup> maleimide,<sup>57</sup> and so on, to facilitate their conjugation with bioreceptors. Like organic redox labels, the metal-based redox labels also feature extensive conjugation in their nitrogenous ligands or cyclopentadienyl rings.

### 1.5.1 Metal-based Redox Labels

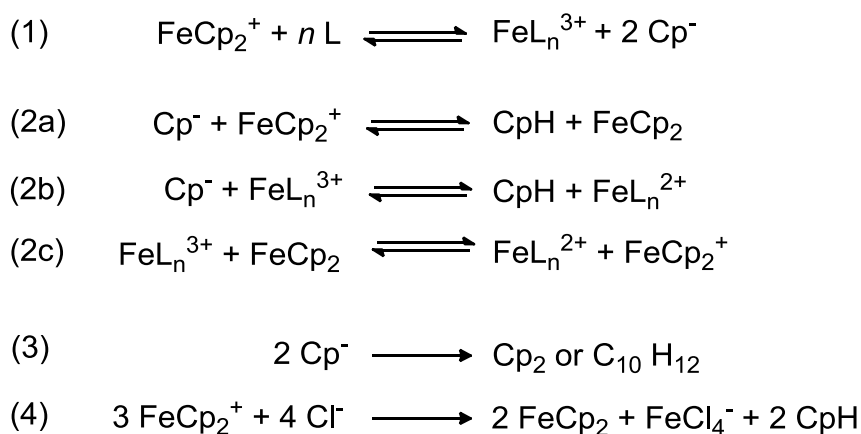
Albeit widely used, some organic redox labels suffer from problems such as autoxidation, poor stability and pH dependence on their  $E_{1/2}$  in different media – acidic, neutral and basic – in which they are active.<sup>3,32,34</sup> In addition, the possibility of polymerisation exists for highly aromatic organic redox labels, for instance, phenazines.<sup>34</sup> The sensitivity towards pH makes the use of organic redox labels impractical in samples where pH is not unknown or uncontrolled. Due to the requirements of the certain systems, metal-based redox labels are able to yield better results and as such are preferred over their organic counterparts.<sup>60</sup>

Ferrocene has been used extensively as a redox label in electrochemical biosensors since its first application in the glucose biosensors.<sup>33</sup> Due to fluctuations in oxygen concentration, 1,1-dimethylferrocene was employed by Cass and co-workers as the first transition-metal based redox mediator to mediate electron transfer in glucose biosensors where it was shown to work independent of pH.<sup>61</sup> Since then, ferrocene has been widely used in sensing applications, as minor modifications on the cyclopentadienyl ring allow the derivatisation of ferrocene with a multitude of functionalities for distinctive properties, e.g., through the introduction of carbohydrates or sulfonates to render these conjugates hydrophilic.<sup>62-64</sup>

### 1.5.2 The Instability of Ferricenium Ion in Biological Samples

The large amount of literature present clearly demonstrates the popularity of ferrocene-based label in biological applications. While ferrocene ( $\text{FeCp}_2$ ) is a stable compound, its oxidised form, ferricenium ion ( $\text{FeCp}_2^+$ ), is unstable in the presence of chloride salts and other strongly nucleophilic reagents ultimately leading to free  $\text{Fe}^{3+}$ ,

Cp<sup>-</sup> and organic coupling products.<sup>65-67</sup> Studies carried out by Prins and co-workers<sup>65</sup> established that this decomposition is started off by a primary ligand exchange step at FeCp<sub>2</sub><sup>+</sup> with L (Scheme 1.1, Equilibrium 1, where L is either a solvent molecule, a neutral nucleophilic agent or a mononegative anion), followed by reduction of FeCp<sub>2</sub><sup>+</sup> and FeL<sub>n</sub><sup>3+</sup> by strongly reducing Cp<sup>-</sup> anions (Scheme 1.1, Equilibriums 2a and 2b). The potential difference between the couples FeCp<sub>2</sub>-FeCp<sub>2</sub><sup>+</sup> and FeL<sub>n</sub><sup>2+</sup>-FeL<sub>n</sub><sup>3+</sup> and subsequently their equilibrium constant (Scheme 1.1, Equilibrium 2c) influence the total decomposition reaction of FeCp<sub>2</sub><sup>+</sup>.<sup>65</sup> Finally, the Cp radicals irreversibly combine to form Cp<sub>2</sub> or dimerise to C<sub>10</sub>H<sub>12</sub>. Equation 4 (Scheme 1.1) describes the progressive decomposition of Fc<sup>+</sup> by chloride ions:<sup>65</sup>



**Scheme 1.1** Steps 1 – 4 detailing the progressive decomposition of ferricenium ion, FeCp<sub>2</sub><sup>+</sup>, by L, where L is either a solvent molecule, a neutral nucleophilic agent or a mononegative anion.<sup>65</sup>

The prevalence of chloride salt in biological samples means that ferrocene labels will have limited stability in biological applications. High concentration of perchlorate ions in chloride-containing buffers have been shown to stabilise Fc<sup>+</sup> during electrochemical measurement by ion pairing with Fc<sup>+</sup>.<sup>68</sup> However, it does not always prevent signal loss caused by the degradation of Fc<sup>+</sup>.<sup>69</sup> It is therefore desirable to explore other transition-metal based complexes to substitute for ferrocene as redox labels in electrochemical sensing devices. Aside from ferrocene, metal complexes with porphyrins, polypyridines, polyphenanthrolines and phthalocyanines ligands have been used as redox labels.<sup>58</sup> In the following sections, selected ruthenium complexes that have been applied as redox labels will be discussed.

## 1.6 Redox Labels Using Transition-metal Complexes

The main challenges in utilising metal-based redox labels in biosensors are the tuning of their  $E_{1/2}$  and their solubility in the working environment. The  $E_{1/2}$  of metal complexes can be modified by ligand selection and/or substituent introduction on ligand through redistribution of electron density around the metal centre. In this regard, ruthenium and osmium complexes provide greater flexibilities in ligand selection than ferrocene, and consequently provide a wider range of potentials. An ideal redox label should fulfil the following requirements:<sup>1,3,70</sup>

1. low  $E_{1/2}$  window: -0.3 V to +0.5 V (vs Ag/AgCl)
2. pH-independent  $E_{1/2}$
3. reversible electron transfer kinetics
4. chemically stable in oxidised and reduced forms
5. easily tuneable potentials

The low  $E_{1/2}$  of the ideal redox labels would reduce interference from oxidisable species in sample matrices during detection whereas the pH-independent  $E_{1/2}$  of an ideal redox label would allow the detection in samples where pH is unknown or uncontrolled. Also, solubility of the redox label is pertinent to the ease of its incorporation at the sensing interface.<sup>70</sup> Some redox mediators of transition-metal complexes will be reviewed here as they draw on similar design motives and desired criteria in order to be applicable in biosensing devices.

### 1.6.1 Redox Mediators Based on Transition-metal Complexes

Zakeeruddin *et al.*<sup>70</sup> studied a series of tris-(4,4-substituted-2,2'-bipyridyl) complexes of iron, ruthenium and osmium as redox mediators to find comparable performances to ferrocene. Complexes with ionisable carboxyl and hydroxyl groups were shown to display pH dependency linked to their  $pK_{as}$ , but those with amino groups did not.<sup>70,71</sup> Following this, Zhang and co-workers screened a series of ruthenium and osmium substituted phen and bpy complexes as solution-based redox mediators for glucose oxidase.<sup>72</sup> A general trend was observed: osmium complexes of the same ligand

systems displayed more negative  $E_{1/2}$  than their ruthenium equivalents, and the ligands bearing electron-donating groups give lower  $E_{1/2}$ .

Warren *et al.* studied the performance of two cationic ruthenium and osmium picolinate complexes electrostatically adsorbed within an anionic polymer/ enzyme layer as redox mediators for glucose sensing.<sup>73</sup> The authors noticed that the strength of the interaction between the complex and polymer during redox cycles had a direct impact on the mechanism – diffusion or hopping – by which electrons could be transported.<sup>73</sup> The diffusion and kinetics parameters of the immobilisation matrix were shown to heavily affect the performance of the glucose sensor. Electrodes modified with anionic polymers have been found to amplify signals as they pre-concentrated cationic species in close proximity to the electrode surface.<sup>36</sup>

Another representative example is an osmium(4,4-dimethyl-2,2-bipyridyl)<sub>2</sub> chloride complex cross-linked to poly(1-vinylimidazole) developed by Heller's group (Figure 1.6a).<sup>35</sup> Noting the interfering currents from oxidisable species in their previous work, they lowered the  $E_{1/2}$  of the polymer by substituting bipyridyl ligand with one that has two electron-donating methyl groups – interferant currents at this potential then become negligible, thus allowing the detection of glucose and lactate.<sup>35</sup>

Coordination modification of a protein with metal complexes is known to be a viable solution in increasing electron transfer efficiency between redox enzymes and transducers without compromising the physicochemical properties of the proteins.<sup>74</sup> [Ru(LL)<sub>2</sub>(X)<sub>2</sub>] complexes, where LL is either phen or bpy and X an acido ligand, are known to readily coordinate to certain oxidases.<sup>74,75</sup> Schuhmann and co-workers assessed the performance of a series of ruthenium complexes as redox mediators for oxygen-independent redox enzymes in modified carbon paste.<sup>75</sup> The potentials of these complexes were varied by changing the ligand X surrounding the ruthenium centre. The change of ligand LL from bpy to phen (complex 3 and 5) resulted in a significant potential shift (Figure 1.6b).

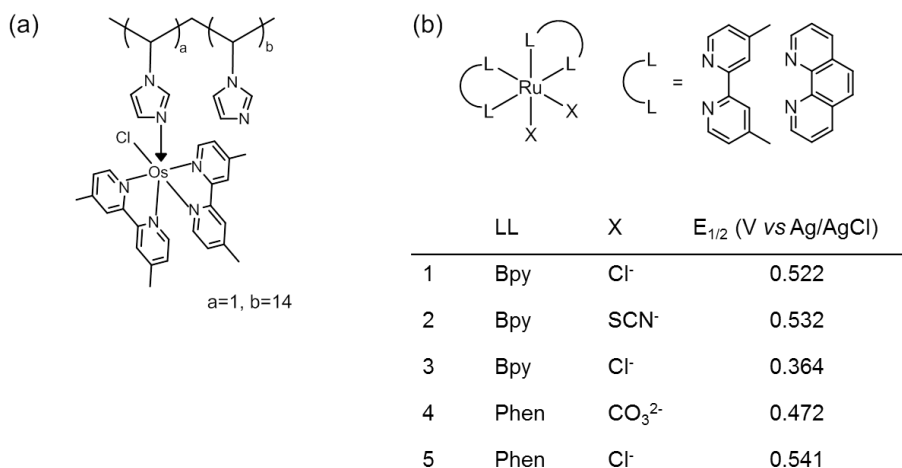


**Figure 1.6** (a) Osmium(4,4-dimethyl-2,2'-bipyridyl)<sub>2</sub> chloride cross-linked to poly(1-vinylimidazole). (b) Structure of [Ru(LL)<sub>2</sub>(X)<sub>2</sub>] and their potentials.

### 1.6.2 Ruthenium Complexes as Redox Labels

The earlier examples cited in Section 1.5.3 establish that ruthenium complexes are able to function as redox mediators in biosensing systems. Since then, a number of reports on the use of ruthenium complexes as redox labels have been generated, where variations of the ligands surrounding the metal centre are shown to influence the redox properties of the complexes in a predictable manner. Two major strategies on the systematic tuning of  $E_{1/2}$  of ruthenium complexes are laid out below.

Structurally similar complexes of significantly varied and wide-ranging potentials can be accessed through cyclometalation.<sup>76</sup> The cyclometalated ruthenium complex stems from the covalent Ru-C bond between the metal centre and the cyclometalated ligand.<sup>77</sup> The changes introduced by a combination of benziimidazole-based bis-tridentate ligands of cyclometalated and non-cyclometalated ruthenium complexes allows for progressive and systematic modulation of the metal-associated  $E_{1/2}$  in a wide scope of 0.26 to 1.32 V vs Ag/AgCl (see Figure 1.7).<sup>77</sup> In this report, anionic cyclometalating ligands led to more significant anodic shifts in  $E_{1/2}$ , as their contribution to the electron richness around metal centre is higher compared to the non-cyclometalated analogues.<sup>77</sup>

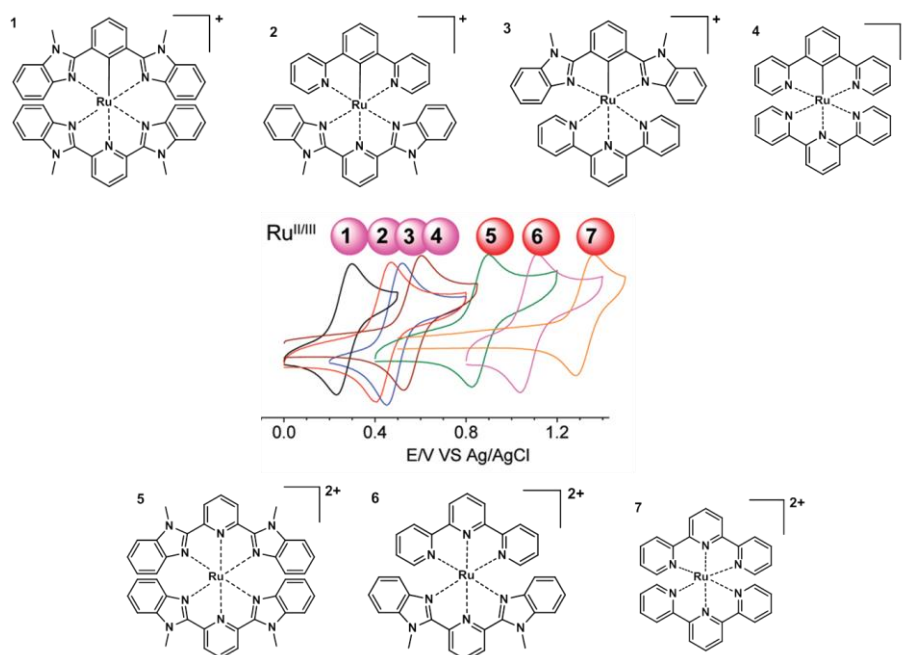


**Figure 1.7** Cyclometalated (top) and non-cyclometalated (bottom) ruthenium complexes, along with their  $E_{1/2}$ .<sup>77</sup>

A second method to tuning  $E_{1/2}$  is by varying the substituents on the ligands or by substituting a ligand from one with another to induce changes in the electronic properties at the metal centre. Kalinina and co-workers prepared a group of ruthenium complexes bearing two acetylacetonato (acac) ligands and one benzoquinonediimine (bqdi) ligand where substituents can be introduced on bqdi (Figure 1.8) to adjust the level of  $\pi$ -back-donation.<sup>78</sup> This in turn influences the electron-richness around the metal centre and consequently their  $E_{1/2}$  from which correlations between the nature of substituents and the quantitative extent of  $\pi$ -back-donation and  $\sigma$ -forward donation can be drawn.

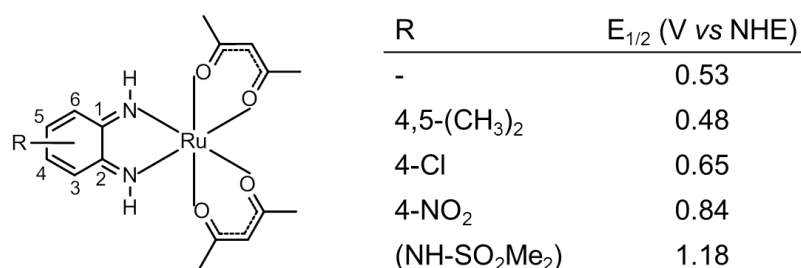


**Figure 1.8** Structure of  $\text{Ru}(\text{acac})_2(\text{R-bqdi})$  complexes and their  $E_{1/2}$ .

Vrabel *et al.*<sup>43</sup> labelled purines on nucleic acids with ruthenium complexes bearing bpy, phen and terpyridine ligands where the values of  $E_{1/2}$  were observed to be

affected by the changing ligands. On the other hand, Meade's group prepared ruthenium-labelled nucleosides of both high and low potentials by adding metal-binding nucleosides, 5'-O-(4,4'-dimethoxytrityl)-2'-iminomethylpyridyl-2'-deoxyuridine (DMTO)<sup>79</sup> and 2'-iminomethylpyridyl-2'-deoxyuridine (IMPy)<sup>80</sup> to Ru(bpy)<sub>2</sub>(Cl)<sub>2</sub> and Ru(acac)<sub>2</sub>(MeCN)<sub>2</sub> respectively to give a difference of around 1 V in reduction potentials between these two groups of complexes. Weizman and Tor synthesised nine ruthenium and osmium complexes consisting of two bpy ligands and one substituted acac ( $\beta$ -diketonato) or hydroxamic acid bearing linker groups to label nucleotides (Figure 1.9).<sup>81</sup> In short, the  $E_{1/2}$  of these redox-labelled nucleosides was modulated by means of the selection of metal centre, modification at the ligand and substitution of one ligand with another.

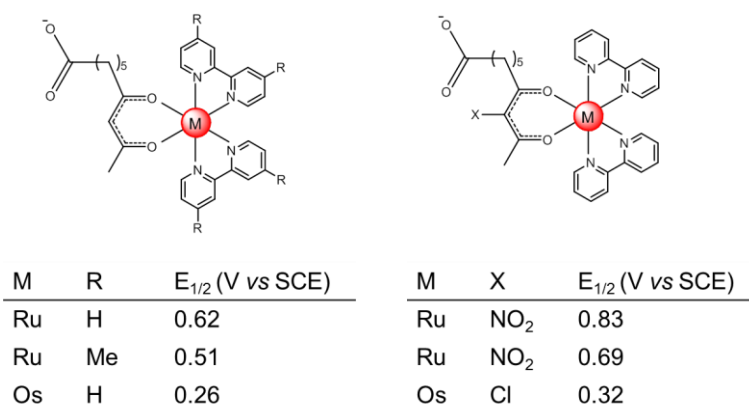


**Figure 1.9** Ruthenium and osmium complexes bearing two bpy ligands and one substituted  $\beta$ -diketonato/hydroxamic acid with linker groups to conjugate with nucleosides.<sup>81</sup>

## 1.7 Surface-Bound Redox Labels: Advantages in Stability and Conformation on Sensing Surfaces

As ruthenium complexes have been shown to be successfully conjugated to biomolecules and their  $E_{1/2}$  can be tuned by proper ligand selection or substitution, the next step is to functionalise the chelating ligands with reactive groups through which attachments can be made to both bioreceptor and the electrode to allow anchoring of the redox label on electrode. The main driver for developing surface-bound redox labels is the “surface enhancement effect” obtained when previously solvated sensors are immobilised onto a surface.<sup>82</sup> This effect is the result of a combination of an increase in

thermodynamic stability of complexes formed with target analytes and the restricted vibrational and rotational degrees of freedom of these sensors when confined to the electrodes.<sup>82</sup>

The immobilisation of a redox label onto an electrode means that this direct electronic contact produces current that is unlikely to be affected by diffusive processes<sup>33,52,83</sup> that result in an amplification in signals.<sup>84</sup> In addition, immobilisation of redox labels eliminates the need for the labels to be water-soluble for them to work in aqueous environment.<sup>84</sup> Most importantly, the integration of biorecognition elements and redox labels fixed onto electrodes rely solely on the change in the intrinsic properties of the redox label upon analyte binding for signal transductions, essentially making these biosensors reagentless.<sup>57</sup>

Ruthenium complexes immobilised onto SAMs have been reported for a variety of applications: redox switches,<sup>85</sup> electrochemiluminescent label,<sup>86,87</sup> molecular electronics,<sup>88</sup> and construction of electroactive self-assembled monolayers (SAMs).<sup>89-91</sup> The principles of immobilising biomolecules on transducer surfaces mentioned earlier in Section 1.3 are equally applicable to the immobilisation of metal complexes on SAMs. As electrostatic binding of complexes onto a SAM can be adversely affected by pH,<sup>92,93</sup> covalent binding of metal complex on SAMs is the preferred method of immobilisation.

## 1.8 SAMs on Gold Electrodes

To enable the construction of sensing surfaces with better control over molecular orientation, surface reproducibility and durability, organised monomolecular layers are often used first to modify the electrode surface. Organosulfur compounds such as thiols, sulfides and disulfides (Figure 1.10) form organised monolayers, commonly known as SAMs, by spontaneous chemisorption onto gold electrodes.<sup>83,94,95</sup> SAMs can be formed on a gold electrode simply by immersing the electrode in a dilute solution containing organosulfur compound for a time period. To create mixed SAMs, the solution may contain different compounds in a set mole ratio, or part of a pre-formed SAM may be displaced by a more stable SAM by exchange.<sup>83</sup>

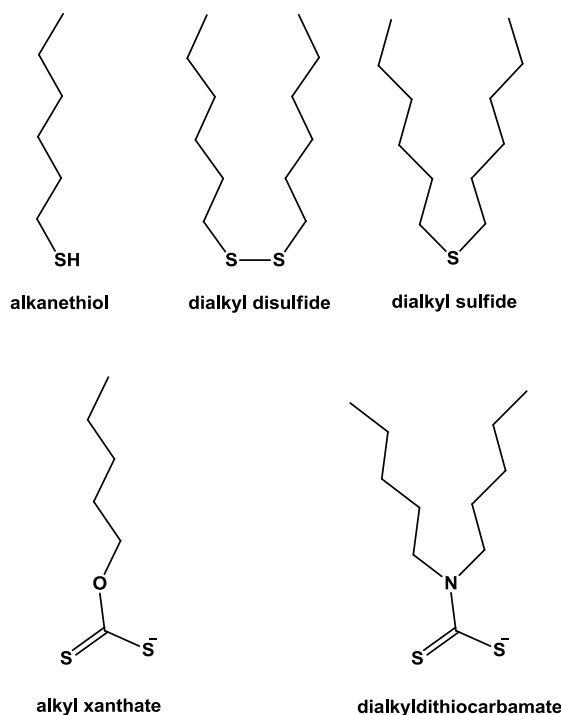
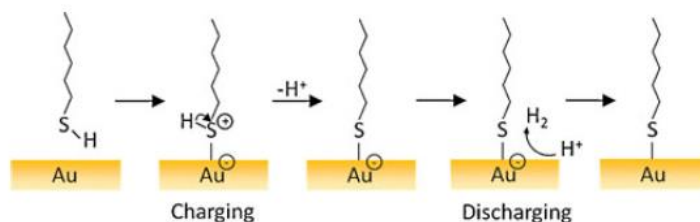


**Figure 1.10** Structures of organosulfur compounds capable of forming SAMs.<sup>95</sup>

SAM formation is thought to consist of two steps: the initial fast adsorption by oxidative addition of the S-H or S-S bond followed by a much slower process of organisation of alkyl chains by van der Waals interactions (Scheme 1.1).<sup>28,95,96</sup> Factors influencing SAM formation include substrate morphology, cleanliness of substrate, adsorbate purity, structure of adsorbate, deposition solvent, concentration of deposition solution and deposition time.<sup>83,94,96</sup> Defects such as pinholes, disorder along alkane chains, domains and islands however exist in SAMs due to variations in packing process and surface structures in polycrystalline substrates.<sup>83,97</sup>



**Scheme 1.2** Adsorption of thiols on gold surfaces.<sup>28</sup>

Ideally, SAMs are arranged in an  $(\sqrt{3} \times \sqrt{3})R30^\circ$  ordering and the alkane chains in *trans* conformation, tilted at  $30^\circ$  as the area occupied by the chains is slightly smaller than the area dictated by the spacing of the sulfur head groups on the gold electrodes so

that a densely packed layer can be formed.<sup>83,94</sup> These highly ordered and well-organised monolayers retain structural order and their high packing density during electrochemical studies when electrode potentials are kept in certain windows, especially in aqueous electrolytes.<sup>94</sup> The ease with which SAMs can be prepared, functionalised and modified, along with their biomimetic and biocompatibility properties makes them very popular in electrochemical sensing studies.<sup>28,96,98</sup> SAMs usually possesses secondary chemical residues available as linkage points to which the desired structural elements can be attached.

Longer chain thiols have been shown to produce much more stable layers, subsequently, more stable affinity biosensors.<sup>6</sup> Nonetheless, thinner monolayers are employed in most cases because the longer chain thiols tend to passivate the electrode.<sup>21</sup> A compromise needs to be struck between SAM stability and the rate of electron transfer influenced mainly by the proximity of redox labels to the electrodes.

## 1.9 Surface-bound Redox Labels in Affinity Biosensors

The electrochemical changes a redox label experiences upon the binding of a target analyte are manifested in the form of potential shifts and/or changes in the magnitude of the current of the redox label. Amperometric monitoring of the kinetics and thermodynamics of electron transfer of a redox-labelled antigen permits an effective and sensitive transduction mechanism for the detection of a target antibody.<sup>99</sup> The same can be applied for peptide-protein interactions. For instance, Kraatz's group fabricated two ferrocene-peptide conjugates on SAMs for the detection of human immunodeficiency virus type I protease (HIV1-PR)<sup>51</sup> (Figure 1.11) and papain, a cysteine protease.<sup>52</sup> In both systems, once the proteases were bound to the peptides, the  $E_{1/2}$  of the ferrocene was shifted anodically, in conjunction with a decrease in current. The anodic shift was explained by an environmental change experienced by the ferrocene as the binding of protease to the peptide would encapsulate the ferrocene redox centre, making it more difficult to oxidise<sup>52</sup> while the slight decrease in current intensity was likely due to the less efficient penetration of the peptide-protein film by the supporting electrolyte.<sup>51,52</sup>

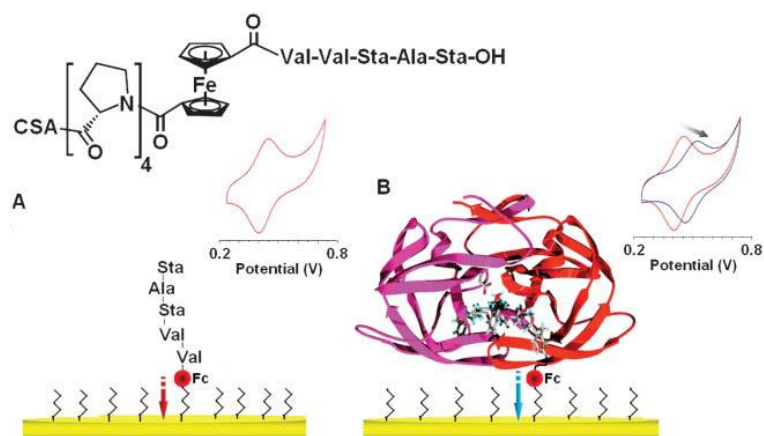


**Figure 1.11** Potential shift and decrease in current density when the target analyte, human immunodeficiency virus type I protease, HIV1-PR, is bound to the ferrocene-peptide conjugate.<sup>51</sup>

In a different approach, the Gooding group constructed immunosensors where the electrochemistry of the ferrocene label was suppressed upon the binding of anti-biotin IgG.<sup>100,101</sup> The ferrocene label engulfed by the large anti-biotin IgG was shown to have its electrochemistry attenuated (Figure 1.12b) – this pronounced decrease in current is rationalised by the perturbations the ferrocene label experiences in its immediate microenvironment from the formation of an immunocomplex, where the access of counterions was restricted.<sup>100</sup> This proof-of-concept has been further expanded to realise a displacement assay in which free biotin was introduced to displace anti-biotin IgG to reverse the attenuation of the current (Figures 1.12c and 1.12d).<sup>101</sup> The same model was successfully applied using epitopes to selectively recognise veterinary antibacterial drug residues in milk samples.<sup>102</sup>

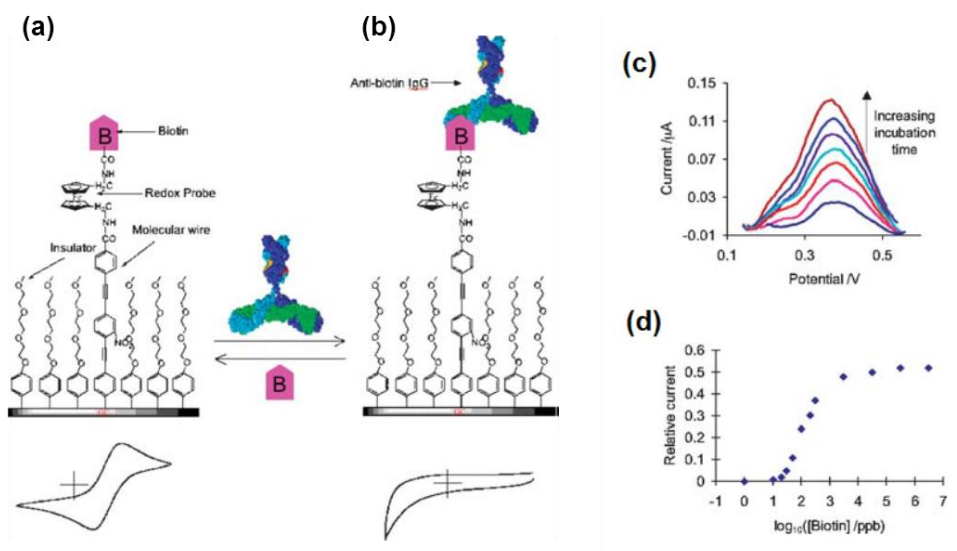


**Figure 1.12** Schematic of a fabricated immunosensor which displays a current attenuation upon binding of a target analyte, anti-biotin IgG: (a) Prior to incubation with the anti-biotin IgG; (b) after incubation with the anti-biotin IgG.<sup>100</sup> A displacement assay in which free biotin displaces anti-biotin IgG to cause a current increase: (c) SWV of the sensing surface after exposure to biotin in increasing time interval; (d) calibration plot showing the increase in relative current (before and after exposure to free biotin) against the concentration of biotin.<sup>101</sup>

The surface architecture of biorecognition surfaces assembled by covalent bonds in a step-wise manner are likely to be affected by coupling efficiency, as each coupling step is rarely quantitative,<sup>103</sup> which invariably causes discrepancies in packing density of the bioreceptors. High packing density of bioreceptors is shown to hinder access of target analytes to the receptor sites, resulting in a decrease in responses.<sup>99</sup> In light of this, Plaxco and co-workers investigated the effects of the fabrication and operational parameters, among them, packing density and location of redox labels of electrode-immobilised oligonucleotide on the performance of electrochemical DNA sensors.<sup>104</sup> They found that equilibration time and signalling of the binding event is highly dependent on the density of the probe oligonucleotides, while improved signalling is achieved when redox label is located closer to the electrode surface. In a later publication, they showed the magnitude of the signal change upon target binding can be enhanced by tuning the frequency of SWV potential pulse.<sup>105</sup> These findings specify that surface architecture, equilibration time and signal transduction need to be optimised in order to maximise signal output of redox labels when binding occurs.

## 1.10 Thesis Aims: Preparation of a Series of Ruthenium Complexes as Redox Labels for Biosensing Applications

Akin to a “mediator soup” in which a solution containing a mixture of redox mediators with a range of different  $E_{1/2}$  are employed to facilitate electron transfer,<sup>39</sup> surface-bound redox labels can be made up by a homologous series of ruthenium complexes of different  $E_{1/2}$  brought on by substituents on their ligands. A binding event leading to a change in the local environment of the redox labels, hence their electrochemical properties – either current or potential or both – allows the selective detection and quantification of target analytes.

This thesis aims to develop ruthenium-based complexes which can serve as redox labels in electrochemical biosensors. The basic structure of the ruthenium-based redox labels to be investigated in this thesis bears both  $\beta$ -diketonato and bpy ligands (Figure 1.13). Both these ligands will not contain ionisable side groups as their  $E_{1/2}$  may then be pH-dependent.<sup>70</sup> The synthetic flexibility afforded by the use of  $\beta$ -diketonato ligands (see Figure 1.9) will make it possible to introduce substituents (R, R', R'' group) to modulate the  $E_{1/2}$  of ruthenium complexes. The bpy ligand is to be functionalised with pendant amine groups (bpy-NH<sub>2</sub>) to enable immobilisation of the redox label to the surface and attachment of biorecognition elements once suitable ruthenium complexes are identified.

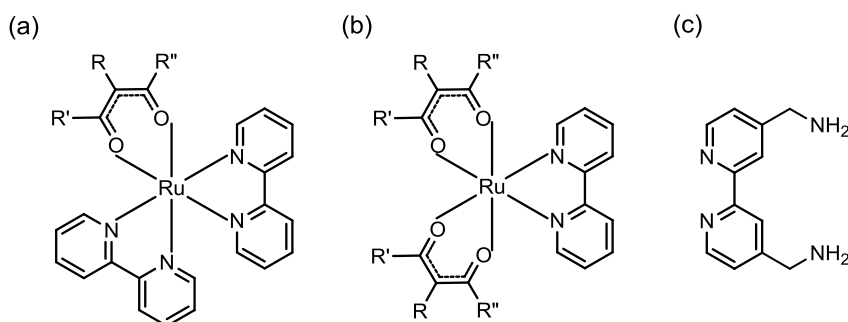


**Figure 1.13** Structures of (a) and (b) ruthenium complexes bearing  $\beta$ -diketonato and bpy ligands; (c) bpy-NH<sub>2</sub>.

The aims of the thesis are as follows:

1. Ruthenium complexes bearing  $\beta$ -diketonato and bpy ligands will be prepared;
2. The complexes electrochemically will be studied to identify suitable candidates as redox labels;
3. The ideal candidate will be modified with bpy-NH<sub>2</sub> to allow attachment of redox label onto SAMs formed on gold electrodes;
4. Covalent binding of an epitope, N-glycosylated-VHLTP (GPP), a pentapeptide which selectively recognises Hb1Ac, a diabetes marker protein, onto the redox label;
5. Evaluation of the performance of the redox label on the detection of Hb1Ac.

## 1.11 Thesis Chapter Overview

The chapters are summarised as follows:

### **Chapter 1: Redox Labels in Electrochemical Affinity Biosensors**

This chapter gives a general introduction on electrochemical biosensors, with particular focus on amperometric biosensors followed by a discussion on redox labels in this class of biosensors. The deficiency of ferrocene and organic compounds as redox labels leads to the intention of developing ruthenium-based redox labels for sensing applications.

### **Chapter 2: Synthesis, Instrumentation and Experimental Procedures**

General considerations of the synthesis of ruthenium complexes, description of instrumentation and experimental procedures for the work carried out in Chapters 3 and 4 are detailed here.

### **Chapter 3: Synthesis and Electronic Tuning of $\beta$ -diketonate Ligands on Heteroleptic Ruthenium<sup>II</sup>( $\beta$ -diketonato)<sub>x</sub>(bpy)<sub>y</sub> Complexes (x and y = 1 or 2)**

This chapter starts by introducing metal complexes formed by ruthenium and bpy and  $\beta$ -diketonato ligands followed by the synthesis of such ruthenium complexes.

Electrochemical studies on the effects of substituents on  $\beta$ -diketonato ligands on the  $E_{1/2}$  of ruthenium complexes are highlighted. Correlations between Hammett constants, ligand electrochemical parameter, UV-vis data to  $E_{1/2}$  of these complexes are described.

#### **Chapter 4: Evaluation of Ruthenium-Based Redox Label in an Electrochemical Biosensor**

The bpy ligand of the ruthenium complex was functionalised with amino groups to enable amide bond coupling for the immobilisation of the redox label onto SAMs. The sensing surface was fabricated step-wise on gold surfaces and characterised by CV and X-ray photoelectron spectroscopy. Finally the attachment of pentapeptide, GPP, onto the free amino group on the redox label for the detection of Hb1Ac is reported.

#### **Chapter 5: Concluding Remarks and Future Work**

The thesis concludes by a brief summary on the use of ruthenium complex as redox label and the future directions of this work.

#### **1.12 References**

- (1) Grieshaber, D.; MacKenzie, R.; Vörös, J.; Reimhult, E. *Sensors* **2008**, *8*, 1400.
- (2) Thévenot, D. R.; Toth, K.; Durst, R. A.; Wilson, G. S. *Biosens. Bioelectron.* **2001**, *16*, 121.
- (3) Chaubey, A.; Malhotra, B. D. *Biosens. Bioelectron.* **2002**, *17*, 441.
- (4) Leech, D. *Chem. Soc. Rev.* **1994**, *23*, 205.
- (5) Borisov, S. M.; Wolfbeis, O. S. *Chem. Rev.* **2008**, *108*, 423.
- (6) Holford, T. R. J.; Davis, F.; Higson, S. P. J. *Biosens. Bioelectron.* **2012**, *34*, 12.
- (7) Sassolas, A.; Leca-Bouvier, B. D.; Blum, L. J. *Chem. Rev.* **2008**, *108*, 109.
- (8) Labuda, J.; Brett, A. M. O.; Evtugyn, G.; Fojta, M.; Mascini, M.; Ozsoz, M.; Palchetti, I.; Paleček, E.; Wang, J. *Pure & Appl. Chem.* **2010**, *82*, 1162.
- (9) Cagnin, S.; Caraballo, M.; Guiducci, C.; Martini, P.; Ross, M.; SantaAna, M.; Danley, D.; West, T.; Lanfranchi, G. *Sensors* **2009**, *9*, 3122
- (10) Mikkelsen, S. R. *Electroanal.* **1996**, *8*, 15.
- (11) Domínguez-Renedo, O.; Alonso-Lomillo, M. A.; Arcos-Martínez, M. J. *Crit. Rev. Env. Sci. Technol.* **2013**, *43*, 1042.
- (12) Castillo, J.; Gáspár, S.; Leth, S.; Niculescu, M.; Mortari, A.; Bontidean, I.; Soukharev, V.; Dorneanu, S. A.; Ryabov, A. D.; Csöregi, E. *Sens. Act. B* **2004**, *102*, 179.
- (13) Rodriguez-Mozaz, S.; Lopez de Alda, M. J.; Barcelo, D. *Anal. Bioanal. Chem.* **2006**, *386*, 1025.
- (14) Wang, J. *Biosens. Bioelectron.* **2006**, *21*, 1887.
- (15) D'Orazio, P. *Clinica Chimica Acta* **2003**, *334*, 41.

- (16) Wang, J.; Rivas, G.; Cai, X.; Palecek, E.; Neilsen, P.; Shiraishi, H.; Dontha, N.; Luo, D.; Parrado, C.; Chicharro, M.; Farias, P. A. M.; Valera, F. S.; Grant, D. H.; Ozsoz, M.; Flair, M. N. *Anal. Chim. Acta* **1997**, *347*, 1.
- (17) Ronkainen, N. J.; Halsall, H. B.; Heineman, W. R. *Chem. Soc. Rev.* **2010**, *39*, 1747.
- (18) Zhang, S.; Wright, G.; Yang, Y. *Biosens. Bioelectron.* **2000**, *15*, 273.
- (19) Mehrvar, M.; Abdi, M. *Analytical Sciences* **2004**, *20*, 1113.
- (20) Wang, J. *Chem. Rev.* **2008**, *108*, 814.
- (21) Chow, E.; Hibbert, D. B.; Gooding, J. J. *Anal. Chim. Acta* **2005**, *543*, 167.
- (22) Chow, E.; Wong, E. L. S.; Böcking, T.; Nguyen, Q. T.; Hibbert, D. B.; Gooding, J. J. *Sens. Act. B* **2005**, *111-112*, 540.
- (23) Yang, W.; Chow, E.; Willett, G. D.; Hibbert, D. B.; Gooding, J. J. *Analyst* **2003**, *128*, 712.
- (24) Wang, J. *Trends in Anal. Chem.* **2002**, *21*, 226.
- (25) Mir, M.; Homs, A.; Samitier, J. *Electrophoresis* **2009**, *30*, 3386.
- (26) O'Dea, J. J.; Osteryoung, J.; Osteryoung, R. A. *Anal. Chem.* **1981**, *53*, 695.
- (27) Chapman, R. G.; Ostuni, E.; Liang, M. N.; Meluleni, G.; Kim, E.; Yan, L.; Pier, G.; Warren, H. S.; Whitesides, G. M. *Langmuir* **2001**, *17*, 1225
- (28) Mandler, D.; Kraus-Ophir, S. *J. Solid State Electrochem.* **2011**, *15*, 1535.
- (29) Willner, I.; Katz, E. *Angew. Chem. Int. Ed.* **2000**, *39*, 1180.
- (30) Sassolas, A.; Blum, L. J.; Leca-Bouvier, B. D. *Biotech. Adv.* **2012**, *30*, 489.
- (31) Bordes, A.-L.; Schöllhorn, B.; Limoges, B.; Degrand, C. *Talanta* **1999**, *48*, 201.
- (32) Lange, U.; Roznyatovskaya, N. V.; Mirsky, V. M. *Anal. Chim. Acta* **2008**, *614*, 1.
- (33) Cass, A. E. G. In *Volume 12. Applications III: Functional Materials, Environmental and Biological Applications*; O'Hare, D., Ed.; Elsevier: Oxford, 2007; Vol. 12, p 589.
- (34) Pauliukaite, R.; Ghica, M. E.; Barsan, M. M.; Brett, C. M. A. *Anal. Lett.* **2010**, *43*, 1588.
- (35) Ohara, T. J.; Rajagopalan, R.; Heller, A. *Anal. Chem.* **1994**, *66*, 2451.
- (36) Limoges, B.; Degrand, C.; Brossier, P. *J. Electroanal. Chem.* **1996**, *402*, 175.
- (37) Green, M. J. *Phil. Trans. R. Soc. Lond. B* **1987**, *316*, 135.
- (38) Wang, J. *Electroanal.* **2001**, *13*, 983.
- (39) Fultz, M. L.; Durst, R. A. *Anal. Chim. Acta* **1982**, *140*, 1.
- (40) Foulds, N. C.; Lowe, C. R. *Anal. Chem.* **1988**, *60*, 2473.
- (41) Heineman, W. R.; Anderson, C. W.; Halsall, H. B. *Science* **1979**, *204*, 865.
- (42) Weber, S. G.; Purdy, W. C. *Anal. Lett.* **1979**, *12*, 1.
- (43) Vrábel, M.; Hocek, M.; Havran, L.; Fojta, M.; Votruba, I.; Klepetář, B.; Pohl, R.; Rulišek, L.; Zendlová, L.; Hobza, P.; Shih, I.; Mabery, E.; Mackman, R. *Eur. J. Inorg. Chem.* **2007**, 1752.
- (44) Li, F.; Chen, W.; Tang, C.; Zhang, S. *Talanta* **2008**, *77*, 1
- (45) Fojta, M.; Havran, L.; Pivoňková, H.; Horáková, P.; Hocek, M. *Curr. Org. Chem.* **2011**, *15*, 2936.
- (46) Hocek, M.; Fojta, M. *Chem. Soc. Rev.* **2011**, *40*, 5802.
- (47) Myers, C. P.; Williams, M. E. *Coord. Chem. Rev.* **2010**, *254*, 2416.
- (48) Wang, P.; Miller, J. E.; Henling, L. M.; Stern, C. L.; Frank, N. L.; Eckermann, A. L.; Meade, T. J. *Inorg. Chem.* **2007**, *46*, 9853.
- (49) Hurley, D. J.; Tor, Y. *J. Am. Chem. Soc.* **2002**, *124*, 3749.
- (50) Khan, S. I.; Beilstein, A. E.; Grinstaff, M. W. *Inorg. Chem.* **1999**, *38*, 418.
- (51) Kerman, K.; Mahmoud, K. A.; Kraatz, H.-B. *Chem. Commun.* **2007**, 3829.

- (52) Mahmoud, K. A.; Kraatz, H.-B. *Chem. Eur. J.* **2007**, *13*, 5585.
- (53) Wring, S. A.; Hart, J. P. *Analyst* **1992**, *117*, 1215.
- (54) Hayes, F. J.; Halsall, H. B.; Heineman, W. R. *Anal. Chem.* **1994**, *66*, 1860.
- (55) Ahrens, M. J.; Bertin, P. A.; Gaustad, A. G.; Georganopoulou, D.; Wunder, M.; Blackburn, G. F.; Gray, H. B.; Meade, T. J. *Dalton Trans.* **2011**, *40*, 1732.
- (56) Hromadová, M.; Salmain, M.; Sokolová, R.; Pospíšil, L.; Jaouen, G. *J. Organometal. Chem.* **2003**, *668*, 17.
- (57) Trammell, S. A.; Goldston, H. M.; Tran, P. T.; Tender, L. M. *Bioconjugate Chem.* **2001**, *12*, 643.
- (58) Zheng, D.; Wang, N.; Wang, F.-Q.; Dong, D.; Li, Y.-G.; Yang, X.-Q.; Guo, L.-H.; Cheng, J. *Anal. Chim. Acta* **2004**, *508*, 225.
- (59) Beer, P. D.; Szemes, F.; Passaniti, P.; Maestri, M. *Inorg. Chem.* **2004**, *43*, 3965.
- (60) Ferapontova, E. E.; Gothelf, K. V. *Electroanal.* **2009**, *21*, 1261.
- (61) Cass, A. E. G.; Davis, G.; Francis, G. D.; Hill, H. A. O. *Anal. Chem.* **1984**, *56*.
- (62) Trivedi, R.; Deepthi, S. B.; Giribabu, L.; Sridhar, B.; Sujitha, P.; Kumar, C. G.; Ramakrishna, K. V. S. *Eur. J. Inorg. Chem.* **2012**, 2267.
- (63) Tustin, G. J.; Lafitte, V. G. H.; Banks, C. E.; Jones, T. G. J.; Smith, R. B.; Davis, J.; Lawrence, N. S. *J. Organometal. Chem.* **2007**, *692*, 5173.
- (64) Seiwert, B.; Karst, U. *Anal. Bioanal. Chem.* **2008**, *390*, 181.
- (65) Prins, R.; Korwagen, A. R.; Kortbeek, A. G. T. G. *J. Organometal. Chem.* **1972**, *39*, 335.
- (66) Ge, D.; Levicky, R. *Chem. Commun.* **2010**, *46*, 7190.
- (67) Kraatz, H.-B. *J. Organometal. Chem.* **1999**, *579*, 222.
- (68) Rowe, G. K.; Creager, S. E. *Langmuir* **1991**, *7*, 2307.
- (69) Kang, D.; Zuo, X.; Yang, R.; Xia, F.; Plaxco, K. W.; White, R. J. *Anal. Chem.* **2009**, *81*, 9109.
- (70) Zakeeruddin, S. M.; Fraser, D. M.; Nazeeruddin, M. K.; Grätzel, M. *J. Electroanal. Chem.* **1992**, *337*, 253.
- (71) Fraser, D. M.; Zakeeruddin, S. M.; Grätzel, M. *J. Electroanal. Chem.* **1993**, *359*, 125.
- (72) Zhang, C.; Haruyama, T.; Kobatake, E.; Aizawa, M. *Anal. Chim. Acta* **2000**, *408*, 225.
- (73) Warren, S.; McCormac, T.; Dempsey, E. *Bioelectrochemistry* **2005**, *67*, 23.
- (74) Federova, T. V.; Vilesov, A. S.; Kurzeev, S. A.; Stepanova, E. V.; Landesman, E. O.; Koroleva, O. V. *Appl. Biochem. Microbiol.* **2006**, *42*, 550.
- (75) Ivanova, E. V.; Sergeeva, V. S.; Oni, J.; Kurzawa, C.; Ryabov, A. D.; Schuhmann, W. *Bioelectrochemistry* **2003**, *60*, 65.
- (76) Cerón-Camacho, R.; Hernández, S.; Lagadec, R. L.; Ryabov, A. D. *Chem. Commun.* **2011**, *47*, 2823.
- (77) Yang, W.-W.; Zhong, Y.-W.; Yoshikawa, S.; Shao, J.-Y.; Masaoka, S.; Sakai, K.; Yao, J.; Haga, M. *Inorg. Chem.* **2012**, *51*, 890.
- (78) Kalinina, D.; Dares, C.; Kaluarachchi, H.; Potvin, P. G.; Lever, A. B. P. *Inorg. Chem.* **2008**, *47*, 10110.
- (79) Rack, J. J.; Krider, E. S.; Meade, T. J. *J. Am. Chem. Soc.* **2000**, *122*, 6287.
- (80) Frank, N. L.; Meade, T. J. *Inorg. Chem.* **2003**, *42*, 1039.
- (81) Weizman, H.; Tor, Y. *J. Am. Chem. Soc.* **2002**, *124*, 1568.
- (82) Cormode, D. P.; Evans, A. J.; Davis, J. J.; Beer, P. D. *Dalton Trans.* **2010**, *39*, 6532.
- (83) Love, J. C.; Estroff, L. A.; Kriebel, J. K.; Nuzzo, R. G.; Whitesides, G. M. *Chem. Rev.* **2005**, *105*, 1103.

- (84) Evans, N. H.; Rahman, H.; Davis, J. J.; Beer, P. D. *Anal Bioanal. Chem.* **2012**, *402*, 1739.
- (85) Sortino, S.; Petralia, S.; Conoci, S.; Di Bella, S. *J. Am. Chem. Soc.* **2003**, *125*, 1122.
- (86) Zanarini, S.; Rampazzo, E.; Bich, D.; Canteri, R.; Della Ciana, L.; Marcaccio, M.; Marzocchi, E.; Montalti, M.; Panciatichi, C.; Pederzoli, C.; Paolucci, F.; Prodi, L.; Vanzetti, L. *J. Phys. Chem. C* **2008**, *112*, 2949.
- (87) Kang, C. H.; Choi, Y.-B.; Kim, H.-H.; Choi, H. N.; Lee, W.-Y. *Electroanal.* **2011**, *23*, 2131.
- (88) Terada, K.; Kobayashi, T.; Haikita, J.; Haga, M. *Chem. Lett.* **2009**, *38*, 416.
- (89) Murphy, F. A.; Suárez, S.; Figgemeier, E.; Schofield, E. R.; Draper, S. M. *Chem. Eur. J.* **2009**, *15*, 5740.
- (90) Tuccitto, N.; Torrisi, V.; Cavazzini, M.; Morotti, T.; Puntoriero, F.; Quici, S.; Campagna, S.; Licciardello, A. *Chem. Phys. Chem.* **2007**, *8*, 227.
- (91) Smalley, J. F.; Finklea, H. O.; Chidsey, C. E. D.; Linford, M. R.; Craeger, S. E.; Ferraris, J. P.; Chalfant, K.; Zawodzinsk, T.; Feldberg, S. W.; Newton, M. D. *J. Am. Chem. Soc.* **2003**, *125*, 2004.
- (92) Freire, R. S.; Kubota, L. T. *Analyst* **2002**, *127*, 1502.
- (93) Jhaveri, S. D.; Trammell, S. A.; Lowy, D. A.; Tender, L. M. *J. Am. Chem. Soc.* **2004**, *126*, 6540.
- (94) Finklea, H. O. In *Electrochemistry. A Series of Advances*; Bard, A. J., Rubinstein, I., Eds.; Marcel Dekker: New York, 1996; Vol. 19, p 109.
- (95) Ulman, A. *Chem. Rev.* **1996**, *96*, 1533.
- (96) Matharu, Z.; Bandodkar, A. H.; Gupta, V.; Malhotra, B. D. *Chem. Soc. Rev.* **2012**, *41*, 1363.
- (97) Eckermann, A. L.; Feld, D. J.; Shaw, J. A.; Meade, T. J. *Coord. Chem. Rev.* **2010**, *254*, 1769.
- (98) Gooding, J. J.; Mearns, F.; Yang, W.; Liu, J. *Electroanal.* **2003**, *15*, 81.
- (99) Yan, J.; Tender, L. M.; Hampton, P. D.; López, G. P. *J. Phys. Chem. B* **2001**, *105*, 8905.
- (100) Liu, G.; Gooding, J. J. *Electrochem. Commun.* **2009**, *11*, 1982.
- (101) Liu, G.; Paddon-Row, M. N.; Gooding, J. J. *Chem. Commun.* **2008**, 3870.
- (102) Khor, S. M.; Liu, G.; Peterson, J. R.; Iyengar, S. G.; Gooding, J. J. *Electroanal.* **2011**, *23*, 1797.
- (103) Gooding, J. J.; Ciampi, S. *Chem. Soc. Rev.* **2011**, *40*, 2704.
- (104) Lubin, A. A.; Hunt, B. V. S.; White, R. J.; Plaxco, K. W. *Anal. Chem.* **2009**, *81*, 2150.
- (105) White, R. J.; Plaxco, K. W. *Anal. Chem.* **2010**, *82*, 73.

## *Chapter 2*

# *Synthesis, Instrumentation and Experimental Procedures*

## 2.1 General Considerations

All manipulations of metal complexes and air-sensitive reagents were carried out using standard Schlenk or vacuum techniques.<sup>1</sup> Solvents were dried and distilled under an atmosphere of nitrogen using standard procedures<sup>2</sup> and stored under nitrogen in glass ampoules, each fitted with a Youngs<sup>®</sup> Teflon valve prior to use. Ethanol (EtOH) was distilled from diethoxymagnesium and dimethylformamide (DMF) was first dried over molecular sieves (4 Å) and distilled.

## 2.2 Chemicals, Reagents, Solvents

All buffers and aqueous solutions were prepared in Milli-Q<sup>™</sup> water (18 mΩ·cm, Millipore, Sydney, Australia). Phosphate buffer (pH 7) was made up of 0.05 M KH<sub>2</sub>PO<sub>4</sub>/K<sub>2</sub>HPO<sub>4</sub> and 0.2 M KCl while phosphate buffer saline (PBS, pH 7.4) was made up of 2.7 mM KCl, 137 mM NaCl, 2 mM KH<sub>2</sub>PO<sub>4</sub> and 10 mM Na<sub>2</sub>HPO<sub>4</sub>. All chemicals used in this thesis are listed in Table 2.1.

**Table 2.1** Chemicals used in this thesis.

Chemical	Formula	Grade	Source
Absolute Ethanol	C <sub>2</sub> H <sub>5</sub> OH	99.5% (w/w)	Ajax Finechem
Acetic anhydride	(CH <sub>3</sub> CO) <sub>2</sub> O	≥99%	Riedel-de-Haën
Acetylacetone	C <sub>5</sub> H <sub>7</sub> O <sub>2</sub>	≥99%	Sigma-Aldrich
Acetonitrile	CH <sub>3</sub> CN	>99.9%	Honeywell Burdick and Johnson
Ammonium hexafluorophosphate	NH <sub>4</sub> PF <sub>6</sub>	≥98%	Fluka
Anhydrous magnesium sulphate	MgSO <sub>4</sub>	62% ≤ x ≤ 70%	Ajax Finechem
Anhydrous sodium acetate	C <sub>3</sub> H <sub>3</sub> O <sub>2</sub> Na	≥99%	Ajax Finechem
Anhydrous sodium sulphate	NaSO <sub>4</sub>	≥99%	Ajax Finechem

Chemical	Formula	Grade	Source
<i>tert</i> - butoxybis(dimethylamino) methane	$(\text{CH}_3)_3\text{COCH}[\text{N}(\text{CH}_3)_2]_2$	90%	Alfa Aesar
<i>N</i> -bromosuccinimide	$\text{C}_4\text{H}_4\text{O}_2\text{NBr}$	99%	Aldrich
2,2'-bipyridine	$\text{C}_{10}\text{H}_{10}\text{N}_2$	$\geq 99\%$	Sigma-Aldrich
Benzene- <i>d</i>	$\text{C}_6\text{D}_6$	99.9% D	CIL
Celite <sup>®</sup> 501 acid-washed	-	-	Fluka
Chloroform- <i>d</i>	$\text{CDCl}_3$	99.9% D	CIL
Copper(II) nitrate trihydrate	$\text{Cu}(\text{NO}_3)_2 \cdot 3\text{H}_2\text{O}$	99%	Prolabo
1,5-cyclooctadiene	$\text{C}_8\text{H}_{12}$	99%	Aldrich
Dibenzoylmethane	$\text{C}_{15}\text{H}_{12}\text{O}_2$	98%	Aldrich
Dichloromethane (drum grade)	$\text{CH}_2\text{Cl}_2$	$\geq 99.5\%$	Ajax Finechem
Dichloromethane (reagent grade)	$\text{CH}_2\text{Cl}_2$	$\geq 99.9\%$	Honeywell Burdick and Johnson
Diethyl ether	$(\text{CH}_3\text{CH}_2)_2\text{O}$	$\geq 98\%$	Ajax Finechem
1-(3-Dimethylaminopropyl)- 3-ethylcarbodiimide hydrochloride	$\text{C}_8\text{H}_{17}\text{N}_3 \cdot \text{HCl}$	98+%	Alfa Aesar
<i>N,N</i> -dimethylformamide	$(\text{CH}_3)_2\text{NCOH}$	>99%	Ajax Finechem
4,4'-dimethyl-2,2'-bipyridine	$\text{C}_{12}\text{H}_{12}\text{N}_2$	99%	Aldrich
Dimethyl sulfoxide- <i>d</i>	$(\text{CD}_3)_2\text{SO}$	99.9%	CIL
Dipotassium hydrogen phosphate	$\text{K}_2\text{HPO}_4$	99.95%	Sigma-Aldrich
Ethanol	$\text{CH}_3\text{CH}_2\text{OH}$	$\geq 99.5\%$	Ajax Finechem
Ethyl acetate	$\text{C}_4\text{H}_8\text{O}_2$	$\geq 99.0\%$	Ajax Finechem
3-ethyl-2,4-pentanedione	$\text{C}_7\text{H}_{12}\text{O}_2$	98%	Aldrich
Ferrocene	$(\text{C}_5\text{H}_5)_2\text{Fe}$	98%	Aldrich
6-(ferrocenyl)hexanethiol	$\text{C}_{16}\text{H}_{22}\text{FeS}$	$\geq 95\%$	Aldrich
<i>N</i> -glycosylated-Val-His-Leu- Thr-Pro	-	>97.5%	Tocris Bioscience

Chemical	Formula	Grade	Source
Hexane	C <sub>6</sub> H <sub>14</sub>	≥95%	Ajax Finechem
1,1,1,5,5,5-hexafluoro-2,4-pentanedione	C <sub>5</sub> H <sub>5</sub> O <sub>2</sub> F <sub>3</sub>	98+%	Lancaster
Hydrochloric acid	HCl	32%	APS
Hydrogen, compressed gas	H <sub>2</sub>	>99%	Linde
Hydrogen peroxide	H <sub>2</sub> O <sub>2</sub>	30% v/v	Univar
Hydroxylamine hydrochloride	NH <sub>2</sub> OH·HCl	-	Pierce
Human Hb1Ac monoclonal antibody IgG (anti-Hb1Ac IgG)	-	-	Abnova
<i>N</i> -hydroxysuccinimide	C <sub>4</sub> H <sub>5</sub> NO <sub>3</sub>	98%	Sigma
<i>N</i> -iodosuccinimide	C <sub>4</sub> H <sub>4</sub> O <sub>2</sub> NI	95%	Aldrich
Lithium chloride	LiCl	99.99%	Aldrich
Methanol	CH <sub>3</sub> OH	>99.8%	Ajax Finechem
3-methyl-2,4-pentanedione	C <sub>6</sub> H <sub>10</sub> O <sub>2</sub>	85%	Aldrich
6-mercaptohexanoic acid	C <sub>6</sub> H <sub>12</sub> O <sub>2</sub> S	90%	Aldrich
2-( <i>N</i> -morpholino)ethanesulfonic acid	C <sub>6</sub> H <sub>13</sub> NO <sub>4</sub> S	99.5%	Sigma
Nitric acid	HNO <sub>3</sub>	70%	Ajax Finechem
Norbornadiene	C <sub>7</sub> H <sub>8</sub>	97%	Lancaster
Palladium on activated charcoal	Pd/C	5% Pd	Fluka
Pentane	C <sub>5</sub> H <sub>12</sub>	≥99%	Ajax Finechem
Potassium carbonate	K <sub>2</sub> CO <sub>3</sub>	≥99.0%	Ajax Finechem
Potassium hydrogen carbonate	KHCO <sub>3</sub>	≥99.0%	Ajax Finechem
Potassium chloride	KCl	≥99.0%	Fluka
Potassium dihydrogen phosphate	KH <sub>2</sub> PO <sub>4</sub>	99.5%	Sigma-Aldrich
Potassium <i>tert</i> -butoxide	C <sub>4</sub> H <sub>9</sub> KO	97%	Alfa Aesar

Chemical	Formula	Grade	Source
Pyridine	C <sub>5</sub> H <sub>5</sub> N	≥99%	Aldrich
Chemical	Formula	Grade	Source
Ruthenium trichloride trihydrate	RuCl <sub>3</sub> ·3H <sub>2</sub> O	Ru: 40-43%	Precious Metals Online
Davisil <sup>®</sup> silica gel	-	60 – 200 micron	Grace Davison
Silver nitrate	AgNO <sub>3</sub>	99.9%	Rhône-Poulenc
Sodium bicarbonate	NaHCO <sub>3</sub>	≥99.7%	Ajax Finechem
Sodium bisulfite	NaHSO <sub>3</sub>	≥99.0%	Ajax Finechem
Sodium carbonate	Na <sub>2</sub> CO <sub>3</sub>	≥99.8%	Ajax Finechem
Sodium hydroxide	NaOH	≥97.0%	Ajax Finechem
Sodium periodate	NaIO <sub>4</sub>	99%	BDH
Sulfuric acid	H <sub>2</sub> SO <sub>4</sub>	98%	Merck
Tetrabutylammonium hexafluorophosphate	(CH <sub>3</sub> CH <sub>2</sub> CH <sub>2</sub> CH <sub>2</sub> ) <sub>4</sub> N (PF <sub>6</sub> )	≥99%	Fluka
Tetrahydrofuran	C <sub>4</sub> H <sub>8</sub> O	≥99.8%	Honeywell Burdick and Jackson
2,2,6,6-tetramethyl-3,5-heptanedione	C <sub>11</sub> H <sub>20</sub> O <sub>2</sub>	≥98%	Aldrich
<i>DL</i> -6,8-thioctic acid	C <sub>8</sub> H <sub>14</sub> O <sub>2</sub> S <sub>2</sub>	99%	Alfa Aesar
Toluene	C <sub>7</sub> H <sub>8</sub>	≥99.8%	Honeywell Burdick and Jackson
1,1,1-trifluoro-2,4-pentanedione	C <sub>5</sub> H <sub>2</sub> O <sub>2</sub> F <sub>6</sub>	98%	Aldrich
Zinc dust, 100 mesh	Zn	97+%	Alfa Aesar

## 2.3 Instrumentation and Techniques

### 2.3.1 Electrochemical Instrumentation

CV and OSWV were performed using an Autolab PGSTAT 12 potentiostat (Eco Chemie, Netherlands) and a BAS 100 B/W electrochemical analyser potentiostat (Bioanalytical Systems, Inc., Lafayette, IN, USA) which were interfaced to computers where data was outputted using Nova and BAS 100W Windows software respectively. This work employed a conventional three-electrode electrochemical cell, which comprises a working electrode (glassy carbon or gold), a counter electrode (platinum wire) and a reference electrode (aqueous or non-aqueous) depending on the solvent system of the experiment. The potential was measured relative to the reference electrode: the aqueous reference electrode was a Ag/AgCl (3 M KCl) electrode (CH Instruments, Inc., TX, USA) while the non-aqueous reference electrode was a Ag/Ag<sup>+</sup> electrode (CH Instruments, Inc., TX, USA) which was referenced against ferrocene, an internal standard. The working electrodes used were glassy carbon and gold electrodes (CH Instruments, Inc., TX, USA). The solutions for electrochemical measurements were deoxygenated with nitrogen gas for 10 min prior to measurements and kept under a blanket of nitrogen during the course of measurements.

### 2.3.2 Cyclic Voltammetry Techniques

In a three-electrode cell, the voltage is measured between the reference electrode and the working electrode, while the current is measured between the working electrode and the counter electrode.<sup>3</sup> In cyclic voltammetry (CV), the voltage applied to the working electrode is varied linearly from an initial potential,  $E_i$ , to a final potential,  $E_f$ , at a constant scan rate; once the  $E_f$  is reached, the direction of the scan is reversed and the potential returned to  $E_i$  (Figure 2.1a) for a cyclic process.<sup>4</sup> This cycle records a current—potential curve, which is termed a cyclic voltammogram. A reversible cyclic voltammogram is shown in Figure 2.1b.

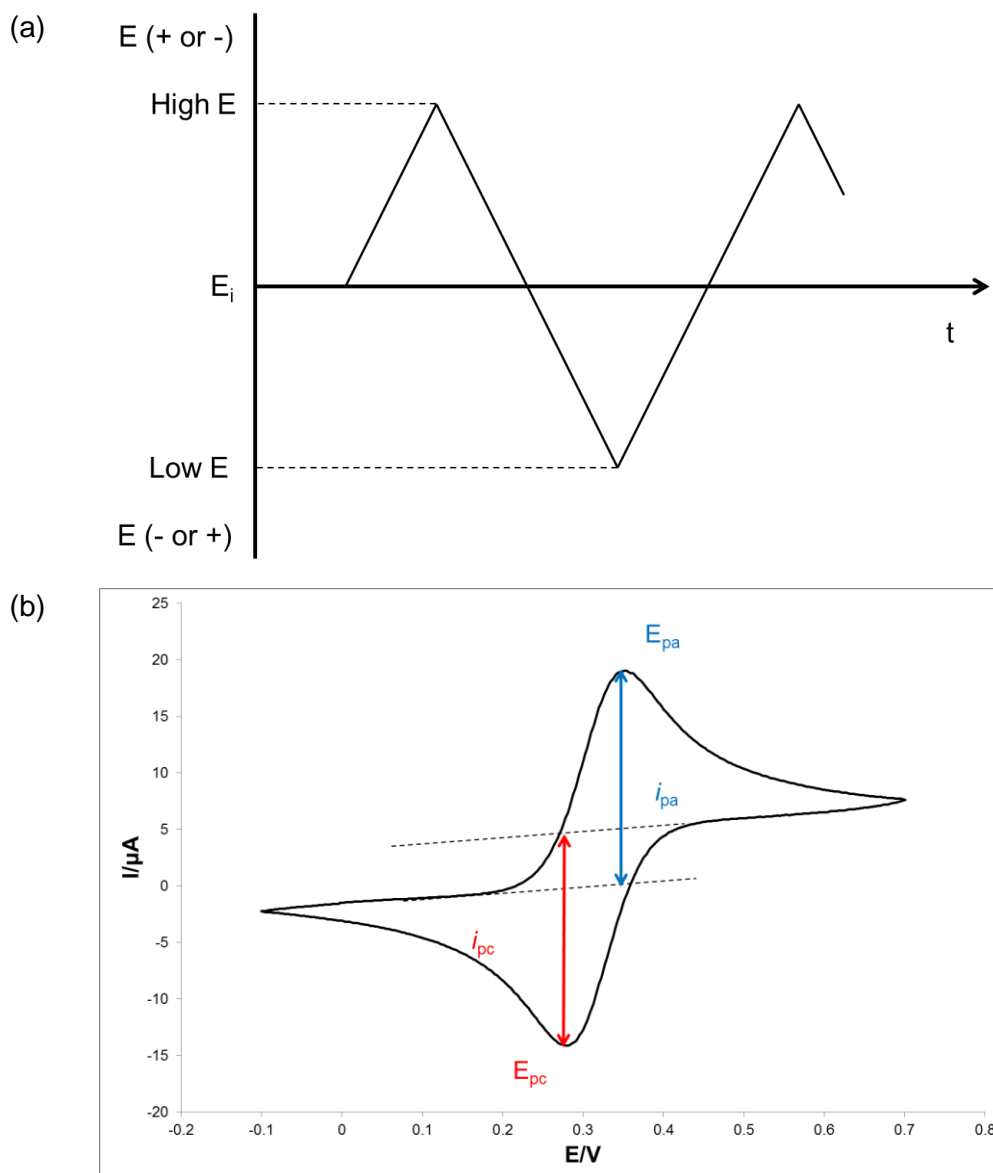


**Figure 2.1** (a) Potential-time pulses in cyclic voltammetry.<sup>4</sup> (b) A cyclic voltammogram of a reversible redox process:  $i_{pa}$  and  $i_{pc}$  are the anodic and cathodic peak current respectively;  $E_{pa}$  and  $E_{pc}$  are the anodic and cathodic peak potential respectively.

A redox reaction is electrochemically reversible when the rate of electron transfer is higher than the rate of mass transport.<sup>4</sup> In order to ensure mass transport is purely a diffusive process, CV measurements are normally carried out in stationary conditions, i.e. the solutions are kept unstirred. The half-wave potential,  $E_{1/2}$ , is determined by  $\frac{1}{2}(E_{pa} + E_{pc})$ , where  $E_{pa}$  and  $E_{pc}$  represent anodic and cathodic cyclic voltammetric peak potentials respectively. A reversible (Nernstian) process is characterised by the following criteria:<sup>4</sup>

1. current ratio,  $i_{pa}/i_{pc}$ , at unity to indicate that the process is chemically reversible;
2.  $E_p$  is independent of scan rate,  $v$  ( $V s^{-1}$ );
3. the peak separation,  $\Delta E_p = E_{pa} - E_{pc} = 59/n$  mV, where  $n$  is the number of electron transferred per redox species; and
4. linear plot of current vs square root of scan rate,  $i_p$  vs  $v^{1/2}$  for diffusion-controlled redox species or linear plot of current vs scan rate,  $i_p$  vs  $v$  for surface-bound redox species.

In organic systems, the reference electrode was freshly prepared before each CV measurement by immersing a silver wire (linked to a gold connector for electrical connection) into a glass tube fitted with Vycor® frit with a solution of 0.01 M  $AgNO_3$  and 0.1 M  $NBu_4PF_6$  in dry MeCN or DCM. CV of complexes were recorded in 1 mM of complex in MeCN or DCM with 0.1 M  $NBu_4PF_6$  as supporting electrolyte, with a bare glassy carbon working electrode (3 mm dia., geometrical area  $0.0707$  cm<sup>2</sup>), a platinum counter electrode, a silver wire/ $AgNO_3$  reference electrode with ferrocene (Fc) as the internal standard<sup>5</sup> and the potentials are reported against  $Fc^{+/0}$ . The electrochemical area of GC electrode,  $0.0492$  cm<sup>2</sup>, was obtained by substituting the known  $D_o$  of Fc ( $2.24 \times 10^{-5}$ /cm<sup>2</sup> s<sup>-1</sup>)<sup>6</sup> into Randles-Sevcik equation (Equation 1).<sup>4</sup>

$$i_p = 2.69 \times 10^5 \cdot n^{3/2} \cdot A \cdot D_o^{1/2} \cdot C \cdot v^{1/2} \quad (1)$$

where  $i_p$  is the peak current in A,  $n$  the number of electron transferred in the redox process,  $A$  the area of the electrode in cm<sup>2</sup>,  $D_o$  the diffusion coefficient in cm<sup>2</sup> s<sup>-1</sup>,  $C$  the concentration in mol cm<sup>-3</sup> and  $v$  the scan rate in V s<sup>-1</sup>.

In aqueous systems, cyclic voltammograms of the sensing surfaces were recorded in phosphate buffer or PBS using Ag/AgCl (3 M KCl) as the reference electrode. For the purpose of conversion between organic and aqueous systems, the  $E_{1/2}$  of Fc in MeCN was determined as 0.443 V vs Ag/AgCl.

### 2.3.3 Square Wave Voltammetry

Square wave voltammetry (SWV) employs pulse techniques which increase the Faradaic currents and at the same time minimise the capacitive currents by exploiting the differences in the decay rates between the Faradaic currents and capacitive currents.<sup>4</sup> The potential waveform for a SWV is a combination of periodic square wave pulses which alternate in direction (forward pulse,  $i_f$  and reverse pulse,  $i_r$ ) and a staircase waveform of small and constant step height to give a sequence of equally spaced steps (Figure 2.2).<sup>4</sup> The current is sampled at the end of either  $i_f$  or  $i_r$  at each step, the resultant current of which is given as the net current of the currents from the forward and reverse half-cycles. The sensitivity of the measurement is therefore enhanced due to low signal-to-noise ratio and the repeated redox cycles of the same analyte species.

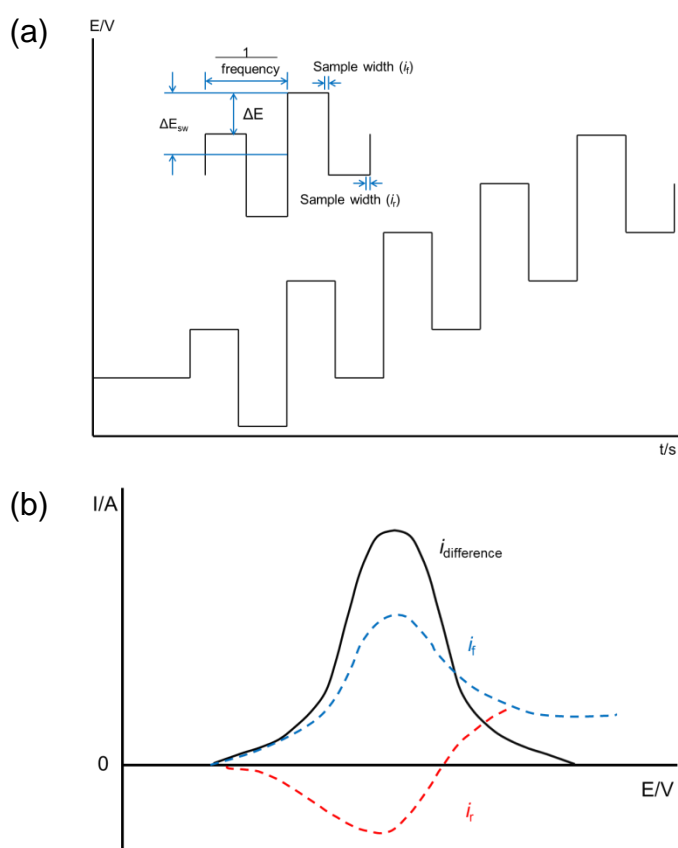


**Figure 2.2** (a) Potential waveform in SWV.  $\Delta E_{sw}$  is the pulse amplitude,  $\Delta E$  the step height and  $\frac{1}{\text{frequency}}$  the square wave period. Currents,  $i_f$  and  $i_r$ , are collected at the end of each pulse. (b) A SWV voltammogram (black line), the net current of which is the sum of currents from  $i_f$  and  $i_r$ .

### 2.3.4 Nuclear Magnetic Resonance Spectroscopy

The  $^1\text{H}$ ,  $^{13}\text{C}$  and  $^{19}\text{F}$  nuclear magnetic resonance (NMR) spectra were recorded in  $\text{CDCl}_3$ ,  $\text{C}_6\text{D}_6$  and  $\text{DMSO-}d_6$  on Bruker Avance III 300 (with an automatic sample charger), Avance III 400, Avance III 500 and Avance III 600 spectrometers, operating at 300.13, 400.23, 500.13, 600.13 MHz ( $^1\text{H}$ ) and 75.49, 100.64, 125.76 and 150.90 MHz ( $^{13}\text{C}$ ).  $^{19}\text{F}$  NMR was recorded on DMX400 at 376.31 MHz. The spectra were collected at 298 K and prepared under air while the NMR sample of  $\text{Ru}(\text{acac})_2(\text{bpy-NH}_2)$  was prepared in a nitrogen glove box. Chemical shifts ( $\delta$ ) are reported in ppm.  $^1\text{H}$  and  $^{13}\text{C}$  NMR chemical shifts were referenced internally to residual solvent resonances. Uncertainties in chemical shifts are typically  $\pm 0.01$  ppm for  $^1\text{H}$  and  $\pm 0.05$  ppm for  $^{13}\text{C}$  NMR. Coupling constants ( $J$ ) are given in Hz and have an uncertainty of  $\pm 0.05$  Hz for  $^1\text{H}$ - $^1\text{H}$  couplings. The following abbreviations are used in reporting the multiplicity of NMR resonances: s, singlet; d, doublet; t, triplet; q, quartet; p, pentet; m, multiplet; br, broad. NMR data were processed using standard Bruker software (Topspin) version 3.1.

### 2.3.5 Mass Spectrometry

Electrospray ionisation mass spectra (ESI/MS) were obtained on Thermo LTQ Orbitrap XL at the Bioanalytical Mass Spectrometry Facility (BMSF), University of New South Wales and reported as mass to charge ratio,  $m/z$ , in either HPLC grade MeOH or MeCN. In reporting mass spectral data,  $M$  is defined as the molecular weight of the compound of interest while  $M^+$  is defined as the molecular weight of the cationic fragments.

### 2.3.6 UV-Vis Spectroscopy

UV-Vis spectra were recorded on Shimadzu UV-2401PC in dry MeCN ( $5 \times 10^{-4}$  M) and reported as  $\lambda_{\text{max}}/\text{nm}$  ( $\epsilon/M^{-1}\text{cm}^{-1}$ ).

### 2.3.7 X-ray Photoelectron Spectroscopy

Gold foils (Goodfellow, 99.9%) were cleaned in piranha solution made up of hydrogen peroxide: concentrate sulphuric acid (1:3), rinsed with copious amount of Milli-Q water and EtOH and dried under a stream of nitrogen before modification. The X-ray photoelectron spectroscopy (XPS) data were collected using a VG ESCALAB 220-iXL spectrometer (VG Scientific, West Sussex, UK) with a monochromatic  $Al_{K\alpha}$  source (1486.6 eV), hemispherical analyser and multichannel detector (6 detectors). Spectra were recorded in normal emission with the analysing chamber operating below  $10^{-9}$  mbar and selecting a spot size of approximately  $1 \text{ mm}^2$ . The take-off angle was set to  $90^\circ$  to the analyser lens. The resolution of the spectrometer was 0.6 eV as measured from the  $Ag3d_{5/2}$  signal (full width at half maximum, fwhm) with a 20 eV pass energy. Survey scans (1100 – 0 eV) were obtained with a 1.0 eV step size, a 100 ms dwell time and analyser pass energy of 100 eV. Narrow scans were run with 0.1 eV step size, a 100 ms dwell time and analyser pass energy of 20 eV. All binding energies were reported in eV and referenced to the  $Au 4f_{7/2}$  peak at 84.0 eV. The XPS spectra were analysed with curve-fitting program XPSEAK4.1 with background subtraction by Shirley routine followed by non-linear least-squares fitting to mixed Gaussian-Lorentzian functions (with Lorentzian/Gaussian ratio of C 1s 20%, N 1s 100% and S 2p 30%). Atomic percentages (At %) of surfaces were calculated by normalised peak areas, which was peak area divided by number of scans and the element sensitivity factor. The sensitivity factors are C 1s 1.00, N 1s 1.80, S 2p 1.67 and  $Ru 3d_{5/2}$  7.39.

### 2.3.8 pH Meter

All pH measurements were taken on Mettler Toledo pH meter that was calibrated using standard buffer solutions (ProSciTech Pty Ltd, Australia): pH 4.0 ( $\pm 0.02$ ) and pH 7.0 ( $\pm 0.02$ ) or pH 10 ( $\pm 0.05$ ). The pH of the aqueous solutions was adjusted by dilute HCl or NaOH solution.

### 2.3.9 Other Characterisation Techniques

Elemental analyses were carried out at the Campbell Microanalytical Laboratory, University of Otago, New Zealand and the Elemental Analysis Unit, The Research School of Chemistry, the Australian National University.

## 2.4 Electrochemical Studies

### 2.4.1 Preparation of Glassy Carbon Electrodes and Calculation of the Electrochemical Surface Area

Glassy carbon (GC) electrodes (2 mm dia.) were polished sequentially in alumina slurries (Milli-Q water suspension) of 1.0, 0.3 and 0.05  $\mu\text{m}$  on micropolishing cloths (Buehler, IL, USA) with rinsing by Milli-Q water between each step. The cleaned GC electrodes were only used to run CV measurements of redox species in organic solvents.

### 2.4.2 Preparation of Gold Electrodes and Calculation of the Electrochemical Surface Area

The levels of cleanliness of gold electrodes affect the reproducibility, packing density and ordering of self-assembled monolayers (SAM).<sup>7,8</sup> Proper pretreatment of gold electrodes will maximise chemisorbed molecular coverage and lead to highly dense and less defects in the SAMs formed. There were two steps to cleaning gold electrodes: mechanical polishing and electrochemical treatment. First, the gold electrodes were cleaned by polishing sequentially in alumina slurries (Milli-Q water suspension) of 1.0, 0.3 and 0.05  $\mu\text{m}$  on micropolishing cloths (Buehler, IL, USA). Second, gold electrodes were cleaned by placing them in 0.5 M  $\text{H}_2\text{SO}_4$  and scanning potentials between 0 to 1.5 V (vs Ag/AgCl) by CV until reproducible scans were obtained in successive scans (Figure 2.2). The potential scan was terminated at 0 V to ensure that the electrodes remained oxide-free.<sup>9</sup>

Electrochemical area of gold electrode was determined from the reduction peak of gold oxide at around 0.9 V by the method of Hoogvliet *et al.* using a conversion

factor of  $482 \mu\text{C cm}^{-2}$ .<sup>10</sup> This calculation was done by using the mean surface concentration of gold atoms based on the density and atomic weight of gold and the assumption that a monolayer of oxygen on gold had been formed with a 1:1 ratio.<sup>10</sup> The working area is calculated at  $0.0613 \text{ cm}^2$  ( $s = 0.0023 \text{ cm}^2$ ,  $n = 6$  cleaned gold electrode surfaces) which gives a roughness factor of 1.94. As the working area varies from one cleaning process to another, current density values are quoted in experiments for a more accurate representation of current across the electrodes used.

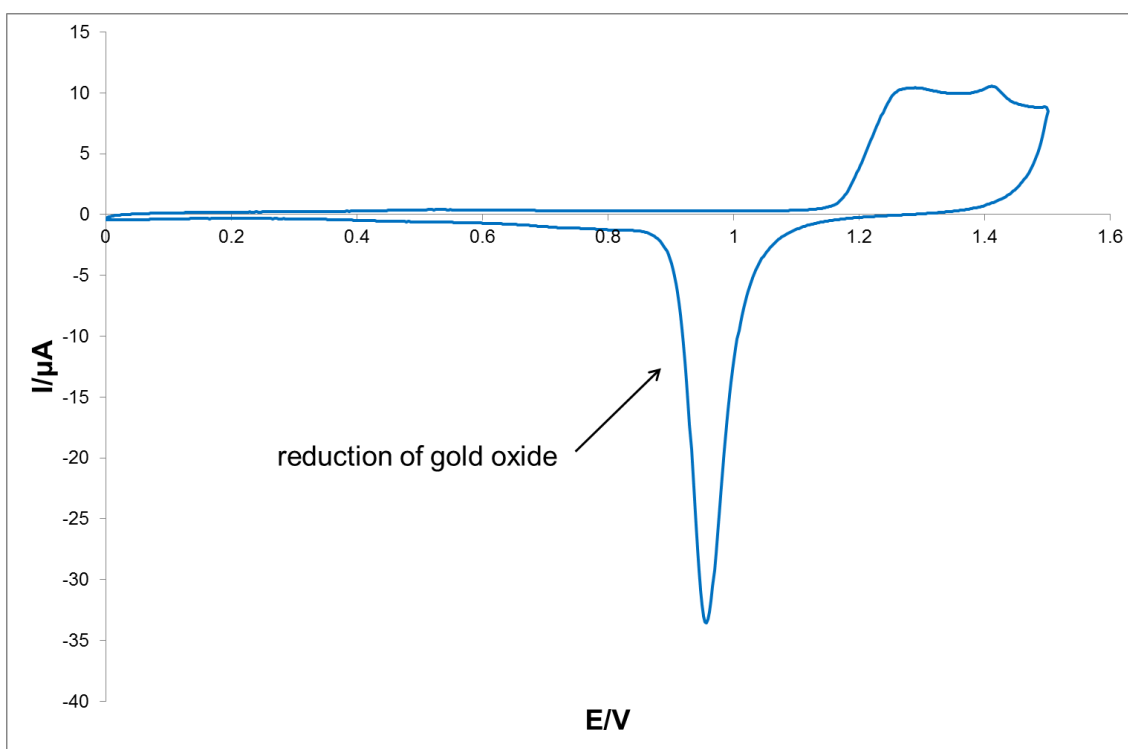


**Figure 2.3** A cyclic voltammogram of a clean gold electrode in 0.5 M  $\text{H}_2\text{SO}_4$ ,  $\nu = 0.1 \text{ V s}^{-1}$ .

### 2.4.3 Modification of Gold Electrodes with Self-assembled Monolayers

Self-assembled monolayers (SAMs) were formed by immersing the cleaned gold electrodes in 1 mM ethanolic solution of 6-mercaptohexanoic acid (MHA) or thioctic acid (TA) for about 4 hours at RT. This process involves two steps: the fast initiation step where a monolayer is formed by a pseudo-covalent bond between the gold surface and the sulphur head group followed by a slow rearrangement step where the hydrocarbon chain are arranged in an  $(\sqrt{3} \times \sqrt{3})\text{R}30$  ordering and the alkane chains in all

*trans*-extended conformation, tilted at 30° from the surface normal.<sup>9,11</sup> After the modification, the gold electrodes were rinsed with EtOH to remove any physisorbed MHA/TA before the next activation step.

#### 2.4.4 Covalent Attachment of Ru(acac)<sub>2</sub>(bpy-NH<sub>2</sub>) onto Gold Electrodes Modified with SAM

After SAM formation, the carboxylic acid end group was activated by coupling agent/additive 1-(3-dimethylaminopropyl)-3-ethylcarbodiimide hydrochloride (EDC) and *N*-hydroxysuccinimide (NHS) (2:1, 100 mM:50 mM) in MES buffer (pH 6.8) for 3 h.<sup>12</sup> The activation surface was rinsed with Milli-Q water and EtOH and dried under a stream of nitrogen. The redox label, Ru(acac)<sub>2</sub>(bpy-NH<sub>2</sub>) was covalently attached to the activated surface by immersing the surface with 1 mM ethanolic solution of redox label overnight at 4 °C.

##### 2.4.4.1 Determination of Surface Coverage of Ru(acac)<sub>2</sub>(bpy-NH<sub>2</sub>) on Gold Electrodes

The surface coverage of the redox label, Ru(acac)<sub>2</sub>(bpy-NH<sub>2</sub>) was determined electrochemically from cyclic voltammograms generated by the redox label bound onto MHA or TA in phosphate buffer by calculating the charge passed in the oxidation process. The surface coverage is calculated using Equation 2:

$$\Gamma = \frac{Q}{nFA} \quad (2)$$

where  $\Gamma$  is the surface coverage Ru(acac)<sub>2</sub>(bpy-NH<sub>2</sub>) at the MHA- or TA-modified gold electrode in mol cm<sup>-2</sup>,  $Q$  the charge passed in coulombs,  $n$  the number of electrons transferred in the redox cycle,  $F$  the Faraday constant (96485.3415 C mol<sup>-1</sup>),  $A$  the electrochemical area of the gold electrode in cm<sup>2</sup> and  $v$  the scan rate in V s<sup>-1</sup>.

### 2.4.5 Attachment of Peptide GPP onto Ru(acac)<sub>2</sub>(bpy-NH<sub>2</sub>) bound to MHA- or TA-modified Gold Surfaces

The attachment of GPP to the redox label, Ru(acac)<sub>2</sub>(bpy-NH<sub>2</sub>) was achieved by incubating 2 mM GPP in EDC/NHS solution (2:1, 20 mM:10 mM, phosphate buffer) for 4 h at 4 °C. The electrodes were rinsed with Milli-Q water/EtOH to wash away physisorbed species and dried under a stream of nitrogen before the next step.

### 2.4.6 Determination of Hb1Ac antibody

The sensing surface was incubated with Hb1Ac antibody (8 µg mL<sup>-1</sup>, PBS) at room temperature for different time periods. The voltammetry responses from the redox label was recorded using square-wave voltammetry (SWV) after each incubation at 130 Hz, 200 Hz or 210 Hz (step potential = 4 mV; amplitude = 25 mV).

## 2.5 References

- (1) Shriver, D. F.; Drezdson, M. A. *The Manipulation of Air Sensitive Compounds*; 2<sup>nd</sup> ed.; John Wiley & Sons: New York, 1986.
- (2) Armarego, W. L. F.; Chai, C. L. L. *Purification of Laboratory Chemicals*; 6<sup>th</sup> ed.; Elsevier, Inc.: Oxford, 2009.
- (3) Grieshaber, D.; MacKenzie, R.; Vörös, J.; Reimhult, E. *Sensors* **2008**, *8*, 1400.
- (4) Zanello, P. *Inorganic Electrochemistry: Theory, Practice and Applications*; The Royal Society of Chemistry: Cambridge, 2003.
- (5) Gagne, R. R.; Koval, C. A.; Lisensky, G. C. *Inorg. Chem.* **1980**, *19*, 2854.
- (6) Tsierkezos, N. G. *J. Solution Chem.* **2007**, *36*, 289.
- (7) Carvalhal, R. F.; Freire, R. S.; Kubota, L. T. *Electroanal.* **2005**, *17*, 1251.
- (8) Tkac, J.; Davis, J. J. *J. Electroanal. Chem.* **2008**, *621*, 117.
- (9) Finklea, H. O. In *Electrochemistry. A Series of Advances*; Bard, A. J., Rubinstein, I., Eds.; Marcel Dekker: New York, 1996; Vol. 19, p 109.
- (10) Hoogvliet, J. C.; Dijksma, M.; Kamp, B.; van Bennekom, W. P. *Anal. Chem.* **2000**, *72*, 2016.
- (11) Love, J. C.; Estroff, L. A.; Kriebel, J. K.; Nuzzo, R. G.; Whitesides, G. M. *Chem. Rev.* **2005**, *105*, 1103.
- (12) Staros, J. V.; Wright, R. W.; Swingle, D. M. *Anal. Biochem.* **1986**, *156*, 220.

## *Chapter 3*

### *Synthesis and Electronic Tuning of $\beta$ -diketonate Ligands on Heteroleptic*

*Ruthenium<sup>2+</sup> ( $\beta$ -diketonato)<sub>x</sub>(bpy)<sub>y</sub>*

*Complexes (x and y = 1 or 2)*

### 3.1 Ruthenium Complexes as Redox Labels

In an electrochemical biosensor, a redox label conducts signals resulting from the binding of target analytes to biorecognition elements. As already discussed in Chapter 1, an ideal redox label satisfies the following criteria:

1. low half-wave potential ( $E_{1/2}$ ) window: -0.3 V to +0.5 V (*vs* Ag/AgCl)
2. pH-independent  $E_{1/2}$
3. reversible electron transfer kinetics
4. chemically stable in oxidised and reduced forms
5. easily tuneable potentials

Ferrocene is the most widely used redox label in electrochemical biosensors. However, the oxidised form of ferrocene, the ferricenium ion, has been shown to decompose in media containing chloride ions.<sup>1-3</sup> Since most biological samples contain chloride ions, it is important to find alternatives to ferrocene complexes for analytical applications. The objective of this chapter is to synthesise stable, tuneable complexes to substitute for ferrocene complexes as redox labels in electrochemical sensors. The design of ruthenium complexes will be discussed, followed by their syntheses and study of their electrochemical behaviour.

### 3.2 Metal Complexes and Their Half-Wave Potentials ( $E_{1/2}$ )

Metal complexes are comprised of a metal ion and ligands that are bound to the metal. The molecular geometry of a complex is determined by the coordination number at the metal centre and in certain instances, the structural rigidity of the ligands.<sup>4</sup> Mononuclear metal complexes can be categorised into three groups according to their electrochemical behaviour, in particular their electrochemical reversibility and structural integrity. In the first, the complexes undergo reversible electrochemical processes whilst remaining structurally intact, which indicates that in the time scale of a redox cycle, no chemical reaction takes place.<sup>4</sup> The most common metal complexes which display chemically reversible behaviour are ferrocene and the related iron, ruthenium and osmium polypyridine complexes.<sup>4</sup> In the second, the complexes undergo irreversible ligand dissociation upon reduction or oxidation, such as  $\text{Co}^{3+}$  complexes with ammine-

type ligands. Finally, in the third, the complexes undergo irreversible structural changes during redox processes, where solvent molecules can coordinate to, or ligands dissociate from, the metal centre.<sup>4</sup>

### 3.2.1 Ruthenium

To be useful as a redox label, it is necessary for the prospective complexes to undergo redox cycles reversibly while retaining their structural integrity. Ruthenium polypyridine complexes, particularly  $\text{Ru}(\text{bpy})_3^{2+}$ , have been one of the most widely studied classes of complexes owing to their chemical stability, redox properties, luminescence emission, excited state reactivity and lifetime.<sup>5</sup> More importantly, when oxidised, these low spin complexes are inert to ligand substitution.<sup>5</sup>

Ruthenium is in the same group as iron (Group 8) and is a second row transition metal with a valence electron configuration of  $4d^7 5s^1$ . Ruthenium has several properties which make it a particularly good metal to be used in electrochemistry: 1) two well-defined oxidation states, i.e.,  $\text{Ru}^{2+}$  and  $\text{Ru}^{3+}$ ; 2) the  $\text{Ru}^{2+/3+}$  redox couple is stable kinetically as evident in the retention of enantiomeric and geometrical configurations of ruthenium complexes during redox cycles, and 3) the small structural differences between octahedral complexes of the two oxidation states allow rapid and reversible electron transfer.<sup>6</sup> Numerous configurationally stable octahedral ruthenium complexes in the +2 oxidation state have been synthesised. Among them, extensive studies have been done on  $\text{Ru}^{2+}$ -polypyridine complexes which exhibit excellent stability in the oxidised as well as reduced forms, a property which directly translates into their electrochemical reversibility.<sup>5</sup>

The electrochemical properties of metal complexes are influenced by the coordination environment and the electron donor/acceptor properties of the ligands.<sup>5</sup> For example,  $\text{Ru}^{2+}$  possesses good  $\pi$  back-bonding capability with  $\pi$ -acceptor ligands such as 2,2'-bipyridine (bpy),<sup>7</sup> which have been shown to stabilise  $\text{Ru}^{2+}$  relative to  $\text{Ru}^{3+}$  by stabilising the occupied metal  $\pi$ -orbitals (HOMO) and reducing interelectronic repulsion in the metal centre.<sup>8,9</sup> Thus, changes in  $E_{1/2}$  of ruthenium complexes can be related to the stabilisation of the  $\text{Ru}^{2+} t_{2g}$  level from which an electron is removed during

oxidation to the level of  $\pi$  back-bonding to a ligand in a  $\text{Ru}^{2+/3+}$  redox couple.<sup>7</sup> A higher  $E_{1/2}$  points to a stronger bond between metal and ligand forming a more stable complex, as the energy required to oxidise the metal is higher.  $E_{1/2}$  values can therefore be treated as an indicator of the relative binding strength of the metal centre to a ligand.

Systematic understanding of the relationships between electronic effects of the ligands and coordination environments on a metal centre can provide the rationale behind the design and modification of the ligands to aid in the synthesis of redox labels with  $E_{1/2}$  suited for sensing applications.

### 3.2.2 Ligands

The changes in  $E_{1/2}$  of heteroleptic  $\text{Ru}^{2+}$  complexes of different combinations of bpy and acetylacetonate (acac) ligands were illustrated by Haga and co-workers.<sup>10</sup> Bpy is a known  $\pi$ -acceptor ligand while acac functions as a  $\sigma$ -donor ligand.  $[\text{Ru}(\text{bpy})_3]^{2+}$  and its derivatives have a filled  $d_{\pi}$  orbital as the highest occupied molecular orbital (HOMO) and an empty  $\pi^*_L$  orbital as the lowest unoccupied molecular orbital (LUMO).<sup>5,10</sup> The HOMO energy level can be raised or lowered depending on the properties of the ligand. A  $\pi$ -acceptor ligand will lower HOMO energy level to result in an anodic shift whereas a  $\pi$ -donor ligand causes the opposite effect.<sup>10</sup> Additionally, due to a decreasing capacity of ruthenium for  $\pi$  back-donation as the HOMO – LUMO gap increases and the electrons in the  $\text{Ru } t_{2g}$  level are more stabilised,  $E_{1/2}$  will be shifted anodically.<sup>11</sup>

**Table 3.1**  $E_{1/2}$  of  $[\text{Ru}(\text{bpy})_{3-n}(\text{acac})_n]^{x+}$  complexes.<sup>10</sup>

Complex	$E_{1/2}/\text{V}$ (vs SCE)	$E_{1/2}/\text{V}^\dagger$ (vs Ag/AgCl)
$\text{Ru}(\text{bpy})_3^{2+}$	1.26	1.305
$\text{Ru}(\text{bpy})_2(\text{acac})^+$	0.59	0.635
$\text{Ru}(\text{bpy})(\text{acac})_2$	-0.08	-0.035
$\text{Ru}(\text{acac})_3$	-0.77	-0.725

<sup>†</sup>  $E_{1/2}$  (vs SCE) + 0.045 V =  $E_{1/2}$  (vs Ag/AgCl)

It has been shown that stepwise substitution of a bpy in  $[\text{Ru}(\text{bpy})_3]^{2+}$  complex with an acac ligand causes a significant cathodic shift in  $E_{1/2}$  (Table 3.1).<sup>10</sup> This was attributed to a progressive decrease in the HOMO – LUMO gap by the increasing

number of acac ligand in the complexes. It was shown that acac was able to stabilise  $\text{Ru}^{3+}$  more effectively on the basis of its anionic charge.<sup>12,13</sup> Hence, the overall effects of these two ligands on the  $E_{1/2}$  of the metal centre were additive, where both ligands exerted their influences on the ease of oxidation of the ruthenium centre.

With appropriate selection of ligands one is able to tune the  $E_{1/2}$  of metal complexes to suit their applications. As  $E_{1/2}$  of  $[\text{Ru}(\text{bpy})_2(\text{acac})]^+$  and  $\text{Ru}(\text{bpy})_2(\text{acac})$  were reported to be at 0.635 V and -0.035 V (*vs* Ag/AgCl) respectively, they present themselves as suitable starting complexes for development as redox labels.

### 3.2.2.1 2,2'-Bipyridine (bpy)

Bipyridine is made up of two planar pyridyl rings linked covalently by their carbon atoms (Figure 3.1). The availability of a large number of modified bipyridine ligands greatly showcases the structural versatility of this ligand. Of these, the 2,2'-bipyridine (bpy) ligand is the most widely used metal chelating ligand in coordination chemistry due to its robust redox stability and ease of functionalisation.<sup>14</sup> Functionalisation of bpy can provide anchoring points to allow attachment of the complex onto transducers and biorecognition elements, which will be elaborated on in Chapter 4, Section 4.1.4.

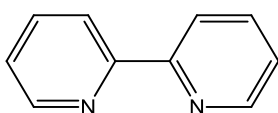


**Figure 3.1** Structure of bpy.

### 3.2.2.2 Acetylacetonate (acac)

2,4-Pentanedione, also known as acetylacetone (acacH), is the simplest form of  $\beta$ -diketone ligand available. AcacH undergoes keto-enol tautomerism with its enolic form more stable due to delocalisation of electron through a  $\pi$ -conjugated system and by intramolecular hydrogen bonding (Figure 3.2).<sup>15,16</sup> After undergoing a mild deprotonation, acetylacetone loses a proton to become a monoanionic ligand, acac.

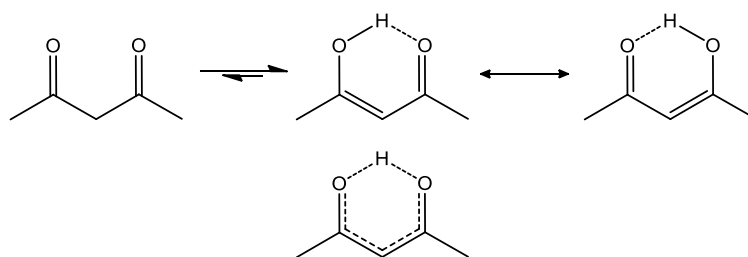


**Figure 3.2** Keto/enol tautomerism of acacH, resulting in the more stable delocalised enol isomer.

A large number of acac ligands with a variety of substituents is available to coordinate to metal ions.<sup>17-19</sup> The three binding modes for acac ligand to chelate to a metal centre are: oxygen-coordinated, carbon-coordinated and a mix of both oxygen and carbon-coordination complexes.<sup>18</sup> The vast majority of coordination modes involve bidentate coordination at the two oxygen atoms of the acac ligand to generate metal complexes of the general formula,  $M(\text{acac})_3$ , with six-membered chelate rings (Figure 3.3). This denticity is advantageous because it confers higher stability and robustness in resultant complexes.

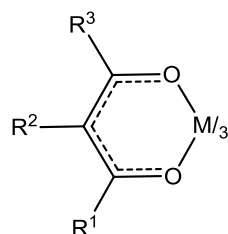


**Figure 3.3** Six-membered chelate ring in  $M(\text{acac})_3$ .

It is important to note that the substituents on acac (substituted variants are hereafter referred to as  $\beta$ -diketones) can be modified to modulate the  $E_{1/2}$  of metal complexes containing  $\beta$ -diketone ligands. The introduction of an electron-donating group (EDG) or electron-withdrawing group (EWG) as a substituent imposes electronic effects around the metal which govern the ease of oxidation of the metal centre. More specifically, a metal centre is harder to oxidise, i.e., lose an electron, when an EWG is present; therefore  $E_{1/2}$  is shifted anodically. Conversely, an EDG induces a cathodic shift in  $E_{1/2}$ .<sup>6</sup>

The ease of deprotonation of the methine proton of  $\beta$ -diketones largely depends on the degree of keto/enol tautomerism of the  $\beta$ -diketone, which is influenced by the electronic and steric effects of the substituents.  $\beta$ -diketones can be substituted at the methine and/or terminal carbons, where donor property and bulkiness of the substituents affect tautomeric equilibria of the ligands. Firstly, an EWG on the methine carbon lessens electron density around the carbon, consequently a  $\beta$ -diketone bearing an EWG is more stable in its enolic form; an EDG, on the contrary, favours keto form.<sup>20</sup> Secondly, the bulkier a substituent is at the methine carbon the lesser enolic content there is due to steric effects.<sup>20</sup> At the terminal carbons, however, the bulkier the terminal substituents the more enolic content there is due to steric interaction which forces the carbonyls closer together resulting in a higher enolic content in order to reduce electrostatic repulsion between the two carbonyls.<sup>21</sup> The chelating ability of these ligands and subsequently the stability of metal chelates are affected to a certain extent by the nature of the substituents and the resultant tautomeric ratios of these ligands – the more electron-donating the substituent is, the more stable the metal chelate as the coordination bonds are stronger due to higher electron density around the metal centre.<sup>20</sup>

### 3.3 Approaches to Immobilising Redox Labels on Electrode Surface

The most common immobilisation techniques for surface bound species are physical adsorption, cross-linking, entrapment, covalent bonds, or a combination of all these techniques. The stability of the binding of redox label on the surface determines the sensitivity and reliability of the biosensor.<sup>22</sup> The immobilisation of the redox label used in this thesis will be discussed in detail in Chapter 4, Section 4.1.

### 3.4 Objectives

The objectives of this chapter are to firstly demonstrate that the  $E_{1/2}$  of ruthenium complexes can be finely tuned through a selection of substituents on the  $\beta$ -diketone ligands and secondly prepare a series of ruthenium complexes with  $E_{1/2}$  within the range of -0.3 V to +0.5 V (vs Ag/AgCl) for biosensing applications.

### 3.5 Experimental Section

#### 3.5.1 Chemicals

All chemicals and reagents used in this chapter are listed in Chapter 2, Section 2.2.

#### 3.5.2 Experimental Techniques

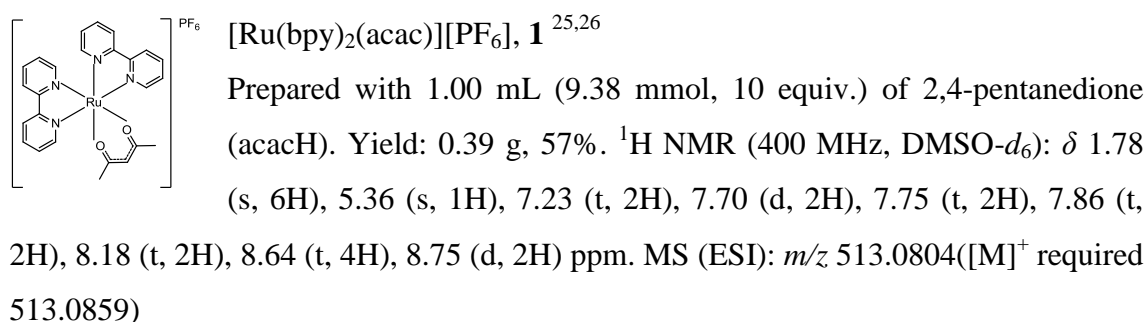
Mass spectrometry, NMR spectrometry, cyclic voltammetry (CV) and UV-Vis absorption measurements were conducted as described in Chapter 2, Section 2.3.

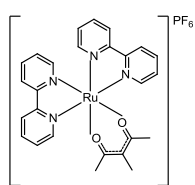
#### 3.5.3 Synthesis

##### Series I: Ruthenium Mono( $\beta$ -diketonato) complexes, $[\text{Ru}(\text{bpy})_2(\beta\text{-diketonato})][\text{PF}_6]$

Unless otherwise noted, complexes of Series I,  $[\text{Ru}(\text{bpy})_2(\beta\text{-diketonato})][\text{PF}_6]$  (**1** – **7**), were prepared using the following method:  $\text{Ru}(\text{bpy})_2(\text{Cl})_2 \cdot 2\text{H}_2\text{O}$  (1 equiv.) was dissolved in degassed water or a 1:1 water:ethanol mix and heated to 75 °C for 30 min.  $\beta$ -diketone was added to the solution followed by *t*-BuOK (1 – 1.5 equiv). The mixture was stirred at 75 °C for 1 h and cooled to room temperature before  $\text{NH}_4\text{PF}_6$  (5.5 equiv.) was added to precipitate the products. The solids were collected, washed with water and diethyl ether or recrystallised with DCM/hexane to give the products as dark solids.

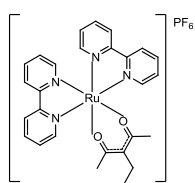
Ligands 3-(4-methoxybenzyl)-2,4-pentanedione (mbpd) and 3-(4-nitrobenzyl)-2,4-pentanedione (nbpd) were synthesised according to the procedure reported by Jana *et al.*<sup>23</sup> and by Andrey Tregubov.<sup>24</sup>





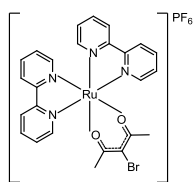
$[\text{Ru}(\text{bpy})_2(\text{macac})][\text{PF}_6]$ , **2**<sup>25,26</sup>

Prepared with 1.12 g (9.81 mmol, 10 equiv.) of 3-methyl-2,4-pentanedione (macac). Yield: 0.60 g, 90%. <sup>1</sup>H NMR (400 MHz, DMSO-*d*<sub>6</sub>):  $\delta$  1.81 (s, 3H), 1.89 (s, 6H), 7.21 (t, 2H), 7.65 (d, 2H), 7.75 (t, 2H), 7.83 (t, 2H), 8.17 (t, 2H), 8.62 (d, 4H), 8.75 (d, 2H) ppm. MS (ESI): *m/z* 527.0954 ([M]<sup>+</sup> required 527.1016).



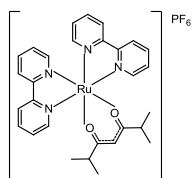
$[\text{Ru}(\text{bpy})_2(\text{eacac})][\text{PF}_6]$ , **3**<sup>26</sup>

Prepared with 0.100 g (0.780 mmol, 1.5 equiv.) of 3-ethyl-2,4-pentanedione (eacac). Purified by column chromatography (silica gel, DCM/MeCN 4:1). Yield: 0.05 g, 15%. <sup>1</sup>H NMR (400 MHz, DMSO-*d*<sub>6</sub>):  $\delta$  0.92 (t, 3H), 1.90 (s, 6H), 2.21 (d, 2H), 7.21 (t, 2H), 7.66 (d, 2H), 7.74 (t, 2H), 7.83 (t, 2H), 8.16 (t, 2H), 8.62 (d, 4H), 8.75 (d, 2H) ppm. <sup>13</sup>C NMR (150.90 MHz, DMSO-*d*<sub>6</sub>):  $\delta$  15.32, 23.51, 27.02, 109.61, 123.34, 123.45, 125.61, 126.37, 134.60, 136.44, 149.77, 152.73, 157.34, 158.76, 184.99 ppm. MS (ESI): *m/z* 541.1166 ([M]<sup>+</sup> required 541.1172). Anal Calcd for C<sub>27</sub>H<sub>27</sub>O<sub>2</sub>N<sub>4</sub>PF<sub>6</sub>Ru: C, 47.30; H, 3.97; N, 8.17; Found: C, 46.93; H, 3.94; N, 7.91. CV (MeCN, 0.1 M NBu<sub>4</sub>PF<sub>6</sub>, 0.1 V s<sup>-1</sup>, vs Fc<sup>+0</sup>) E<sub>1/2</sub> (Ru<sup>2+/3+</sup>) = 0.181 V, | $\Delta E$ | = 0.066V.



$[\text{Ru}(\text{bpy})_2(\text{Br-acac})][\text{PF}_6]$ , **4**<sup>26</sup>

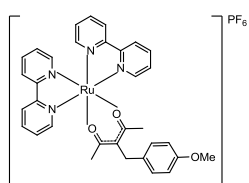
*N*-bromosuccinimide (0.0400 g, 0.225 mmol) was added to a DCM solution of [Ru(bpy)<sub>2</sub>(acac)](PF<sub>6</sub>) (0.140 g, 0.213 mmol). The mixture was stirred for an hour under nitrogen followed by the addition of NH<sub>4</sub>PF<sub>6</sub> (0.200 g, 1.22 mmol) before the DCM was evaporated. The complex was purified by chromatography (silica gel, DCM/MeCN 4:1) to give the product as a black solid. Yield: 0.07 g, 40%. <sup>1</sup>H NMR (400 MHz, DMSO-*d*<sub>6</sub>):  $\delta$  2.14 (s, 6H), 7.24 (t, 2H), 7.68 (d, 2H), 7.80 (t, 2H), 7.87 (t, 2H), 8.22 (t, 2H), 8.66 (t, 4H), 8.78 (d, 2H) ppm. MS (ESI): *m/z* 590.9890 ([M]<sup>+</sup> required 590.9890 for <sup>79</sup>Br), *m/z* 592.9882 ([M]<sup>+</sup> required 592.9949 for <sup>81</sup>Br).



$[\text{Ru}(\text{bpy})_2(\text{dmhd})][\text{PF}_6]$ , **5**<sup>26</sup>

Prepared with 0.100 g (0.640 mmol, 1.2 equiv.) of 2,6-dimethyl-3,5-heptanedione (dmhd). Yield: 0.37 g, 60%. <sup>1</sup>H NMR (300 MHz,

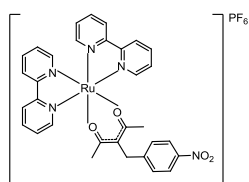
DMSO- $d_6$ ):  $\delta$  0.58 (d, 6H), 0.80 (d, 6H), 2.25 (sp, 2H), 7.73 (t, 2H), 7.73 (t, 2H), 7.90-7.83 (m, 4H), 8.16 (t, 2H), 8.50 (d, 2H), 8.64 (d, 2H), 8.75 (d, 2H) ppm.  $^{13}\text{C}$  NMR (150.90 MHz, DMSO- $d_6$ ):  $\delta$  19.98, 38.18, 94.27, 123.01, 123.21, 125.40, 126.03, 134.74, 136.35, 149.63, 153.11, 157.46, 158.75, 192.85 ppm. MS (ESI):  $m/z$  569.1547 ( $[\text{M}]^+$  569.1485). Anal Calcd for  $\text{C}_{31}\text{H}_{35}\text{O}_2\text{N}_4\text{PF}_6\text{Ru}$ : C, 48.81; H, 4.38; N, 7.85. Found: C, 48.15; H, 4.52; N, 7.70. CV (MeCN, 0.1 M  $\text{NBu}_4\text{PF}_6$ , 0.1  $\text{V s}^{-1}$ , vs  $\text{Fc}^{+/0}$ )  $E_{1/2}(\text{Ru}^{2+/3+}) = 0.201 \text{ V}$ ,  $|\Delta E| = 0.070 \text{ V}$ .



$[\text{Ru}(\text{bpy})_2(\text{mbpd})][\text{PF}_6]$ , **6**<sup>26</sup>

Prepared with 0.111 g (0.503 mmol, 1.2 equiv.) of mbpd. Yield: 0.20 g, 53%.  $^1\text{H}$  NMR (400 MHz, DMSO- $d_6$ ):  $\delta$  1.79 (s, 6H), 3.57 (s, 2H), 3.73 (s, 3H), 6.86 (dd, 4H), 7.22 (t, 2H), 7.71 (d, 2H), 7.88

– 7.80 (m, 4H), 8.22 (t, 2H), 8.67 (dd, 4H), 8.78 (d, 2H) ppm.  $^{13}\text{C}$  NMR (100.64 MHz, DMSO- $d_6$ ):  $\delta$  27.56, 34.70, 54.99, 106.26, 113.76, 123.38, 123.44, 125.57, 126.37, 128.03, 133.26, 134.64, 136.51, 149.74, 152.79, 157.28, 157.36, 158.68, 185.82 ppm. MS (ESI):  $m/z$  633.1420 ( $[\text{M}]^+$  required 633.1434). Anal Calcd for  $\text{C}_{33}\text{H}_{31}\text{O}_3\text{N}_4\text{PF}_6\text{Ru}$ : C, 50.97; H, 4.02; N, 7.20. Found: C, 50.34; H, 4.04; N, 7.24. CV (MeCN, 0.1 M  $\text{NBu}_4\text{PF}_6$ , 0.1  $\text{V s}^{-1}$ , vs  $\text{Fc}^{+/0}$ )  $E_{1/2}(\text{Ru}^{2+/3+}) = 0.167 \text{ V}$ ,  $|\Delta E| = 0.066 \text{ V}$ .



$[\text{Ru}(\text{bpy})_2(\text{nbpd})][\text{PF}_6]$ , **7**<sup>26</sup>

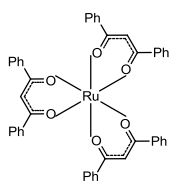
Prepared with 0.113 g (0.480 mmol, 1 equiv.) of nbpd. Yield: 0.20 g, 27%.  $^1\text{H}$  NMR (300 MHz, DMSO- $d_6$ ):  $\delta$  1.79 (s, 6H), 3.81 (s, 2H), 7.23 (t, 2H), 7.28 (d, 2H), 7.72 (d, 2H), 7.88-7.84 (m, 4H),

8.16 (d, 2H), 8.23 (t, 2H), 8.65 (d, 2H), 8.71 (d, 2H), 8.78 (d, 2H) ppm.  $^{13}\text{C}$  NMR (100.64 MHz, DMSO- $d_6$ ):  $\delta$  27.74, 35.82, 105.25, 123.42, 123.46, 123.52, 125.61, 126.49, 128.39, 134.73, 136.65, 145.84, 149.77, 150.49, 152.85, 157.29, 158.68, 185.96 ppm. MS (ESI):  $m/z$  648.1166 ( $[\text{M}]^+$  required 648.1179). Anal Calcd for  $\text{C}_{32}\text{H}_{28}\text{O}_4\text{N}_5\text{PF}_6\text{Ru}$ : C, 48.49; H, 3.56; N, 8.84. Found: C, 47.85; H, 3.53; N, 8.80. CV (MeCN, 0.1 M  $\text{NBu}_4\text{PF}_6$ , 0.1  $\text{V s}^{-1}$ , vs  $\text{Fc}^{+/0}$ )  $E_{1/2}(\text{Ru}^{2+/3+}) = 0.194 \text{ V}$ ,  $|\Delta E| = 0.070 \text{ V}$ .

Series II: Ruthenium Bis( $\beta$ -diketonato) complexes, Ru(bpy)( $\beta$ -diketonato)<sub>2</sub>

Complex Ru(acac)<sub>3</sub> (**9**),<sup>27</sup> and precursors Ru(bpy)(Cl)<sub>4</sub>,<sup>28</sup> [Ru(COD)(Cl)<sub>2</sub>]<sub>n</sub> and [Ru(NBD)(Cl)<sub>2</sub>]<sub>n</sub><sup>29</sup> were prepared according to literature methods.

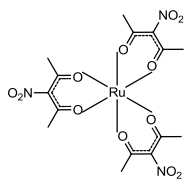
I. Preparation of Ru( $\beta$ -diketonato)<sub>3</sub> Complexes (**11** – **14**)



Ru(dbm)<sub>3</sub>, **11**<sup>30</sup>

RuCl<sub>3</sub>·3H<sub>2</sub>O (1.31 g, 5.01 mmol) was dissolved in a mixture of EtOH (100 mL) and degassed water (25 mL) resulting in a dark brown solution.

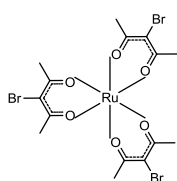
The solution was refluxed for 4 h, during which time a colour change of the solution from dark brown to dark blue was observed. Dibenzoylmethane (3.70 g, 16.5 mmol) was added to the dark blue solution after cooling down to room temperature. The reaction was refluxed for a further 1.5 h before cooling again. KHCO<sub>3</sub> (0.860 g, 8.59 mmol) was added to the now black green solution and the mixture was refluxed again for another 1.5 h, during which time gas evolution was observed. A second portion of KHCO<sub>3</sub> (0.860 g, 8.59 mmol) was added to the cooled yellow-green solution. The reaction was refluxed for a further 2 h, the colour of which was now black. After cooling a dark precipitate was formed and separated from the brown solution. The precipitate was washed with cold EtOH and hexane before being purified by silica gel column chromatography (DCM/hexane 3:7 to 1:1). An insoluble layer remained on top of column while a dark red, later dark brown fraction was collected. The collected fraction was dried *in vacuo*, which upon recrystallisation in DCM/pentane gave the product as a black solid. Yield: 0.96 g, 25%. <sup>1</sup>H NMR (300 MHz, CDCl<sub>3</sub>):  $\delta$  - 32.56 (br s, 3H), 6.72 (d, *J* 6.7 Hz, 12 H), 9.20 (t, *J* 6.6 Hz, 6 H), 11.78 (s, 12 H) ppm. MS (ESI): *m/z* 794.1187 ([M + Na]<sup>+</sup> required 794.1213).



Ru(NO<sub>2</sub>-acac)<sub>3</sub>, **12**<sup>31</sup>

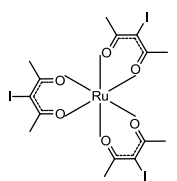
Acetic anhydride (30 mL) was added to Cu(NO<sub>3</sub>)<sub>2</sub>·3H<sub>2</sub>O (2.35 g, 9.73 mmol) to give a light blue suspension. The contents were stirred at 0 °C for 15 min after the flask was fitted with a calcium chloride drying tube. **9** (1.20 g, 3.01 mmol) was added to the cold deep blue solution. The mixture was stirred at 0 °C for 2 h and a further 2 h at room temperature. Ice (100 g), deionised water

(100 g) and anhydrous sodium acetate (2.14 g, 26.1 mmol) were added to the now reddish brown mixture. The colour immediately turned greenish blue. The solution was left to stir until a gummy substance was no longer present in the mixture. The contents were filtered to give bright red powder. The solid was washed with water to give product as a bright red powder. Yield: 1.12 g, 70%.  $^1\text{H}$  NMR (400 MHz,  $\text{CDCl}_3$ ):  $\delta$  -3.55 (s) ppm. MS (ESI):  $m/z$  556.9813 ( $[\text{M} + \text{Na}]^+$  required 556.9826). Anal Calcd for  $\text{C}_{15}\text{H}_{18}\text{O}_{12}\text{N}_3\text{Ru}$ : C, 33.78; H, 3.40; N, 7.88. Found: C, 33.01; H, 3.54; N, 7.65. CV (MeCN, 0.1 M  $\text{NBu}_4\text{PF}_6$ , 0.1  $\text{V s}^{-1}$ , vs  $\text{Fc}^{+/0}$ )  $E_{1/2}(\text{Ru}^{2+/3+}) = -0.786 \text{ V}$ ,  $|\Delta E| = 0.068 \text{ V}$ .



**Ru(Br-acac)<sub>3</sub>, 13**<sup>32</sup>

*N*-bromosuccinimide (1.18 g, 2.01 mmol) was added to  $\text{Ru}(\text{acac})_3$  (0.800 g, 6.64 mmol) followed by DCM (30 mL). The mixture turned dark violet instantly. The mixture was left to stir at room temperature overnight before solvent was removed under vacuum. The dark solids were then redissolved in a minimum amount of DCM before passing through a column of silica gel to remove unidentified dark purple (top) and pink (middle) bands. The dark violet solvent collected was evaporated to give dark solids which upon recrystallisation by DCM/pentane gave product **13**. Yield: 0.82 g, 64%.  $^1\text{H}$  NMR (400 MHz,  $\text{CDCl}_3$ ):  $\delta$  -7.78 (s) ppm. MS (ESI):  $m/z$  655.7571 ( $[\text{M} + \text{Na}]^+$  required for  $^{79}\text{Br}$  655.7567), 661.7544 ( $[\text{M} + \text{Na}]^+$  required for  $^{81}\text{Br}$  661.7559).

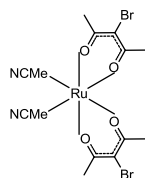


**Ru(I-acac)<sub>3</sub>, 14**<sup>32</sup>

*N*-iodosuccinimide (2.03 g, 9.02 mmol) was added to  $\text{Ru}(\text{acac})_3$  (0.402 g, 1.01 mmol) dissolved in toluene (50 mL). The reaction mixture was refluxed for 2 h. After toluene was removed the solids were redissolved in a minimum amount of DCM and passed through a column of silica gel. A major dark violet band was collected and solvent evaporated. The solids were recrystallised with DCM/pentane to give **14** as a dark solid. Yield: 0.65 g, 85%.  $^1\text{H}$  NMR (400 MHz,  $\text{CDCl}_3$ ):  $\delta$  -7.54 (s) ppm. MS (ESI):  $m/z$  776.7279 ( $[\text{M}]^+$  required 776.7275).

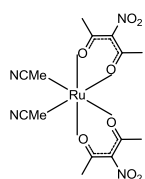
## II. Preparation of Ru( $\beta$ -diketonato)<sub>2</sub>(acetonitrile)<sub>2</sub> Complexes (**10**, **15** – **17**)

Ru(acac)<sub>2</sub>(MeCN)<sub>2</sub> (**10**) was prepared according to literature procedure.<sup>33</sup>



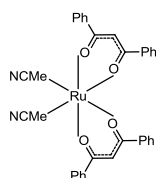
Ru(Br-acac)<sub>2</sub>(MeCN)<sub>2</sub>, **15**<sup>33</sup>

**9** (0.330 g, 0.855 mmol) and *N*-bromosuccinimide (0.301 g, 1.71 mmol) were added to a flask followed by DCM (15 mL). The colour turned from orange to dark purple the instant DCM was introduced to the mixture. The reaction mixture was left to stir under nitrogen overnight. The solution was washed with aqueous NaHSO<sub>3</sub> solution (20 mL,  $\times$  3) followed by deionised water (20 mL  $\times$  2). The brown-green DCM layer was dried with MgSO<sub>4</sub> and the solvent removed to give product as a dark brown solid. Yield: 0.33 g, 87%. <sup>1</sup>H NMR (300 MHz, C<sub>6</sub>D<sub>6</sub>):  $\delta$  0.96 (s, 6H), 2.54 (s, 6H), 2.56 (s, 6H) ppm. MS (ESI):  $m/z$  539.8633 ([M]<sup>+</sup> 539.8651 required).



Ru(NO<sub>2</sub>-acac)<sub>2</sub>(MeCN)<sub>2</sub>, **16**<sup>33</sup>

**12** (0.574 g, 1.08 mmol) was stirred in EtOH with activated zinc dust (0.5 g) for 1 h, during which time the colour changed from bright red to brown. MeCN (5 mL) was added to the brown mixture and refluxed for 4 h. The mixture was filtered through a bed of celite on which a brown layer remained. The crude product (filtrate) was subjected to silica gel column chromatography to first elute unreacted **12** with DCM followed by EtOAc to flush the product out from the column as an orange fraction. Solvent was removed to give the product **16** as an orange solid. Yield: 0.46 g, 92%. <sup>1</sup>H NMR (400 MHz, DMSO-*d*<sub>6</sub>):  $\delta$  2.09 (s, 6H), 2.11 (s, 6H), 2.73 (s, 6H) ppm. <sup>13</sup>C NMR (100.64 MHz, DMSO-*d*<sub>6</sub>):  $\delta$  3.83, 26.59, 26.83, 128.46, 139.13, 183.15, 184.52 ppm. MS (ESI):  $m/z$  495.0052 ([M + Na]<sup>+</sup> 495.0060).



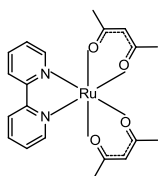
Ru(dbm)<sub>2</sub>(MeCN)<sub>2</sub>, **17**<sup>34</sup>

**11** (0.581 g, 0.752 mmol) was added to a flask containing activated zinc dust (0.5 g) followed by EtOH (15 mL). The suspension was refluxed for 1 h, during which time a colour change from black to dark blue was observed. MeCN (10 mL) was added to the mixture under nitrogen and colour changed from dark blue, to brown, to green, to dark green, then red to dark red was observed over 2 h of reflux. The dark red reaction mixture was refluxed for a further 3.5 h before

being filtered through a bed of celite to give a clear red solution. The solution was dried *in vacuo* to give a dark red powder. The powder was purified by silica gel column chromatography with DCM to firstly remove dibenzylmethane, followed by pure EtOAc to elute the complex as a dark red powder. Yield: 0.25 g, 50%.  $^1\text{H}$  NMR (400 MHz, acetone- $d_6$ ):  $\delta$  2.69 (s, 6H), 6.77 (s, 2 H), 7.24 – 7.36 (m, 6H), 7.39 – 7.50 (m, 6H), 7.88 (d,  $J$  6.8 Hz, 4H), 8.05 (d,  $J$  8.1 Hz, 4H) ppm. MS (ESI):  $m/z$  630.1082 ( $[\text{M}]^+$  required 630.1087).

### III. Preparation of Ru(bpy)( $\beta$ -diketonato) $_2$ Complexes (**8**, **18**, **19** – **21**)

Ru(acac) $_2$ (bpy) (**8**) was prepared by Routes 1 – 3 with varying yields.



Route 1 – *via* Ru(acac) $_2$ (MeCN) $_2$ <sup>35</sup>

**10** (0.096 g, 0.252 mmol) and bpy (0.0395 g, 0.253 mmol) were dissolved in EtOH (10 mL). The reaction mixture was refluxed overnight. The initially orange mixture turned deep green. Ethanol was removed to give dark solids. The solids were subjected to column chromatography (silica gel, DCM/MeOH 9:1) to give the product **10** as a dark solid. Yield: 0.12 g, 66%.  $^1\text{H}$  NMR (400 MHz,  $\text{C}_6\text{D}_6$ ):  $\delta$  1.60 (s, 6H), 2.21 (s, 6H), 5.38 (s, 2H), 6.41 (t,  $J$  6.5 Hz, 2H), 6.61 (t,  $J$  7.8 Hz, 2H), 7.08 (d,  $J$  8.0 Hz, 2H), 9.17 (d,  $J$  5.6 Hz, 2H) ppm. MS (ESI):  $m/z$  479.0512 ( $[\text{M} + \text{Na}]^+$  required 479.0515).

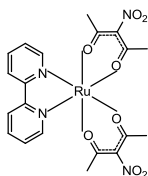
Route 2 – *via* Ru(bpy)(Cl) $_4$ <sup>36</sup>

Ru(bpy)(Cl) $_4$  (0.402 g, 1.01 mmol) was added to a flask containing activated zinc dust (1.5 g) followed by a mixture of EtOH – degassed water (10 mL each). The contents were stirred for 15 min during which colour change from black to deep violet was observed. AcacH (1.56 g, 15.6 mmol) was added to the flask followed by Na $_2$ CO $_3$  (1.20 g, 11.3 mmol) in portions. The reaction mixture was refluxed for 1 h. A colour change from violet to maroon was noted. The reaction was cooled to room temperature and filtered to give a dark maroon solution; the solid was washed with copious amount of cold abs. EtOH until the runoff was no longer green. The green-maroon coloured filtrate was reduced and extracted with DCM (20 mL  $\times$  3). The combined green DCM layer was dried with MgSO $_4$ , filtered and solvent removed *in vacuo* to give dark solid. The

dark solid was subject to column chromatography (silica gel, DCM/MeOH 9:1) to remove an unidentified red and brown band before the elution of product. Yield: 0.18 g, 40%.

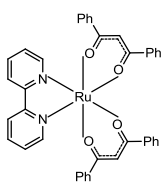
### Route 3 – Ru(COD)(acac)<sub>2</sub><sup>37</sup>

Ru(COD)(acac)<sub>2</sub> (0.203 g, 0.498 mmol) and bpy (0.0850 g, 0.544 mmol) were placed in a pressure tube and underwent vacuum/nitrogen fill cycles three times. Toluene (15 mL) was added to the tube under nitrogen to give a light yellow solution. The reaction mixture was heated at 175 °C for 72 h, by which point the solution had turned green. Solvent was removed to give a dark solid which was subjected to column chromatography (silica gel, DCM/MeOH 9:1) to first elute a faint yellow band, followed by a dark green band with a pink band trailing on top of it. The dark green band was collected and solvent removed to give the product as a dark solid which was recrystallised with DCM/pentane. Yield: 0.015 g, 7%.



### Ru(NO<sub>2</sub>-acac)<sub>2</sub>(bpy), **18**

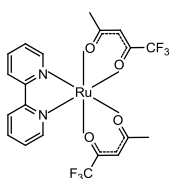
**18** (0.200 g, 0.424 mmol) and bpy (0.0660 g, 0.423 mmol) were added to a Schlenk flask followed by EtOH (~15 mL). The reaction mixture was refluxed for 5 h before solvent was taken off to give a dark brown solid. The solid was purified by column chromatography (silica gel, MeCN/DCM 1:5) to give a dark brown solid. Yield: 0.030 g, 13%. <sup>1</sup>H NMR (500 MHz, DMSO-*d*<sub>6</sub>): δ 1.76 (s, 6H), 2.28 (s, 6H), 7.52 (t, *J* 6.6 Hz, 2H), 7.90 (t, *J* 7.8 Hz, 2H), 8.59 (d, *J* 8.0 Hz, 2H), 8.68 (d, *J* 5.4 Hz, 2H) ppm. <sup>13</sup>C NMR (150.90 MHz, DMSO-*d*<sub>6</sub>): δ 3.82, 13.97, 22.07, 26.57, 26.66, 26.81, 27.11, 30.96, 122.74, 125.21, 128.44, 134.66, 139.11, 139.47, 152.07, 159.82, 182.14, 183.12, 183.94, 184.49 ppm. MS (ESI): *m/z* 569.0209 ([*M* + Na]<sup>+</sup> required 569.0217). Anal Calcd for C<sub>20</sub>H<sub>20</sub>N<sub>4</sub>O<sub>8</sub>Ru: C, 44.04; H 3.70; N 10.27. Found: C, 44.17; H, 3.77; N, 10.04. CV (MeCN, 0.1 M NBu<sub>4</sub>PF<sub>6</sub>, 0.1 V s<sup>-1</sup> vs Fc<sup>+0</sup>) E<sub>1/2</sub> (Ru<sup>2+/3+</sup>) = -0.389V, |ΔE| = 0.069 V.



### Ru(dbm)<sub>2</sub>(bpy), **19**

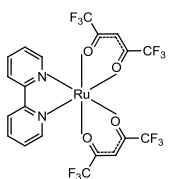
**19** (0.0650 g, 0.102 mmol) and bpy (0.0170 g, 0.109 mmol) were added to a flask followed by EtOH (20 mL). The reaction mixture was refluxed for 3 h during which a colour change from brown to black was observed

in the first 30 min. The reaction mixture was cooled to room temperature, solvent removed and solids redissolved in a minimal amount of DCM before being added dropwise to excess pentane to precipitate the product as a black solid. The solid was filtered, washed twice with pentane and dried *in vacuo*. Yield: 0.050 g, 70%.  $^1\text{H}$  NMR (400 MHz,  $\text{DMSO-}d_6$ ):  $\delta$  6.72 (s, 2H), 7.28 (t,  $J$  7.7 Hz, 4H), 7.35 – 7.49 (m, 10 H), 7.60 (d,  $J$  7.3 Hz, 4 H), 7.79 (t,  $J$  7.7 Hz, 2 H), 8.02 (d,  $J$  7.1 Hz, 4H), 8.59 (d,  $J$  8.1 Hz, 2H), 8.84 (d,  $J$  5.6 Hz, 2H) ppm. MS (ESI):  $m/z$  704.1217 ( $[\text{M}]^+$  704.1244). CV (MeCN, 0.1 M  $\text{NBu}_4\text{PF}_6$ , 0.1  $\text{V s}^{-1}$  vs  $\text{Fc}^{+/0}$ )  $E_{1/2}(\text{Ru}^{2+/3+}) = -0.416 \text{ V}$ ,  $|\Delta E| = 0.059 \text{ V}$ .



$\text{Ru}(\text{tfac})_2(\text{bpy})$ , **20**<sup>36</sup>

$\text{Ru}(\text{bpy})(\text{Cl})_4$  (0.200 g, 0.500 mmol) was added to a flask containing activated zinc dust (0.5 g) followed by EtOH – degassed water (15 mL each). The mixture was stirred for 15 min to result in a deep violet colour. Colour changed to maroon upon addition of trifluoroacetylacetone (tfac) (0.900 mL, 7.42 mmol) and  $\text{Na}_2\text{CO}_3$  (0.583 g, 5.50 mmol). The reaction was refluxed for 3 h. The maroon mixture was filtered; the filtrate was reduced to 5 mL and extracted by DCM (20 mL x 3). The DCM layer was washed with water, dried with  $\text{MgSO}_4$  and solvent removed *in vacuo* to give a dark solid. The solid was purified by column chromatography (silica gel, MeCN/toluene 1:5) to give the product as a dark maroon solid. Yield: 0.070 g, 25%.  $^1\text{H}$  NMR (400 MHz,  $\text{C}_6\text{D}_6$ ), a mixture of three isomers:  $\delta$  1.34 (s, 3H), 1.39 (s, 3H), 1.96 (s, 3H), 1.97 (s, 3H), 5.89 (s, 2H), 6.23 – 6.32 (m, 4H), 6.52 – 6.61 (m, 4H), 6.86 (d,  $J$  8.0 Hz, 2H), 6.91 (t,  $J$  8.0 Hz, 2H), 8.69 (d,  $J$  5.7 Hz, 1H), 8.78 (d,  $J$  5.5 Hz, 1H), 8.91 (d,  $J$  5.6 Hz, 1H), 9.00 (d,  $J$  5.5 Hz, 1H) ppm.  $^{19}\text{F}$  NMR (376 MHz,  $\text{C}_6\text{D}_6$ ):  $\delta$  -73.16, -73.17, -73.31, -73.40 ppm. MS (ESI):  $m/z$  586.9939 ( $[\text{M}]^+$  required 586.9939). CV (MeCN, 0.1 M  $\text{NBu}_4\text{PF}_6$ , 0.1  $\text{V s}^{-1}$  vs  $\text{Fc}^{+/0}$ )  $E_{1/2}(\text{Ru}^{2+/3+}) = -0.087 \text{ V}$ ,  $|\Delta E| = 0.073 \text{ V}$ .



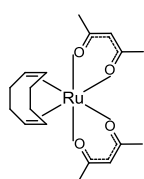
$\text{Ru}(\text{hfac})_2(\text{bpy})$ , **21**<sup>36</sup>

$\text{Ru}(\text{bpy})(\text{Cl})_4$  (0.201 g, 0.502 mmol) was added to a flask containing activated Zn dust followed by EtOH (15 mL) and degassed water (15 mL). The mixture was left to stir at room temperature for 15 min whereupon its colour changed from dark to deep purple. Hexafluoroacetylacetone (hfac) (0.970 mL, 6.85 mmol) was added to the stirring mixture followed immediately by

Na<sub>2</sub>CO<sub>3</sub> (0.581 g, 5.48 mmol). The reaction mixture was refluxed for one hour. The resulting maroon mixture was filtered, the filtrate reduced to 5 mL and extracted with DCM (50 mL, 30 mL × 3). The combined organic extracts was then dried with MgSO<sub>4</sub>, filtered and solvent removed to give a reddish brown solid. The solid was purified by column chromatography (silica gel, MeCN/toluene 1:5) to give reddish brown solids. Yield: 0.11 g, 33%. <sup>1</sup>H NMR (400 MHz, C<sub>6</sub>D<sub>6</sub>): δ 6.12 (t, 2H), 6.45 (s, 2H), 6.52 (t, 2H), 6.71 (d, 2H), 8.44 (d, 2H) ppm. MS (ESI): *m/z* 694.9374 ([M + Na]<sup>+</sup> required 694.9385).

#### IV. Preparation of Ru(diene)(β-diketonato)<sub>2</sub> Complexes (**22** – **28**)

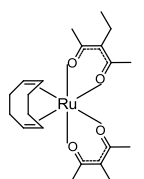
Ru(diene)(β-diketonato)<sub>2</sub> complexes (diene = 1,5-cyclooctadiene, COD or norbornadiene, NBD) were prepared following methods described by Powell<sup>29</sup> and Bennett *et al.*<sup>38</sup>, respectively. Complexes **23** – **26** were prepared in a way analogous to **22** while **28** was prepared in a similar fashion to that used for the preparation of **27**.



Ru(COD)(acac)<sub>2</sub>, **22**<sup>29</sup>

[Ru(COD)(Cl)<sub>2</sub>]<sub>n</sub> (0.280 g, 1.00 mmol) and Na<sub>2</sub>CO<sub>3</sub> (1.01 g, 9.44 mmol) added to a flask followed by DMF (10 mL). AcacH (0.300 mL, 2.92 mmol) was added to the brown mixture. The reaction mixture was heated at

140 °C. The brown mixture turned into a dark orange colour after 15 min. After cooling to room temperature sodium salt was removed from the organic layer and washed with MeOH until the filtrate ran clear. Methanol was removed from the DMF layer *in vacuo*. Water was added to the DMF layer to crash out yellow solids. Yield: 0.24 g, 59%. <sup>1</sup>H NMR (300 MHz, CDCl<sub>3</sub>): δ 1.85 – 1.95 (m, 8H), 2.15 – 2.21 (m, 10H), 2.36 – 2.40 (m, 2H), 4.00 – 4.05 (m, 2H), 4.11 – 4.17 (m, 2H), 5.36 (s, 2H) ppm. MS (ESI): *m/z* 408.0879 ([M]<sup>+</sup> required 408.0875).

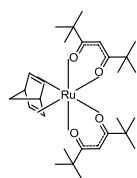


Ru(COD)(eacac)<sub>2</sub>, **23**<sup>29</sup>

Prepared with 0.400 mL (2.98 mmol, 3 equiv.) of eacac. Yield: 0.25 g, 69%. <sup>1</sup>H NMR (400 MHz, CDCl<sub>3</sub>): δ 1.06 (t, 6H), 1.98 – 1.99 (m, 2H), 2.01 (s, 6H), 2.08 – 2.14 (m, 4H), 2.27 (s, 6H), 2.31 (d, 4H), 2.36 – 2.43 (m, 2H),



(s, 2H), 1.89 (s, 6H), 2.17 (s, 6H), 3.81 (s, 2H), 4.39 – 4.41 (m, 2H), 4.63 – 4.66 (m, 2H), 5.31 (s, 2H) ppm. MS (ESI):  $m/z$  415.0439 ( $[M + Na]^+$  required 415.0454).



Ru(NBD)(tmhd)<sub>2</sub>, **28**<sup>38</sup>

Prepared with 0.5 mL (2.40 mmol, 2.4 equiv.) of tmhd. Yield: 0.23 g, 36 %.

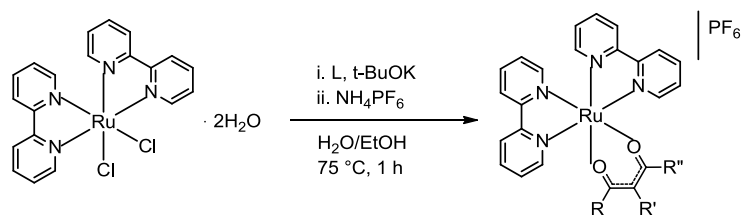
<sup>1</sup>H NMR (400 MHz, CDCl<sub>3</sub>):  $\delta$  0.95 (s, 18H), 1.23 (s, 18H), 1.16 (s, 2H), 3.85 (s, 2H), 4.14 – 4.15 (m, 2H), 4.52 – 4.54 (m, 2H), 5.47 (s, 2H) ppm.

MS (ESI):  $m/z$  583.2309 ( $[M + Na]^+$  required 583.2332).

### 3.6 Results and Discussion

#### 3.6.1 Synthesis of Series I: Ruthenium Mono( $\beta$ -diketonato) Complexes, [Ru(bpy)<sub>2</sub>( $\beta$ -diketonato)](PF<sub>6</sub>)

Complexes of Series I, ruthenium mono( $\beta$ -diketonato) complexes (**1** – **7**) (Scheme 3.1) were prepared as a starting point to investigate the effects of substituents on the  $E_{1/2}$  of the complexes containing both the  $\beta$ -diketonato and bpy ligands. The complexes were prepared by displacing chloride ligands in Ru(bpy)(Cl)<sub>2</sub>·2H<sub>2</sub>O with  $\beta$ -diketones in the presence of a stoichiometric amount of *t*-BuOK in a hot mixture of EtOH – water, and the product was precipitated by NH<sub>4</sub>PF<sub>6</sub> in moderate to high yields (Scheme 3.1). Munery *et al.*<sup>26</sup> noted that the use of *t*-BuOK, a base which deprotonates  $\beta$ -diketones, would increase reaction yields. **1** was brominated by *N*-bromosuccinimide in DCM and purified by column chromatography to give **4** in moderate yield.<sup>26</sup> Proton chemical shift values of the 3 and 3' protons in bpy follow similar trends to those found for *cis*-[Ru(bpy)<sub>2</sub>(L)]<sup>2+</sup> complexes, where L =  $\alpha,\alpha'$ -diimine ligand, in that protons at 3,3'-positions are most deshielded,<sup>39,40</sup> but no trend was observed for the rest of the protons which occupied the remaining positions on the bpy rings.

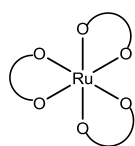
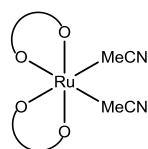
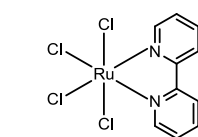
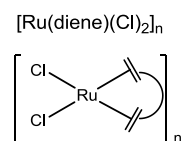
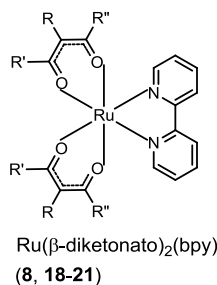
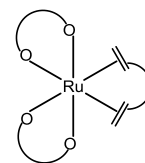
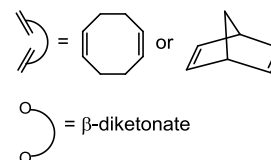


$\beta$ -diketone, Complex	R	R'	R''
2,4-pentanedione, <b>1</b>	CH <sub>3</sub>	H	CH <sub>3</sub>
3-methyl-2,4-pentanedione, <b>2</b>	CH <sub>3</sub>	CH <sub>3</sub>	CH <sub>3</sub>
3-ethyl-2,4-pentanedione, <b>3</b>	CH <sub>3</sub>	C <sub>2</sub> H <sub>5</sub>	CH <sub>3</sub>
3-bromo-2,4-pentanedione, <b>4</b>	CH <sub>3</sub>	Br	CH <sub>3</sub>
2,6-dimethyl-3,5-heptanedione, <b>5</b>	C <sub>2</sub> H <sub>7</sub>	H	C <sub>2</sub> H <sub>7</sub>
3-(4-methoxybenzyl)-2,4-pentanedione, <b>6</b>	CH <sub>3</sub>	C <sub>8</sub> H <sub>9</sub> O	CH <sub>3</sub>
3-(4-nitrobenzyl)-2,4-pentanedione, <b>7</b>	CH <sub>3</sub>	C <sub>7</sub> H <sub>6</sub> NO <sub>2</sub>	CH <sub>3</sub>

**Scheme 3.1** Preparation of Ru(bpy)<sub>2</sub>( $\beta$ -diketonato) complexes.

### 3.6.2 Routes to Prepare Series II: Ruthenium Bis( $\beta$ -diketonato) Complexes, Ru(bpy)<sub>2</sub>( $\beta$ -diketonato)

Three synthetic pathways were explored in an attempt to find the most efficient route for preparing ruthenium bis( $\beta$ -diketonato) complexes (Scheme 3.2). Ru(acac)<sub>2</sub>(bpy) (**8**) was prepared by all three routes with varying yields. Route 1 gave **18** and **19**, Route 2 led to complexes **20** and **21** and finally Route 3 led to complex **19**.

Route 1: Ru( $\beta$ -diketonato)<sub>2</sub>(MeCN)<sub>2</sub>  
(**10**, **15-17**)Route 2: Ru(bpy)(Cl)<sub>4</sub>Route 3: Ru( $\beta$ -diketonato)<sub>2</sub>(diene)  
(**22-28**)Ru( $\beta$ -diketonato)<sub>3</sub> (**9**, **11-14**)EtOH  
Δ, 2 - 5 h  
50 - 92%  
i. Zn,  
ii. MeCNbpy  
EtOH  
Δ, 3 - 5 h  
13 - 70%EtOH/ H<sub>2</sub>O  
Δ, 1 h  
25 - 33 %  
i. Zn  
ii. L, Na<sub>2</sub>CO<sub>3</sub>DMF  
Δ, 10 min  
22 - 81 %  
β-diketone,  
Na<sub>2</sub>CO<sub>3</sub>bpy  
toluene  
Δ, 14 days  
2 - 7 %

$\beta$ -diketone, Complex	R'	R	R''
2,4-pentanedione, <b>8</b>	CH <sub>3</sub>	H	CH <sub>3</sub>
3-nitro-2,4-pentanedione, <b>18</b>	CH <sub>3</sub>	NO <sub>2</sub>	CH <sub>3</sub>
Dibenzoylmethane, <b>19</b>	C <sub>6</sub> H <sub>5</sub>	H	C <sub>6</sub> H <sub>5</sub>
1,1,1-trifluoro-2,4-pentanedione, <b>20</b>	CF <sub>3</sub>	H	CH <sub>3</sub>
1,1,1,5,5,5-hexafluoro-2,4-pentanedione, <b>21</b>	CF <sub>3</sub>	H	CF <sub>3</sub>

**Scheme 3.2** Routes to Ru( $\beta$ -diketonato)<sub>2</sub>(bpy) complexes.**3.6.2.1 Route 1: Ru( $\beta$ -diketonato)<sub>2</sub>(MeCN)<sub>2</sub>****I. Preparation of Ru( $\beta$ -diketonato)<sub>3</sub> Complexes (**9** and **11**)**

This first route necessitates the preparation of the complex Ru(acac)<sub>3</sub> (**9**) to give the complex *cis*-Ru(acac)<sub>2</sub>(MeCN)<sub>2</sub> (**10**). Complex **9** was prepared in 60% yield by reacting RuCl<sub>3</sub>·3H<sub>2</sub>O with 12 equiv. of acacH. The use of dilute acid and toluene in this reaction creates an equilibrium established by the acacH as it partitions itself between the two phases as depicted in Figure 3.4.<sup>27</sup> Once the metal salt dissolves in the dilute acid, acac coordinates with ruthenium(III) and the resultant neutral precursor **9** formed partitions to the toluene phase before it can react with the aqueous acid.<sup>27</sup> Although this

is an efficient route for the synthesis of **9**, attempts to synthesise analogues with other  $\beta$ -diketones were unsuccessful in producing the necessary  $\text{Ru}(\beta\text{-diketonato})_3$  complexes.

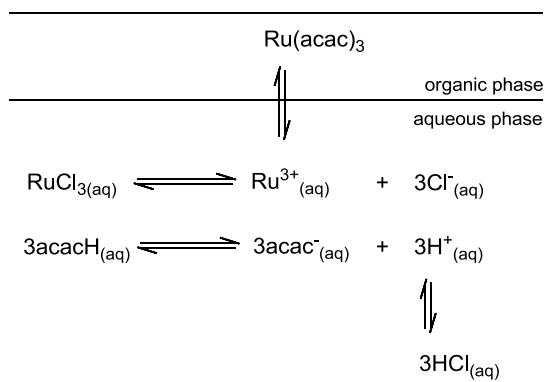


**Figure 3.4** Phase-transfer equilibria in the reaction of  $\text{Ru(acac)}_3$ .

A slightly complicated ‘ruthenium blue’ method was employed to prepare  $\text{Ru}(\text{dbm})_3$  (**11**) (dbm = dibenzoylmethanato). The refined ‘ruthenium blue’ method reported by Endo *et al.* involves firstly the preparation of a ‘ruthenium blue’ solution of  $\text{RuCl}_3 \cdot 3\text{H}_2\text{O}$  in a refluxing mixture of EtOH – water for 4 – 5 h; a series of colour changes was observed during the reductive activation of the ruthenium species by aq. EtOH, until a dense colour of blue resulted.<sup>30</sup> The nature of this highly air-sensitive blue species has not been confirmed, but it was reported that it may be a cluster of anions  $[\text{Ru}_5\text{Cl}_2]^{2-}$ .<sup>27</sup> Caution was taken so as not to over-reduce the ruthenium species, which was evident when a deposit of black solid or mirror is present.<sup>30</sup>

Complex **11** was synthesised by introducing dibenzoylmethane to the ‘ruthenium blue solution’, refluxing for a period of time until the blue changed colour, cooled, its hydrogen ions neutralised by  $\text{KHCO}_3$  and refluxed; this step was repeated once to give the product in 25% yield.<sup>30</sup> Although no ruthenium mirror was observed during this reaction, there was an insoluble solid present when **11** was purified by column chromatography, which points to a possibility of over-reduction of the  $\text{RuCl}_3 \cdot 3\text{H}_2\text{O}$  species even though care was taken during reaction.

## II a. Substituted Ru( $\beta$ -diketonato)<sub>3</sub> Complexes (**12** – **14**) by Direct Modification of Ru(acac)<sub>3</sub>

Direct modification of the acac ligand of complex **9** was employed to expand the scope of available complexes for this route. It has been proposed that, owing to the structural similarity of metal-diketonates to a benzene ring, they display pseudo-aromatic properties when subjected to electrophilic substitution to give mono-, di- and tri-substituted products depending on the stoichiometry of the reagent or the intramolecular deactivating properties of the already substituted acac.<sup>41,42</sup> The methine proton on acac has been shown to undergo electrophilic substitution reactions to give complexes with substituted chelates, e.g., halogenation,<sup>32,43-45</sup> nitration,<sup>46,47</sup> formylation,<sup>47</sup> chlorosulfonylation,<sup>48</sup> thiocyanogenation and acylation.<sup>49</sup>

Substantial research on the substitution behaviour of various metal-diketonates has been performed, however very little has involved ruthenium complexes.<sup>41,42</sup> Although some metal-diketonates are known to be acid-labile, Ru( $\beta$ -diketonato)<sub>3</sub> complexes are robust enough to undergo modification at the methine proton. Following the method of Collman *et al.*,<sup>47</sup> nitration of **9** with Cu(NO<sub>3</sub>)<sub>2</sub> in acetic anhydride was achieved to give Ru(NO<sub>2</sub>-acac)<sub>3</sub> (**12**) in 70% yield.

Precursor **9** underwent bromination with *N*-bromosuccinimide immediately to give Ru(Br-acac)<sub>3</sub> (**13**) in 90% yield. Ru(I-acac)<sub>3</sub> (**14**) was also synthesised using *N*-iodosuccinimide in 85% yield.<sup>32</sup> The mechanism of bromination was determined by Kluiber: the bromination proceeds without any intermediate ring cleavage on **9** which acted similarly to a metalloheterocycle (Figure 3.5).<sup>44</sup>

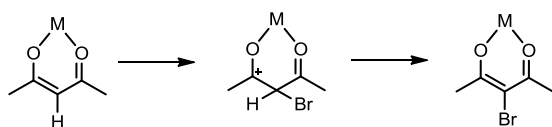


**Figure 3.5** Bromination on metal( $\beta$ -diketonates).

## II b. Proton NMR of Ru( $\beta$ -diketonato)<sub>3</sub> complexes (**9**, **11-14**)

Paramagnetic complexes often give broad, poorly resolved proton signals as a consequence of rapid nuclear spin relaxation. Despite the fact that Ru( $\beta$ -diketonato)<sub>3</sub> complexes are paramagnetic, useful information about these complexes can be gleaned from <sup>1</sup>H NMR.<sup>30,50-52</sup> Table 3.2 summarises the NMR data of the proton chemical shifts of the complexes **9** and **11 – 14** recorded in C<sub>6</sub>D<sub>6</sub>.

**Table 3.2** <sup>1</sup>H NMR data for Ru( $\beta$ -diketonato)<sub>3</sub> complexes in C<sub>6</sub>D<sub>6</sub>.

complex	<sup>1</sup> H chemical shift, $\delta$ (ppm)		
	methine H	methyl H	substituents on $\beta$ -diketone
<b>9</b>	-30.12	-5.55	
<b>11</b>	-32.56		6.72, 9.20, 11.78
<b>12</b>		-3.41	
<b>13</b>		-7.78	
<b>14</b>		-7.21	

In the case of **9**, a sharp singlet at -5.55 ppm and a broad singlet -30.12 ppm were assigned to methyl protons and methine protons based on integrals. Complete disappearance of the broad singlet indicated that **12 – 14** have undergone electrophilic substitution at the methine carbon, while proton peaks belonging to both the phenyl ring and methine proton are present in **11**. Due to the similar properties displayed by halogenated complexes **13** and **14**, their chemical shift values are close together.

The proton chemical shifts of  $\beta$ -diketonates in these complexes show large upfield shifts due to their interactions with the paramagnetic Ru<sup>3+</sup> centre.<sup>50</sup> The shifts, called isotropic shifts, arise from contact and pseudo-contact interactions: a contact shift is the result of electron spin imbalance on the ligand due to spin transfer between metal and ligand whereas pseudo-contact shift results from a through-space coupling between ligand nuclei and the unpaired electron on the metal ion, where a dependency on molecular geometry is shown.<sup>53,54</sup> Both contact and pseudo-contact interactions contribute to the isotropic shifts in Ru<sup>3+</sup> complexes.<sup>55,56</sup> In this group of Ru( $\beta$ -diketonato)<sub>3</sub> complexes, the protons at the methine carbon are shown to interact with the ruthenium centre more directly, as they experience larger upfield shifts.

### II c. Preparation of *cis*-Ru( $\beta$ -diketonato)<sub>2</sub>(MeCN)<sub>2</sub> complexes (**10**, **15** – **17**)

Due to the substitution-inert nature of Ru( $\beta$ -diketonato)<sub>3</sub> complexes, one approach to the synthesis of the mixed  $\beta$ -diketonato and bpy complexes was to prepare an intermediate that allowed clean ligand substitution reactions with bpy.<sup>50</sup> Ru( $\beta$ -diketonato)<sub>2</sub>(MeCN)<sub>2</sub> complexes were targeted as MeCN should be sufficiently labile to be displaced readily by bpy. Although there was a previous report of the synthesis of Ru(acac)<sub>2</sub>(bpy) complexes obtained in one step from Ru(acac)<sub>3</sub>,<sup>35</sup> the yields achieved here on the attempts with bpy were extremely low.

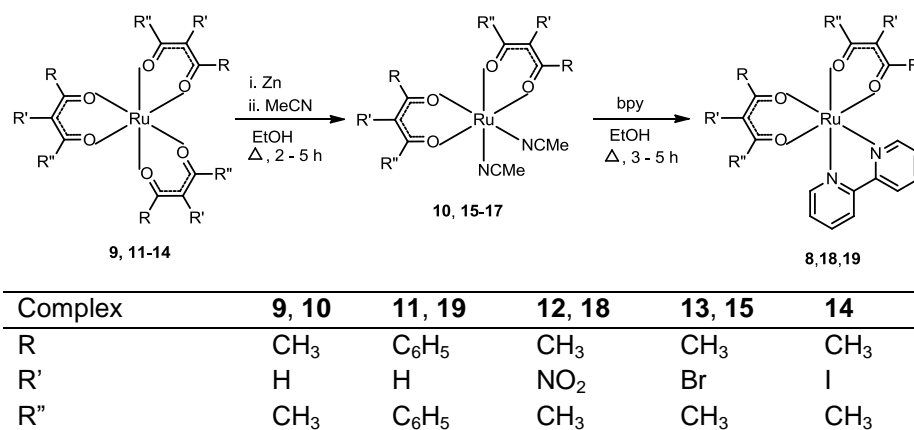
In this chapter, intermediate Ru(acac)<sub>2</sub>(MeCN)<sub>2</sub> (**10**) was accessed by the reduction of precursor **9** with activated zinc dust following heating in EtOH for 1 h then cooling and the addition of an excess of MeCN. The mixture was finally refluxed for a further 2 h.<sup>33</sup> An intense colour change of bright red to dark red and finally bright orange was observed over the course of this reaction. Air-stable **10** was isolated in near quantitative yield as a bright orange solid. It is critically important that the zinc dust be properly activated prior to the reaction to ensure full reduction of **9**.<sup>57</sup>

On reacting complexes **12** and **13** in the same fashion with zinc dust, they both yielded **10** rather than the expected halogenated species. This is consistent with the report of Collman *et al.* which noted that zinc powder in hot EtOH decomposed brominated complexes.<sup>43</sup> Intermediate **10** was then brominated to give Ru(Br-acac)<sub>2</sub>(MeCN)<sub>2</sub> (**15**) as a dark brown solid. The reaction of **11** and **14** gave Ru(dbm)<sub>2</sub>(MeCN)<sub>2</sub> (**17**) as a brown solid at 60% yield and Ru(NO<sub>2</sub>-acac)<sub>2</sub>(MeCN)<sub>2</sub> (**16**) as a dark orange solid at 92% respectively.

### III. Preparation of Ru( $\beta$ -diketonato)<sub>2</sub>(bpy) Complexes (**8**, **18** and **19**) via Ru( $\beta$ -diketonato)<sub>2</sub>(MeCN)<sub>2</sub> complexes

A literature survey found a number of reactions utilising intermediate **10** and Ru( $\beta$ -diketonato)<sub>2</sub>(MeCN)<sub>2</sub> complexes as intermediates to prepare heteroleptic bis( $\beta$ -diketonato)(L) Ru<sup>2+</sup> complexes (L = N, N'-donor).<sup>12,34,35,51,58-60</sup> Treatment of intermediate **10** with an equimolar amount of bpy in refluxing EtOH under nitrogen

gave Ru(acac)<sub>2</sub>(bpy) (**8**) as a black green solid in 60% yield (Scheme 3.3). Aromatic signals in <sup>1</sup>H NMR in **8** were found to correspond to the number and symmetry of the protons in bpy, along with three singlets belonging to acac, to confirm formation of product.



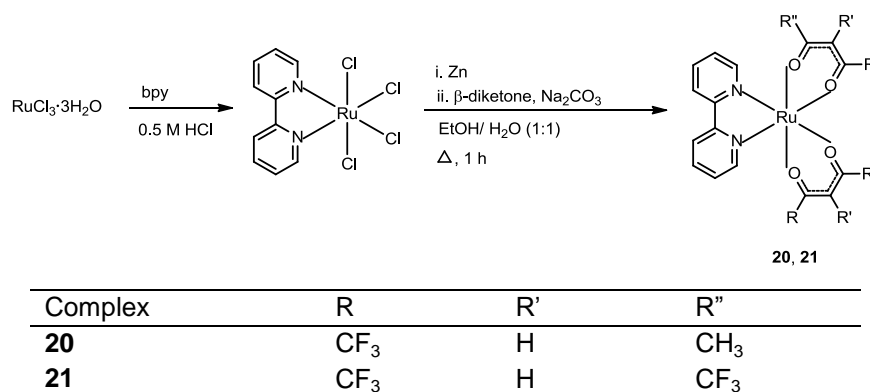
**Scheme 3.3** Synthesis of Ru(β-diketonato)<sub>2</sub>(bpy) complexes *via* Route 1.

Ru(NO<sub>2</sub>-acac)<sub>2</sub>(bpy) (**18**) and Ru(dbm)<sub>2</sub>(bpy) (**19**) were prepared from complexes **16** and **17** in the same fashion in low to moderate yields. **18** was purified by column chromatography to remove a small amount of bpy, the presence of which could be explained by incomplete reaction. Nonetheless, prolonged reaction time resulted in the decomposition of **18**, hence the reflux was limited to less than 6 h.

### 3.6.2.2 Route 2: Preparation of Ru(β-diketonato)<sub>2</sub>(bpy) Complexes (**8**, **20** and **21**) *via* Ru(bpy)(Cl)<sub>4</sub>

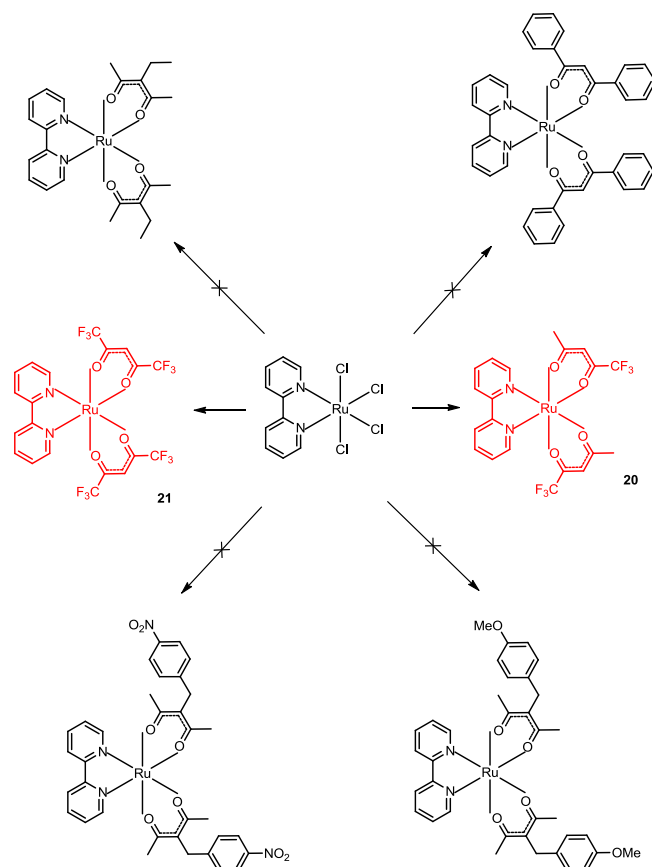
A second approach involving the preparation of precursor of the Ru(β-diketonato)<sub>2</sub>(bpy) complexes *via* Ru(bpy)(Cl)<sub>4</sub> was investigated concurrently. Ru(bpy)(Cl)<sub>4</sub> was obtained by dissolving RuCl<sub>3</sub>·3H<sub>2</sub>O in dilute HCl to which 1.2 equiv. of bpy was added and allowed to stand for 21 days at 85% yield.<sup>28</sup> In an analogous fashion to that of Route 1, Ru(bpy)(Cl)<sub>4</sub> was stirred with activated zinc dust in a mixture of EtOH – water for 15 min followed by the addition of the β-diketones, acac, tfac and hfac, respectively and Na<sub>2</sub>CO<sub>3</sub>. The mixtures were refluxed for 1 h to give Ru(acac)<sub>2</sub>(bpy) (**8**), Ru(tfac)<sub>2</sub>(bpy) (**20**) and Ru(hfac)<sub>2</sub>(bpy) (**21**) (tfac = 1,1,1-trifluoro-2,4-pentanedione, hfac = 1,1,1,5,5,5-hexafluoro-2,4-pentanedione) respectively in

moderate to high yields. Because of its asymmetric  $\beta$ -diketone, **20** exists as a mixture of three geometrical isomers in 1:1:2 ratio of *cis*- and *trans*-isomers. This was confirmed by  $^1\text{H}$  NMR where the following configurations were observed: *trans*- $\text{CF}_3$ -*cis*-H-[Ru(tfac) $_2$ (bpy)], *cis*- $\text{CF}_3$ -*cis*-H-[Ru(tfac) $_2$ (bpy)] and *cis*- $\text{CF}_3$ -*trans*-H-[Ru(tfac) $_2$ (bpy)]. This is further supported by the presence of four signals in  $^{19}\text{F}$  NMR. No attempts were made to resolve the isomers.



**Scheme 3.4** Synthesis of Ru( $\beta$ -diketonato) $_2$ (bpy) via Route 2.

Route 2 is a more direct way of preparing ruthenium bis( $\beta$ -diketonato) complexes compared to Route 1. Nonetheless efforts to prepare complexes using other  $\beta$ -diketonates such as eacac, dbm, mbpd and nbpd in the presence of *t*-BuOK did not give products.



**Scheme 3.5** Attempted syntheses *via* Route 2 to prepare Ru( $\beta$ -diketonato)<sub>2</sub>(bpy).

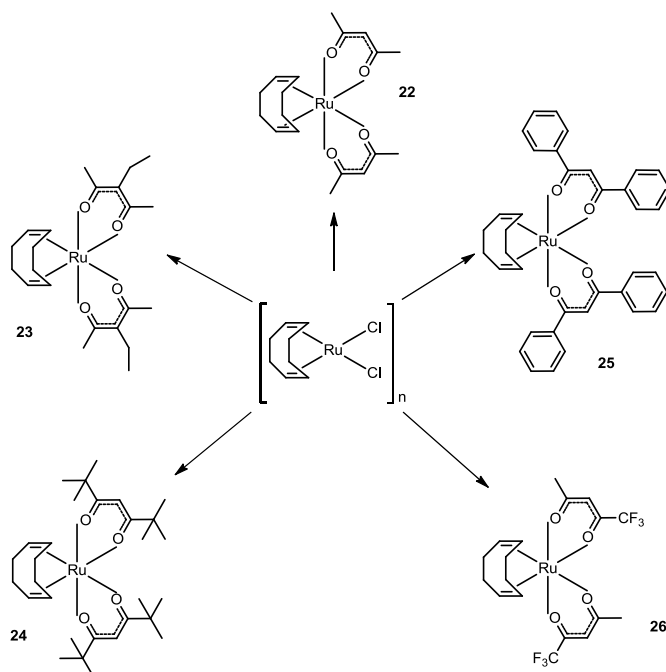
### 3.6.2.3 Route 3: Preparation of Ru( $\beta$ -diketonato)<sub>2</sub>(bpy) Complexes (8 and 19) *via* Ru(diene)( $\beta$ -diketonato)<sub>2</sub> complexes

It has been reported that the complexes Ru(L)<sub>2</sub>(acac)<sub>2</sub> complexes are accessible through Ru(diene)(acac)<sub>2</sub> complexes, where L = triisopropylphosphine, (S)-BINAP, carbon monoxide, trialkylstibenes, tertiary phosphine.<sup>8,61,62</sup> The air-stable diene complexes, Ru(diene)(acac)<sub>2</sub> have been prepared through the binding of acyclic conjugated dienes with the reduced form of Ru(acac)<sub>3</sub> in  $\eta^2$ ,  $\eta^2$  mode; cyclic dienes and mono alkenes on the other hand give the less stable Ru( $\eta^2$ -alkene)(acac)<sub>2</sub> or Ru( $\eta^2$ ,  $\eta^2$ -alkene)(acac)<sub>2</sub> complexes.<sup>8,63</sup> These complexes are composed of labile dienes which can be readily displaced by other ligands, providing an alternative route to the synthesis of mixed ligand complexes. However, these routes require the low yielding preparation of the Ru( $\beta$ -diketonato)<sub>3</sub> complexes, so attention was directed at ruthenium diene starting materials, [Ru(COD)(Cl)<sub>2</sub>]<sub>n</sub> and [Ru(NBD)(Cl)<sub>2</sub>]<sub>n</sub>, where a variety of

$\beta$ -diketones could be incorporated directly by displacement of chloride ligands to give  $\text{Ru}(\beta\text{-diketonato})_2(\text{diene})$  complexes.

The reactions of cycloocta-1,5-diene (COD) and bicyclo[2.2.1]hepta-2,5-diene (norbornadiene, NBD) with  $\text{RuCl}_3 \cdot 3\text{H}_2\text{O}$  gave the products  $[\text{Ru}(\text{COD})(\text{Cl})_2]$  and  $[\text{Ru}(\text{NBD})(\text{Cl})_2]_n$  respectively.<sup>29,38</sup>  $\text{Ru}(\text{COD})(\text{acac})_2$  (**22**) was synthesised from  $[\text{Ru}(\text{COD})\text{Cl}_2]$  in 80% yield.<sup>29</sup> Under the same conditions, the synthesis was expanded to afford  $\text{Ru}(\text{COD})(\text{eacac})_2$  (**23**),  $\text{Ru}(\text{COD})(\text{tmhd})_2$  (**24**),  $\text{Ru}(\text{COD})(\text{dbm})_2$  (**25**) and  $\text{Ru}(\text{COD})(\text{tfac})_2$  (**26**),  $\text{Ru}(\text{NBD})(\text{acac})_2$  (**27**) and  $\text{Ru}(\text{NBD})(\text{tmhd})_2$  (**28**) (tmhd = 2,2,6,6-tetramethyl-3,5-heptanedione).

The presence of bound COD in these intermediates was confirmed by the appearance of COD methine and methylene peaks in  $^1\text{H}$  NMR as multiplets; the same was observed for NBD complexes. Similar to **20**, **26** is made up of a mix of *cis*- and *trans*-isomers in the ratio of 1:1:2 according to its  $^1\text{H}$  NMR data. No efforts were made to distinguish the isomers from one another.



**Scheme 3.6**  $\text{Ru}(\beta\text{-diketonato})_2(\text{COD})$  complexes prepared from Route 3.

Adapting the method of Šmejkal and co-worker,<sup>37</sup> **22** together with an equimolar of bpy in toluene under nitrogen was boiled in a pressure tube at 175 °C for 14 days. Progress of the displacement of COD ligand on **22** was monitored by <sup>1</sup>H NMR, which after such forcing conditions an estimated 50% of **22** still remained to give **8** in 50% yield based on <sup>1</sup>H NMR, 7% after purification by column chromatography; **25** gave **19** in less than 2% yield after column chromatography. An attempt with **24** failed to give any product.

NBD being a more labile ligand than COD was assumed to be more easily replaced by bpy. Disappointingly, no observable products were formed by **27** and **28** under similar reaction conditions. In conclusion, even though Ru(diene)(β-diketonato)<sub>2</sub> complexes can be prepared easily and in high yields, the displacement of diene by bpy proved to be unwieldy.

### 3.7 Summary on the Synthesis of Ruthenium Complexes

Three routes to the synthesis of ruthenium complexes of Series II, Ru(β-diketonato)<sub>2</sub>(bpy), were successfully applied, yielding complexes **8** and **18** – **21**. Table 3.3 summarises the ruthenium complexes prepared by the three routes.

**Table 3.3** Ruthenium complexes synthesised in Series II.

Route	1	2	3
Precursor	Ru(acac) <sub>3</sub> , <b>9</b> Ru(dbm) <sub>3</sub> , <b>11</b> Ru(NO <sub>2</sub> -acac) <sub>3</sub> , <b>12</b> Ru(Br-acac) <sub>3</sub> , <b>13</b> Ru(I-acac) <sub>3</sub> , <b>14</b>	Ru(bpy)(Cl) <sub>4</sub>	[Ru(COD)(Cl) <sub>n</sub> ] [Ru(NBD)(Cl) <sub>n</sub> ]
Intermediate	Ru(acac) <sub>2</sub> (MeCN) <sub>2</sub> , <b>10</b> Ru(Br-acac) <sub>2</sub> (MeCN) <sub>2</sub> , <b>15</b> Ru(dbm) <sub>2</sub> (MeCN) <sub>2</sub> , <b>17</b> Ru(NO <sub>2</sub> -acac) <sub>2</sub> (MeCN) <sub>2</sub> , <b>16</b>		Ru(COD)(acac) <sub>2</sub> , <b>22</b> Ru(COD)(eacac) <sub>2</sub> , <b>23</b> Ru(COD)(tmhd) <sub>2</sub> , <b>24</b> Ru(COD)(dbm) <sub>2</sub> , <b>25</b> Ru(COD)(tfac) <sub>2</sub> , <b>26</b> Ru(NBD)(acac) <sub>2</sub> , <b>27</b> Ru(NBD)(tmhd) <sub>2</sub> , <b>28</b>
Product	Ru(acac) <sub>2</sub> (bpy), <b>8</b> (66%) Ru(NO <sub>2</sub> -acac) <sub>2</sub> (bpy), <b>18</b> (13%) Ru(dbm) <sub>2</sub> (bpy), <b>19</b> (70%)	Ru(acac) <sub>2</sub> (bpy), <b>8</b> (40 %) Ru(tfac) <sub>2</sub> (bpy), <b>20</b> (25%) Ru(hfac) <sub>2</sub> (bpy), <b>21</b> (33%)	Ru(acac) <sub>2</sub> (bpy), <b>8</b> (50% by <sup>1</sup> H NMR, 7% actual yield) Ru(dbm) <sub>2</sub> (bpy), <b>19</b> (2%)

Of the three routes, Route 1 was the most dependable; Route 2 did not work for β-diketones with EDG substituents while Route 3 did not give products in high yields.

### 3.8 Tuning of the Half-Wave Potentials

In Section 3.2.2.2, the effects of EDG and EWG on  $\beta$ -diketonates on  $E_{1/2}$  were introduced. Here the degree of such effects on the  $E_{1/2}$  of ruthenium complexes of both Series I and II was studied by CV. As discussed in Chapter 2, Section 2.3.2, a reversible process fulfils the following criteria: (a)  $i_{pa}/i_{pc}$  at unity; (b)  $\Delta E = 59/n$  mV ( $n$  = number of electron transferred per redox species); (c)  $E_p$  independent of scan rate,  $v$  and (d) linear plot of  $i_p$  vs  $v^{1/2}$  for diffusion-controlled process.<sup>64</sup> All of the complexes in Series I and II were shown to undergo a  $Ru^{2+/3+}$  redox cycle with  $\Delta E$  between 59 to 73 mV, and  $i_{pc}/i_{pa}$  at near unity to show that the complexes were both electrochemically and chemically reversible. The  $E_{1/2}$  of the complexes did not vary with  $v$  and the redox processes were diffusion-controlled as  $i_p$  vs  $v^{1/2}$  is linear. Waves were assigned by comparison to analogous metal complexes.<sup>25</sup>

#### Series I. Ruthenium Mono( $\beta$ -diketonato) Complexes, $[Ru(bpy)_2(\beta\text{-diketonato})](PF_6)$

The  $E_{1/2}$  of the ruthenium complexes in Series I,  $[Ru(\beta\text{-diketonato})(bpy)_2](PF_6)$  is demonstrated to be dependent on the substituents on the  $\beta$ -diketonate ligands. An EDG on the  $\beta$ -diketone ligand increases electron density around the metal centre by inductive effects, thereby weakening its effective nuclear charge which in turn destabilises electrons in the metal  $d$ -orbitals; this leads to a cathodic shift in  $E_{1/2}$  due to the increased ease in oxidising the metal centre. An EWG on the contrary has a stabilising effect on  $d$ -electrons which is reflected by an anodic shift in the  $E_{1/2}$ .<sup>65</sup>

**Table 3.4** Electrochemical data of  $Ru(bpy)_2(\beta\text{-diketonato})$  complexes

Complex	$E_{pa}/V$	$E_{pc}/V$	$E_{1/2}/V^*$	$\Delta E/mV$
<b>1</b>	0.351	0.281	0.228	70
<b>2</b>	0.249	0.183	0.128	66
<b>3</b>	0.303	0.237	0.181	66
<b>4</b>	0.413	0.347	0.292	66
<b>5</b>	0.324	0.254	0.201	70
<b>6</b>	0.288	0.222	0.167	66
<b>7</b>	0.317	0.247	0.194	70

\* $E_{1/2}$  vs  $Fc^{+/0}$  couple in 0.01 M  $AgNO_3$  in MeCN with 0.1 M  $NBu_4PF_6$ ,  $v = 0.1$  V  $s^{-1}$

The effects of EDG and EWG are clearly illustrated in complexes **2** and **4**. Complex **2** has an electron-donating methyl group at the methine position while an electron-withdrawing bromine occupies the same position in **4**. A cathodic shift of 100 mV is observed in **2** while **4** experiences an anodic shift of 64 mV when both are compared to the parent complex **1**.

On closer examination it can be seen that the positioning of the substituents on the  $\beta$ -diketonate ligands plays a significant role in their influence on  $E_{1/2}$ . The substituents on the terminal arms of  $\beta$ -diketone can be seen as *meta* to the metal centre whereas groups on methine position are *para* to the metal centre (Figure 3.6).

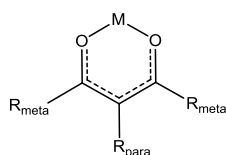


**Figure 3.6** Positions of substituents on  $\beta$ -diketonates.

Consider complexes where the *meta* positions are substituted: complex **1** with a methyl group and **5** with an isopropyl group on both ends. As the inductive effects of methyl and isopropyl groups are similar to each other, the  $E_{1/2}$  of these two complexes were predicted to be close to each other. Indeed there is only a difference of 27 mV between the two. The  $E_{1/2}$  of **5** is slightly more cathodic than **1** showing that the metal centre is slightly more electron rich.

Next, consider complexes where the *para* positions are substituted: complex **2** with a methyl group and **3** with an ethyl group. The methyl group in **2** is shown to be a stronger EDG as it shifts the  $E_{1/2}$  cathodically by 100 mV than the 47 mV by the ethyl group in **3**. A second pair of complexes, **6** and **7**, is modified with substituents which are not in direct conjugation with the  $\beta$ -diketone ring at the *para* position. The methine positions of both these complexes were substituted with benzylic groups containing a methoxy and a nitro group at their 4-position respectively. The presence of benzylic group firstly, distances the EDG and EWG *para* to the metal centre and secondly, either accentuates or diminishes the donating or withdrawing effect of such groups. Methoxy is a stronger electron donor than methyl, however the benzyl group diminished its effect

by disrupting the conjugation of methoxy to the  $\beta$ -diketone ring in **6**, hence there was only a 61 mV cathodic shift. While nitro group is a very strong electron acceptor which is expected to cause an anodic shift, the weakly donating benzyl counteracts the acceptor to result in a 34 mV cathodic shift in **7**.

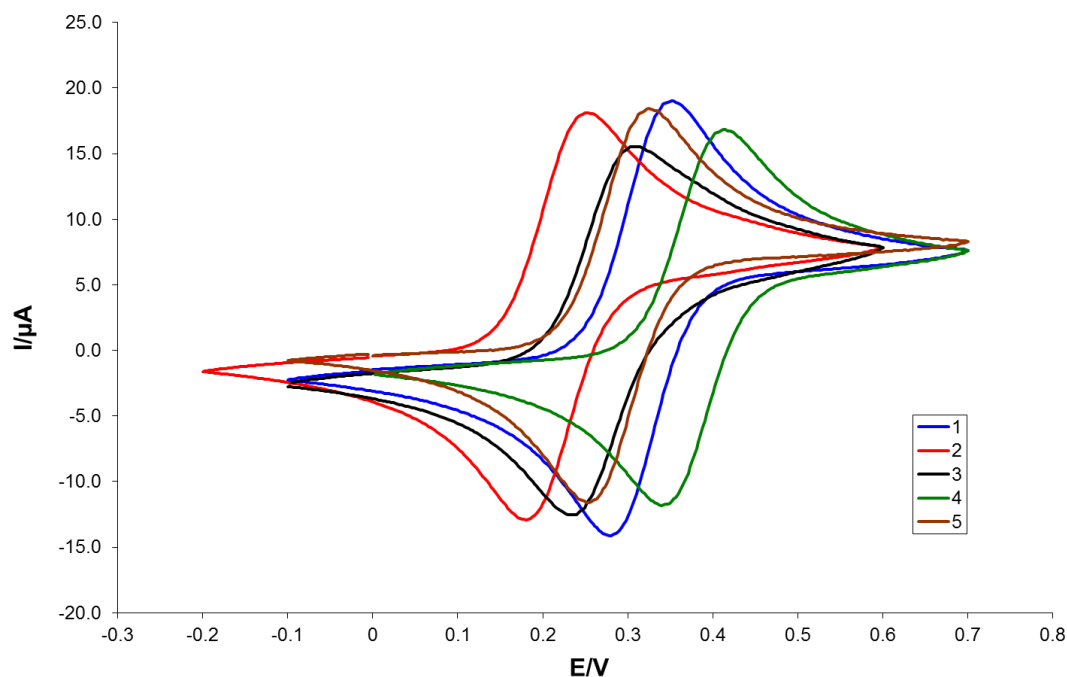


**Figure 3.7** Cyclic voltammograms of complexes **1** – **5**.

#### Series II. Ruthenium Bis( $\beta$ -diketonato) Complexes, $\text{Ru}(\beta\text{-diketonato})_2(\text{bpy})$

First, the  $E_{1/2}$  of  $\text{Ru}(\beta\text{-diketonato})_3$  (**9**, **11-14**) complexes were obtained (Table 3.5). Next, the effects of displacement of  $\beta$ -diketonates by bpy on  $E_{1/2}$  of Series II were investigated. In this series the combined effects of two  $\beta$ -diketonates are clearly manifested on the shifts in  $E_{1/2}$  going from  $\text{Ru}(\beta\text{-diketonato})_3$  complexes to  $\text{Ru}(\beta\text{-diketonato})_2(\text{bpy})$  complexes. The displacement of a  $\beta$ -diketonate in **9** by bpy to form **8** raised the  $E_{1/2}$  by 0.672 V, as bpy is a  $\pi$ -acceptor – the HOMO-LUMO gap of the complex will be increased to result in a more stabilised  $\text{Ru}^{2+}$  complex. Although all of the  $\text{Ru}(\beta\text{-diketonates})_3$  complexes have optical isomers, and **21** has geometrical isomers due to its asymmetrical ligand, no differences in electrochemical behaviour of these isomers were observed.<sup>66</sup>

**Table 3.5**  $E_{1/2}$  for selected complexes from precursors and complexes of Series II.

Ru( $\beta$ -diketonato) <sub>3</sub>	$E_{pa}/V$	$E_{pc}/V$	$E_{1/2}/V^*$	$\Delta E/V$
acac, <b>9</b>	-1.032	-1.095	-1.06	63
dbm, <b>11</b>	-0.870	-0.941	-0.906	71
NO <sub>2</sub> -acac, <b>12</b>	-0.355	-0.424	-0.389	69
Br-acac, <b>13</b>	-0.664	-0.732	-0.786	68
I-acac, <b>14</b> <sup>†</sup>	-0.693	-0.789	-0.829	96
Ru( $\beta$ -diketonato) <sub>2</sub> (bpy)	$E_{pa}/V$	$E_{pc}/V$	$E_{1/2}/V^*$	$\Delta E/V$
acac, <b>8</b>	-0.476	-0.481	-0.478	63
NO <sub>2</sub> -acac, <b>18</b>	-0.051	-0.056	-0.054	71
dbm, <b>19</b>	-0.387	-0.445	-0.416	59
tfac, <b>20</b>	-0.083	-0.090	-0.087	73
hfac, <b>21</b>	0.398	0.393	0.395	71

\* vs Ag/Ag<sup>+</sup> in 0.01 M AgNO<sub>3</sub> in MeCN using Fc<sup>+0</sup> as an internal standard with 0.1 M NBu<sub>4</sub>PF<sub>6</sub> as electrolyte,  $v = 100 \text{ mV s}^{-1}$  † in DCM

The strong electron-withdrawing nitro group on **18** led to an anodic shift of 424 mV when compared to **9**. The phenyl groups – now electron-withdrawing due to their proximity to the carbonyl groups in the ligand – were much weaker in strength in relation to the nitro group, thus the  $E_{1/2}$  of **19** was shifted anodically by just 62 mV compared to **18**. A 482 mV difference was found on comparing the  $E_{1/2}$  of **20** to **21**. This difference corresponds to the number of trifluoromethyl substituents on the ligands: there are four in **21** compared to two in **20**, and the  $E_{1/2}$  of **21** was more anodic than **20**.

### 3.8.1 Summary of the Half-wave potentials of Series I and II

Apart from the coarse tuning of potentials demonstrated by the substitution of a  $\pi$ -accepting bpy with a  $\pi$ -donating acac on the ruthenium centre, the  $E_{1/2}$  of the complexes could be finely tuned by varying the substituents on  $\beta$ -diketones. Changes in  $E_{1/2}$  arising from EDG/EWG and their positions on the  $\beta$ -diketone ligands relative to ruthenium were examined.

The  $E_{1/2}$  from Series I did not meet the desired range of potentials (-0.3 V to +0.5 V vs Ag/AgCl) as their potentials fall in the range of +0.61 to +0.73 V (vs Ag/AgCl) once conversion was applied (Fc<sup>+0</sup> vs Ag/AgCl = 0.443 V). This led to the

synthesis of Series II with lower  $E_{1/2}$  which is more suited to the application of electrochemical biosensors. The  $E_{1/2}$  of the complexes in Series II fall in the range of -0.035 V to +0.838 V (vs Ag/AgCl). Complexes **8** (-0.035 V) and **19** (+0.027 V) present themselves as suitable candidates for redox labels.

### 3.9 Diffusion Coefficient, $D_o$

Given that electrochemical processes are diffusion-controlled the values of the diffusion coefficients,  $D_o$ , of the complexes in Series I and II in acetonitrile were obtained from Randles-Sevcik equation:

$$i_p = 2.69 \times 10^5 \cdot n^{3/2} \cdot A \cdot D_o^{1/2} \cdot C \cdot v^{1/2}$$

where  $i_p$  is the current,  $n$  the number of electrons transferred,  $A$  the electrode area,  $D$  the diffusion coefficient,  $C$  the bulk concentration of redox species and  $v$  the scan rate.

The electrode area,  $A$ , on glassy carbon electrode was obtained by using the known  $D_o$  of ferrocene in acetonitrile ( $2.24 \times 10^{-5} \text{ cm}^2 \text{ s}^{-1}$ ) (Table 3.6).<sup>67</sup>

**Table 3.6** Diffusion coefficients for ruthenium complexes in Series I and II in MeCN.

	$D_o/10^{-9} \text{ m}^2 \text{ s}^{-1}$
Series I [Ru(bpy) <sub>2</sub> (β-diketonato)](PF <sub>6</sub> )	
<b>1</b>	1.7594
<b>2</b>	1.4894
<b>3</b>	1.1815
<b>4</b>	1.3303
<b>5</b>	1.5609
<b>6</b>	1.4953
<b>7</b>	1.3463
Series II Ru(β-diketonato) <sub>2</sub> (bpy)	
<b>8</b>	1.3535
<b>18</b>	0.6454
<b>19</b>	0.1003
<b>20</b>	1.7448
<b>21</b>	1.3693

Complexes with bulky ligands, and those of higher global charge, would be expected to have smaller  $D_o$  values as they would be expected to travel more slowly in

solution.<sup>66,68,69</sup> Additionally, changes in electron density around ruthenium brought on by donor/acceptor groups on  $\beta$ -diketones will affect the degree to which counterions will attach to the reduced complexes.<sup>70</sup> The structurally simplest complex in Series I, **1**, has the largest  $D_o$  while the rest of the complexes are between  $1.1815$  to  $1.5609 \times 10^{-9} \text{ m}^2 \text{ s}^{-1}$ . However, the bulkiest complex of the series did not have the smallest  $D_o$ . This can probably be attributed to the interaction between these charged complexes of Series I with acetonitrile and the supporting electrolytes.

On the contrary, more meaningful comparisons can be made in Series II where the complexes are neutral.  $D_o$  for **19** with the bulkiest ligand, dbm, is about one order of magnitude smaller than **8**, while complex **21** with two trifluoromethyl groups on each  $\beta$ -diketone ligand has a smaller  $D_o$  than **20** with only one on its ligand. **18** has a lower  $D_o$  when compared to **20** and **21**, which can possibly be attributed to its interaction with the supporting electrolyte as the nitro group, although formally neutral, has considerable polarisation between its nitrogen and oxygen atoms.

### 3.10 Relationships between the Nature of Ligands and $E_{1/2}$

Owing to the pseudo-aromaticity of ruthenium complexes described in this chapter, the EDG and EWG on  $\beta$ -diketone ligands can be assumed to influence the  $E_{1/2}$  of the complexes by inductive effects. The Hammett constant can be used to approximate or correlate the combined electronic effects of *para* and *meta* substituents on  $\beta$ -diketones with  $E_{1/2}$  on the basis that such complexes can be thought of as having similar trigonal geometries and a common redox centre, for which linear free energy relationships can be established.<sup>6,71,72</sup>

The sum of Hammett constants for  $\beta$ -diketones in a complex is:<sup>30</sup>  
 $\Sigma\sigma_{\text{pmp}} = n[\sigma_{\text{p}}(\text{R}) + \sigma_{\text{m}}(\text{R}') + \sigma_{\text{p}}(\text{R}'')]$ ,  $n$  = number of  $\beta$ -diketones in complex.

Using available Hammett constants,<sup>71</sup> the sums of Hammett constants ( $\Sigma\sigma_{\text{pmp}}$ ) for ruthenium complexes are tabulated in Table 3.7. Note that for complexes **6** and **7** the substituent constants are only an approximation using a 4-substituted phenyl ring as a model as there is no data available on 4-substituted benzyl ring. It was expected that the

increase in  $\Sigma\sigma_{\text{pmp}}$  is inversely proportional to the strength of donor character of the substituent according to the Hammett constants.

**Table 3.7** Sums of the Hammett constants,  $\Sigma\sigma_{\text{pmp}}$ , for the ruthenium complexes.

	$\sigma_{\text{p}}(\text{R})$	$\sigma_{\text{m}}(\text{R}')$	$\sigma_{\text{p}}(\text{R}'')$	$\Sigma\sigma_{\text{pmp}}$
Series I [Ru(bpy) <sub>2</sub> ( $\beta$ -diketonato)](PF <sub>6</sub> )				
<b>1</b>	-0.07	0	-0.07	-0.14
<b>2</b>	-0.07	-0.17	-0.07	-0.31
<b>3</b>	-0.07	-0.15	-0.07	-0.29
<b>4</b>	-0.07	0.23	-0.07	0.09
<b>5</b>	-0.06	0	-0.06	-0.12
<b>6</b>	-0.07	-0.08*	-0.07	-0.22
<b>7</b>	-0.07	0.26*	-0.07	0.12
Ru( $\beta$ -diketonato) <sub>3</sub>				
<b>9</b>	-0.07	0	-0.07	-0.42
<b>11</b>	0.06	0	0.06	0.36
<b>12</b>	-0.07	0.78	-0.07	1.92
<b>13</b>	-0.07	0.23	-0.07	0.27
<b>14</b>	-0.07	0.18	-0.07	0.12
Series II Ru( $\beta$ -diketonato) <sub>2</sub> (bpy)				
<b>8</b>	-0.07	0	-0.07	-0.28
<b>18</b>	-0.07	0.78	-0.07	1.28
<b>19</b>	0.06	0	0.06	0.24
<b>20</b>	0.43	0	-0.07	0.72
<b>21</b>	0.43	0	0.43	1.72

\* approximation

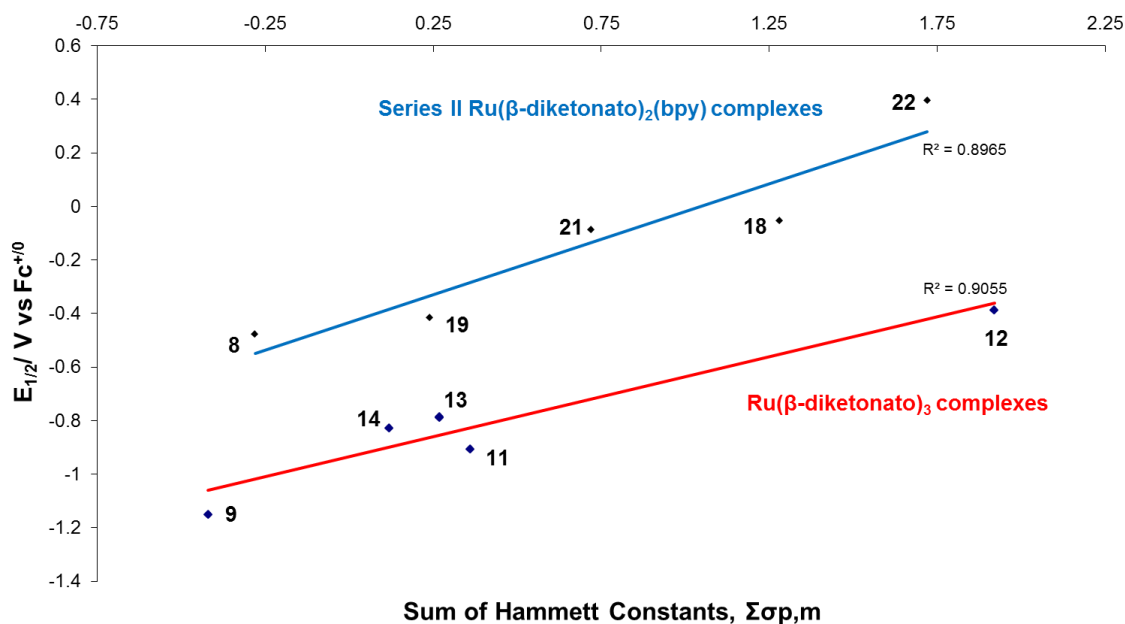


**Figure 3.8**  $E_{1/2}$  vs the sum of the Hammett constants ( $\Sigma\sigma_{pmp}$ ) of  $Ru(\beta\text{-diketonato})_2(\text{bpy})$  (8, 18-21) and  $Ru(\beta\text{-diketonato})_3$  (9, 10-14) complexes.

No linear relationship can be established between  $\Sigma\sigma_{pmp}$  and  $E_{1/2}$  in Series I but a reasonably linear relationship can be found for Series II and  $Ru(\beta\text{-diketonato})_3$  complexes (Figure 3.8). The more acac there is around the metal centre, the more linear the relationship (see  $R^2$  value in Figure 3.8). This is to be expected given that the correlation between  $\Sigma\sigma_{p,m}$  and  $E_{1/2}$  comes entirely from substituents on  $\beta$ -diketones with zero contribution from the unsubstituted bpy in the complex.

A more systematic approach to probing the relationship between the structural and electronic features of a complex and its  $E_{1/2}$  is to consider the additive effects of ligands on the metal centre.<sup>73</sup> Out of the additive models proposed, the ligand electrochemical parameter,  $E_L(L)$ , developed by Lever based on an  $Ru^{2+/3+}$  redox couple, has been most widely applied to examine the correlation between ligands and  $E_{1/2}$  of metal complexes.<sup>74</sup>

A metal-centred redox process in a complex which is electrochemically reversible involves electrons in nonbonding or weakly  $\pi$ -bonding (or anti-bonding)  $t_{2g}$  subsets, and the overall effects of ligands on  $E_{1/2}$  are additive with respect to ligand

variation.<sup>74</sup> For a metal (M) complex with the formula of  $M X_x Y_y Z_z$ ,  $E_L(L)$  is defined as:

$$\Sigma E_{(L)} = x E_L(X) + y E_L(Y) + z E_L(Z)$$

which can be used to predict  $E_{1/2}$  of complexes with an octahedral geometry.<sup>74</sup>

The oxidation potentials of the complexes and  $\Sigma E_{(L)}$  are computed as listed in Table 3.8 along with the  $E_{pc}$ . Apart from a few ligands where values of  $E_{(L)}(L)$  are unavailable, a reasonably linear correlation can be established between  $E_{(L)}(L)$  and  $E_{pc}$  of the complexes of both Series I and II and precursors, suggesting that the ligand contributions are additive. This is in line with reports that  $E_{(L)}(L)$  is a good predictor of  $E_{1/2}$  of metal complexes where applicable. However the limited range of parameters may be preventing this method from widespread adoption in comparison to Hammett constants.

**Table 3.8** Data of  $\Sigma E_{(L)}$  of selected complexes and their  $E_{pc}$  (vs NHE)

	$E_{pc}/V^{\square}$	$\Sigma E_{(L)}/V^{\square}$
Series I [Ru(bpy) <sub>2</sub> (β-diketonato)](PF <sub>6</sub> )		
<b>1</b>	-0.349	0.438
<b>2</b>	-0.447	0.408
<b>4</b>	-0.283	0.488
<b>5</b>	-0.376	0.388
Ru(β-diketonato) <sub>3</sub>		
<b>9</b>	-1.725	-0.24
<b>11</b>	-0.906	0.36
<b>13</b>	-1.326	-0.09
<b>14</b> <sup>†</sup>	-1.323	-0.09
Series II Ru(β-diketonato) <sub>2</sub> (bpy)		
<b>8</b>	-1.111	0.099
<b>19</b>	-1.075	0.179
<b>20</b>	-0.720	0.319
<b>21</b>	-0.237	0.599

<sup>†</sup> in DCM

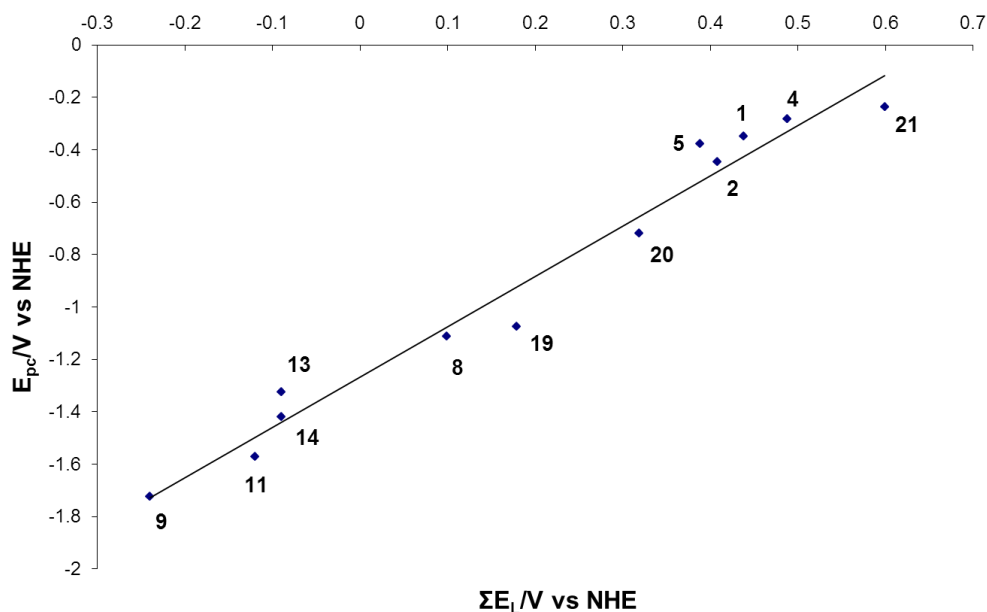


**Figure 3.9**  $\Sigma E_{(L)}$  vs  $E_{pc}$  of selected complexes.

### 3.11 Correlation between UV-Vis Absorbance and $E_{1/2}$

The lowest energy absorption band for ruthenium bpy complexes in the absorbance spectra typically arises from MLCT where the HOMO consists of a ruthenium  $d$ -orbital and the LUMO is a  $\pi^*$ -orbital of the bpy (a  $\pi$ -acceptor ligand); the  $d\pi \rightarrow \pi^*$  transition shows up as the most intense band due to extensive mixing of  $d\pi$  and  $\pi^*$  orbitals.<sup>59,75,76</sup> In contrast,  $d\sigma$  and  $d\delta \rightarrow \pi^*$  bands are usually extremely weak because of the poor overlap between ground state,  $d\sigma$  orbital, and excited state,  $\pi^*$ -orbitals, of the complexes.<sup>59</sup> Hence, there are both weak and strong charge transfer transitions in ruthenium complexes with  $\pi$ -acceptor ligands. The  $\pi$ -donating  $\beta$ -diketone ligands will however stabilise a ruthenium excited state leading to a lower energy shift of MLCT transitions.<sup>77,78</sup> Also in play are the electronic influences of the substituents on these ligands where an EDG will lead to a bathochromic shift and the opposite for an EWG.<sup>79</sup>

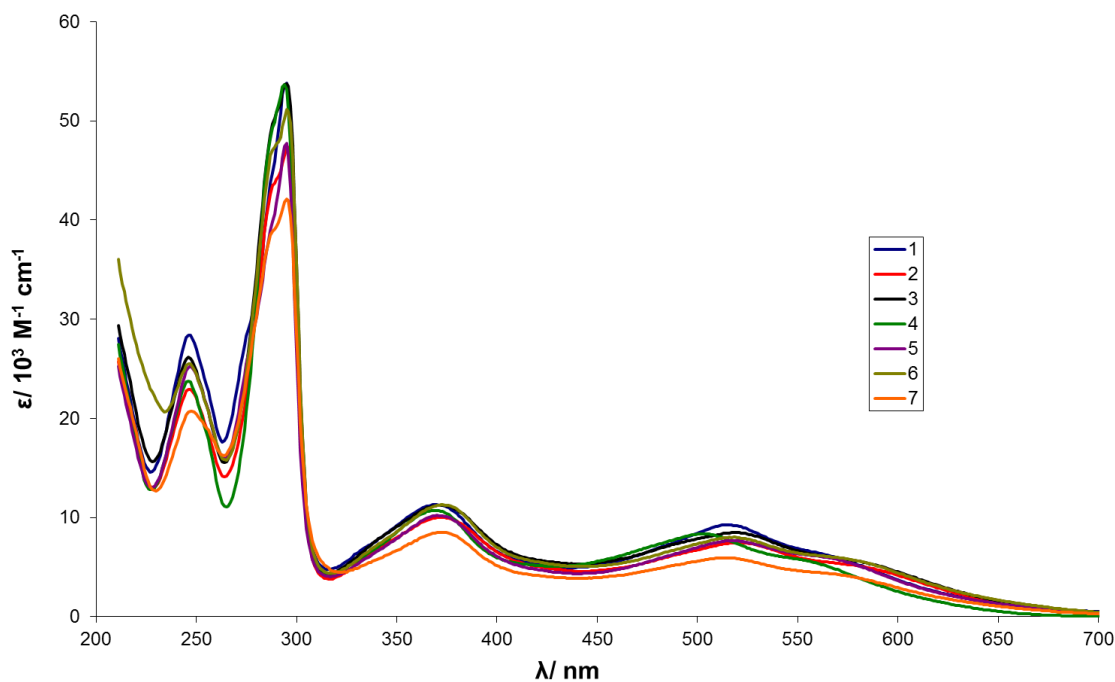
The electronic spectra of the complexes in Series I recorded in MeCN (0.05 mM) are shown in Figure 3.10, with the data presented in Table 3.9. The absorbance peaks of these complexes are very similar to each other due to the presence of a single  $\beta$ -diketone exerting its influence on their electronic character. The broadness of visible

absorbance bands is a result of the interactions between the  $d$ -orbitals on ruthenium and the  $\pi$ ,  $\pi^*$  orbitals on bpy, the MLCT transitions of which are similar in energy influenced by the vibrational modes of the complex.<sup>7,9,80</sup> Also, shoulder absorptions can be observed in the region of 500 nm, which could probably be assigned to  $\beta$ -diketonates after comparison to similar complexes.<sup>77</sup> In total, there are two strong absorption bands assigned to  $\pi \rightarrow \pi^*$  intraligand transitions in the UV region and three MLCT bands  $d\pi$  ( $\text{Ru}^{2+}$ )  $\rightarrow \pi^*$  (L) (L = bpy,  $\beta$ -diketone) in the visible region which concur with the reported UV-Vis spectra of similar  $\text{Ru}^{2+}$ -bipyridine complexes.<sup>25,51,81</sup>

The smaller the HOMO-LUMO gap, the longer the wavelength of the absorption maximum will be, and less energy is needed to oxidise the metal.<sup>65</sup> Looking at the  $E_{1/2}$  of Series I, the increased ease of oxidation follows the trend of  $\mathbf{4} < \mathbf{1} < \mathbf{5} < \mathbf{7} < \mathbf{3} < \mathbf{2} < \mathbf{6}$  (see Table 3.4). It can be concluded that **4** requires slightly higher energy to oxidise which is confirmed by its slight hypsochromic shift in the MLCT bands compared to **1**. The greater stability found in **4** is due to the increase in  $\text{Ru}^{2+}$  to bpy back-bonding. This mirrored the trend of  $E_{1/2}$  values of these complexes.

**Table 3.9** Absorption maxima,  $\lambda_{\text{max}}$ , and molar extinction coefficient,  $\epsilon$  in Series I.

Complex	$\lambda / \text{nm}$ ( $\epsilon / 10^3 \text{ M}^{-1} \text{ cm}^{-1}$ )
<b>1</b>	247 (28.4), 295 (53.8), 369 (11.3), 515 (9.3), 568sh(6.1)
<b>2</b>	247 (22.9), 296 (46.5), 374 (10), 521 (7.5), 586sh (5.1)
<b>3</b>	247 (26.0), 295 (5.9), 373 (11.2), 519 (10.4), 580sh (5.6)
<b>4</b>	246 (23.8), 294 (53.6), 370 (10.7), 504 (8.3), 558sh (5.5)
<b>5</b>	247 (25.2), 295 (47.8), 370 (10.2), 516 (7.7), 574sh (5.5)
<b>6</b>	246 (25.5), 295 (51.1), 376 (11.2), 518 (8.0), 577sh (5.7)
<b>7</b>	247 (20.7), 295 (42.1), 373 (8.5), 512 (5.9), 575sh (4.1)

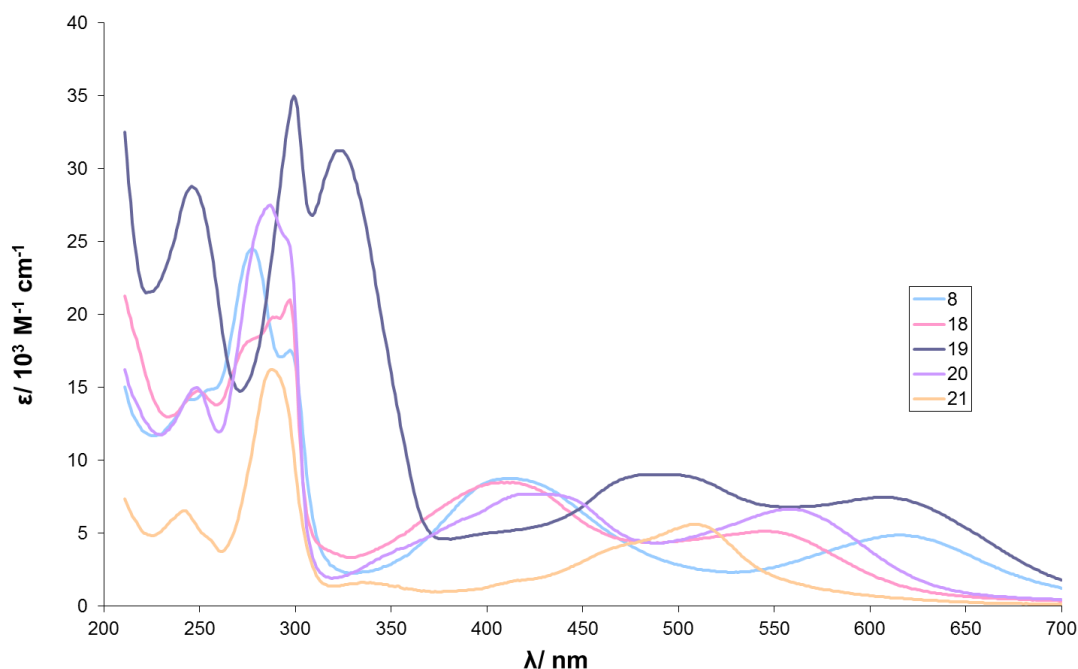


**Figure 3.10** UV-Vis absorbance spectra for complexes in Series I.

Separately, the ease of oxidation of the complexes in Series II is observed to increase from **8** < **19** < **18** < **20** < **21** (see Table 3.5). As **21** has four strongly electron-withdrawing trifluoromethyl groups on its two  $\beta$ -diketone ligands, its absorption maximum should experience a hypsochromic shift. However, it only has only one visible band at lower absorption intensity, which is probably due to its strong electron-withdrawing effect around the metal centre which greatly reduces the MLCT character of the  $d\pi$  ( $\text{Ru}^{2+}$ )  $\rightarrow \pi^*$  (bpy) transition. The distortion of the band around 300 nm for **18** in which no clear maximum was noticeable, can be attributed to an overlap of nitro group absorption onto the  $t_{2g} \rightarrow \pi^*$  (MLCT) band.<sup>8282</sup> Owing to the presence of two phenyl groups on the dbm ligand, not only are the absorptions for **19** hyperchromically shifted, there is also a degree of overlapping in the  $\pi \rightarrow \pi^*$  intraligand transitions of bpy and phenyl on dbm in the region of 300 nm, to give a broad band.

**Table 3.10** Absorption maxima,  $\lambda_{\text{max}}$ , and molar extinction coefficient,  $\epsilon$  in Series II.

Complex	$\lambda / \text{nm}$ ( $\epsilon / 10^3 \text{ M}^{-1} \text{ cm}^{-1}$ )
<b>8</b>	277sh (24.5), 297 (17.5), 411 (8.8), 617 (4.9)
<b>18</b>	249 (14.8), 287 (19.7), 297 (21.0), 408 (8.5), 546 (5.14)
<b>19</b>	246 (28.8), 300 (34.8), 323 (31.2), 485 (9.0), 608 (7.5)
<b>20</b>	248 (15.0), 287sh (27.5), 294 (25.4), 425 (7.7), 559 (6.7)
<b>21</b>	243 (6.5), 289 (16.2), 337 (1.6), 509 (5.6)

**Figure 3.11** UV-Vis absorbance spectra for complexes in Series II.

### 3.12 Summary

In this chapter, ruthenium complexes bearing bpy and  $\beta$ -diketonato ligands were prepared and examined chiefly in terms of their electrochemical behaviour. Two series of ruthenium complexes, Series I (**1** – **7**) of the general formula  $[\text{Ru}(\text{bpy})_2(\beta\text{-diketonato})](\text{PF}_6)$  and Series II (**8**, **18** – **21**) of the general formula  $\text{Ru}(\beta\text{-diketonato})_2(\text{bpy})$  were prepared.

The  $E_{1/2}$  of the complexes was influenced by the substituents on  $\beta$ -diketonato ligand. Complexes in Series II  $\text{Ru}(\beta\text{-diketonato})_2(\text{bpy})$  experienced larger shifts in  $E_{1/2}$  due to a larger number of substituents on  $\beta$ -diketone ligands influencing the electronic character of the ruthenium centre. Correlations between  $E_{1/2}$  and the donor properties of

these substituents were made: EDG shifted the  $E_{1/2}$  cathodically whereas EWG shifted the  $E_{1/2}$  anodically. By varying the substituents on the  $\beta$ -diketone ligand the  $E_{1/2}$  of the complexes could be finely modulated. More correlations were made between  $E_{1/2}$  of complexes with the Hammett constant ( $\Sigma\sigma_{\text{pmp}}$ ), the ligand electrochemical parameter ( $\Sigma E_{(\text{L})}$ ) and UV-Vis absorbance. The Hammett constant gave a reasonably linear relationship between  $E_{1/2}$  of Series II and  $\text{Ru}(\beta\text{-diketonato})_3$  complexes while the ligand electrochemical parameter was shown to have a linear relationship with  $E_{1/2}$  for all of Series I and II and  $\text{Ru}(\beta\text{-diketonato})_3$ . The bathochromic shifts of MLCT band of Series I complexes compared with parent complex 1, and the hypsochromic shifts of Series II complexes compared with parent 8, can both be correlated with the measured  $E_{1/2}$  values.

Out of the complexes prepared, the  $E_{1/2}$  of **8** and **19** at -0.035 V and +0.027 V (vs Ag/AgCl) respectively, present themselves as suitable candidates to be used for redox labels in electrochemical sensors, as their  $E_{1/2}$  are within the desired range (-0.3 V to +0.5 V vs Ag/AgCl). These two complexes were chosen to be immobilised on gold electrodes, as described in the next chapter.

### 3.13 References

- (1) Prins, R.; Korwagen, A. R.; Kortbeek, A. G. T. G. *J. Organometal. Chem.* **1972**, *39*, 335.
- (2) Kraatz, H.-B. *J. Organometal. Chem.* **1999**, *579*, 222.
- (3) Ge, D.; Levicky, R. *Chem. Commun.* **2010**, *46*, 7190.
- (4) Venturi, M.; Credi, A.; Balzani, V. *Coord. Chem. Rev.* **1999**, *185-186*, 233.
- (5) Juris, A.; Balzani, V. *Coord. Chem. Rev.* **1988**, *84*, 85.
- (6) Patterson, G. S.; Holm, R. H. *Inorg. Chem.* **1972**, *11*, 2285.
- (7) Staniewicz, R.; Hendricker, D. G. *J. Am. Chem. Soc.* **1977**, *99*, 6581.
- (8) Bennett, M. A.; Byrnes, M. J.; Kováčik, I. *J. Organometal. Chem.* **2004**, *689*, 4463.
- (9) Sullivan, B. P.; Salmon, D. J.; Meyer, T. J. *Inorg. Chem.* **1978**, *17*, 3334.
- (10) Haga, M.; Matsumura-Inoue, T.; Shimizu, K.; Satô, G. P. *J. Chem. Soc. Dalton Trans.* **1989**, 371.
- (11) Reddy, K. B.; Cho, M. P.; Wishart, J. F.; Emge, T. J.; Isied, S. S. *Inorg. Chem.* **1996**, *35*, 7241.
- (12) Nayak, A.; Patra, S.; Sarkar, B.; Ghumaan, S.; Puranik, V. G.; Kaim, W.; Lahiri, G. K. *Polyhedron* **2005**, *24*, 333.
- (13) Weizman, H.; Tor, Y. *J. Am. Chem. Soc.* **2002**, *124*, 1568.
- (14) Kaes, C.; Katz, A.; Hosseini, M. W. *Chem. Rev.* **2000**, *100*, 3553.
- (15) Drexler, E. J.; Field, J. W. *J. Chem. Educ.* **1976**, *53*, 392.
- (16) Aromí, G.; Gamez, P.; Reedijk, J. *Coord. Chem. Rev.* **2008**, *252*, 964.

- (17) Vigato, P. A.; Peruzzo, V.; Tamburini, S. *Coord. Chem. Rev.* **2009**, 253, 1099.
- (18) Skopenko, V. V.; Amirkhanov, V. M.; Sliva, T. Y.; Vasilchenko, I. S.; Anpilova, E. L.; Garnovskii, A. D. *Russ. Chem. Rev.* **2004**, 73, 737.
- (19) Bray, D. J.; Clegg, J. K.; Lindoy, L. F.; Schilter, D. *Adv. Inorg. Chem.* **2007**, 59, 1.
- (20) Tanaka, M.; Shono, T.; Shinra, K. *Bull. Chem. Soc. Jpn.* **1969**, 42, 3190.
- (21) Schweitzer, G. K.; Benson, E. W. *J. Chem. Eng. Data.* **1968**, 13, 452.
- (22) Mehrvar, M.; Abdi, M. *Analytical Sciences* **2004**, 20, 1113.
- (23) Jana, U.; Biswas, S.; Maiti, S. *Tetrahedron Lett.* **2007**, 48, 4065.
- (24) Terent'ev, A. O.; Borisov, D. A.; Yaramenko, I. A.; Chernyshev, V. V.; Nikishin, G. I. *J. Org. Chem.* **2010**, 75, 5065.
- (25) El-Hendawy, A. M.; Al-Kubaisi, A. H.; Al-Madfa, H. A. *Polyhedron* **1997**, 16, 3039.
- (26) Munery, S.; Jaud, J.; Bonvoisin, J. *Inorg. Chem. Commun.* **2008**, 11, 975.
- (27) Knowles, T. S.; Howells, M. E.; Howlin, B. J.; Smith, G. W.; Amodio, C. A. *Polyhedron* **1994**, 13, 2197.
- (28) Krause, R. A. *Inorg. Chim. Acta* **1977**, 22, 209.
- (29) Powell, P. *J. Organometal. Chem.* **1974**, 65, 89.
- (30) Endo, A.; Kajitani, M.; Mukaida, S.; Shimizu, K.; Satô, G. P. *Inorg. Chim. Acta* **1988**, 150, 25.
- (31) Collman, J. P.; Young, W. L. I. *Inorg. Synth.* **1963**, VII, 205.
- (32) Endo, A.; Shimizu, K.; Satô, G. P. *Chem. Lett.* **1985**, 1985, 581.
- (33) Kobayashi, T.; Nishina, Y.; Shimizu, K.; Satô, G. P. *Chem. Lett.* **1988**, 1137.
- (34) Wang, P.; Miller, J. E.; Henling, L. M.; Stern, C. L.; Frank, N. L.; Eckermann, A. L.; Meade, T. J. *Inorg. Chem.* **2007**, 46, 9853.
- (35) Gupta, A. K.; Poddar, R. K. *Indian J. Chem.* **2000**, 39A, 457.
- (36) Allard, M. M.; Odongo, O. S.; Lee, M. M.; Chen, Y.; Endicott, J. F.; Schlegel, H. B. *Inorg. Chem.* **2010**, 49, 6840.
- (37) Šmejkal, T.; Breit, B. *Organometallics* **2007**, 26, 2461.
- (38) Bennett, M. A.; Chung, G.; Hockless, D. C. R.; Neumann, H.; Willis, A. C. *J. Chem. Soc. Dalton Trans.* **1999**, 3451.
- (39) da Cunha, C. J.; Fielder, S. S.; Stynes, D. V.; Masui, H.; Auburn, P. R.; Lever, A. B. P. *Inorg. Chim. Acta* **1996**, 242, 293.
- (40) Bryant, G. M.; Fergusson, J. E. *Aust. J. Chem.* **1971**, 24, 441.
- (41) Olivier, J.-H.; Harrowfield, J.; Ziessel, R. *Chem. Commun.* **2011**, 47, 11179.
- (42) Collman, J. P. *Angew. Chem. Int. Ed.* **1965**, 4, 132.
- (43) Collman, J. P.; Moss, R. A.; Maltz, H.; Heindel, C. C. *J. Am. Chem. Soc.* **1961**, 83, 531.
- (44) Kluiber, R. W. *J. Am. Chem. Soc.* **1960**, 82, 4839.
- (45) Singh, P. R.; Sahai, R. *Aust. J. Chem.* **1967**, 20, 639.
- (46) Singh, P. R.; Sahai, R. *Aust. J. Chem.* **1967**, 20, 649.
- (47) Collman, J. P.; Marshall, R. L.; Young, W. L. I.; Goldby, S. D. *Inorg. Chem.* **1962**, 1, 704.
- (48) Svistunova, I. V.; Shapkin, N. P.; Nikolaeva, O. V. *Russ. J. Gen. Chem.* **2005**, 75, 335.
- (49) Collman, J. P.; Marshall, R. L.; Young, W. L. I.; Sears, C. T. J. *J. Org. Chem.* **1963**, 28, 1449.
- (50) Baird, I. R.; Rettig, S. J.; James, B. R.; Skov, K. A. *Can. J. Chem.* **1999**, 77, 1821.

- (51) Wu, A.; Masland, J.; Swartz, R. D.; Kaminsky, W.; Mayer, J. M. *Inorg. Chem.* **2007**, *46*, 11190.
- (52) Gordon, J. G. I.; O'Connor, M. J.; Holm, R. H. *Inorg. Chim. Acta* **1971**, *5*, 381.
- (53) Johnson, A.; Everett, G. W., Jr. *J. Am. Chem. Soc.* **1972**, *94*, 1419.
- (54) Drago, R. S.; Zink, J. I.; Richman, R. M.; Perry, W. D. *J. Chem. Ed.* **1974**, *51*, 371.
- (55) Eaton, D. R. *J. Am. Chem. Soc.* **1965**, *87*, 3097.
- (56) Koiwa, T.; Masuda, Y.; Shono, J.; Kawamoto, Y.; Hoshino, Y.; Hashimoto, T.; Natarajan, K.; Shimizu, K. *Inorg. Chem.* **2004**, *43*, 6215.
- (57) Bennett, M. A.; Byrnes, M. J.; Willis, A. C. *Organometallics* **2003**, *22*, 1018.
- (58) Kar, S.; Chanda, N.; Mobin, S. M.; Urbanos, F. A.; Neimeyer, M.; Puranik, V. G.; Jimenez-Aparicio, R.; Lahiri, G. K. *Inorg. Chem.* **2005**, *44*, 1571.
- (59) Kalinina, D.; Dares, C.; Kaluarachchi, H.; Potvin, P. G.; Lever, A. B. P. *Inorg. Chem.* **2008**, *47*, 10110.
- (60) McKinnon, S. D. J.; Patrick, B. O.; Lever, A. B. P.; Hicks, R. G. *J. Am. Chem. Soc.* **2011**, *133*, 13587.
- (61) Ernst, R. D.; Melendez, E.; Stahl, L.; Ziegler, M. L. *Organometallics* **1991**, *10*, 3635.
- (62) Grünwald, C.; Laubender, M.; Wolf, J.; Werner, H. *J. Chem. Soc. Dalton Trans.* **1998**, 833.
- (63) Meléndez, E.; Ilarraza, R.; Yap, G. P. A.; Rheingold, A. L. *J. Organometal. Chem.* **1996**, *522*, 1.
- (64) Zanello, P. *Inorganic Electrochemistry: Theory, Practice and Applications*; The Royal Society of Chemistry: Cambridge, 2003.
- (65) Eskelinen, E.; Haukka, M.; Kinnunen, T.-J. J.; Pakkanen, T. A. *J. Electroanal. Chem.* **2003**, *556*, 103.
- (66) Endo, A.; Hoshino, Y.; Hirakata, K.; Takeuchi, Y.; Shimizu, K.; Furushima, Y.; Ikeuchi, H.; Satô, G. P. *Bull. Chem. Soc. Jpn.* **1989**, *62*, 709.
- (67) Tsierkezos, N. G. *J. Solution Chem.* **2007**, *36*, 289.
- (68) Fraser, D. M.; Zakeeruddin, S. M.; Grätzel, M. *J. Electroanal. Chem.* **1993**, *359*, 125.
- (69) Ikeuchi, H.; Naganuma, K.; Ichikawa, M.; Ozawa, H.; Ino, T.; Sato, M.; Yonezawa, H.; Mukaida, S.; Yamamoto, A.; Hashimoto, T. *J. Solution Chem.* **2007**, *36*, 1243.
- (70) Endo, A. *Bull. Chem. Soc. Jpn.* **1983**, *56*, 2733.
- (71) Hansch, C.; Leo, A.; Taft, R. W. *Chem. Rev.* **1991**, *91*, 165.
- (72) Slattery, S. J.; Bare, W. D.; Jameson, D. L.; Goldsby, K. A. *J. Chem. Soc. Dalton Trans.* **1999**, 1999, 1347.
- (73) Pombeiro, A. J. L. *Eur. J. Inorg. Chem.* **2007**, 1473.
- (74) Lever, A. B. P. *Inorg. Chem.* **1990**, *29*, 1271.
- (75) Kinnunen, T.-J. J.; Haukka, M.; Pesonen, E.; Pakkanen, T. A. *J. Organometal. Chem.* **2002**, *655*, 31.
- (76) Goreslsky, S. I.; Dodsworth, E. S.; Lever, A. B. P.; Vlcek, A. A. *Coord. Chem. Rev.* **1998**, *174*, 469.
- (77) Takahashi, Y.; Arakawa, H.; Sugihara, H.; Hara, K.; Islam, A.; Katoh, R.; Tachibana, Y.; Yanagida, M. *Inorg. Chim. Acta* **2000**, *310*, 169.
- (78) Doveloglou, A.; Adeyemi, S. A.; Meyer, T. J. *Inorg. Chem.* **1996**, *35*, 4120.
- (79) Brooks, S. C.; Vinyard, D. J.; Richter, M. M. *Inorg. Chim. Acta* **2006**, *359*, 4635.

- (80) Brown, G. M.; Weaver, T. R.; Keene, F. R.; Meyer, T. J. *Inorg. Chem.* **1976**, *15*, 190.
- (81) Bryant, G. M.; Fergusson, J. E.; Powell, H. K. J. *Aust. J. Chem.* **1971**, *24*, 257.
- (82) Kuroda, K.; Yoshitani, K.; Kunigita, K.; Kamiiba, Y.; Watanabe, K. *Bull. Chem. Soc. Jpn.* **1976**, *49*, 2445.

## *Chapter 4*

# *Evaluation of a Ruthenium-based Redox Label on a Sensing Surface*

## 4.1 The Monitoring of Blood Glucose Level

The prevalence of Type 2 diabetes in the general population has been rising steadily in the past few decades because of a shift to sedentary lifestyle and poor diets. The complications associated with diabetes are severe, including higher risks of cardiovascular disease, kidney failure and blindness. Stringent disease management, i.e., daily monitoring of blood glucose level, is crucial as a preventative measure against complications arising from this chronic illness. In fact, this monitoring requirement prompted the development of the first biosensors – the glucose biosensors, which now account for about 85% share of the entire biosensor market.<sup>1</sup> As well as the daily monitoring of blood glucose level, the monitoring of Hb1Ac, a diabetes marker protein, provides information on the average blood glucose level over the preceding two to three months to give an indication on the effectiveness of treatment regimes.<sup>2</sup> A number of strategies, such as cation exchange, gel electrophoresis, affinity chromatography, colorimetric, spectroscopic and mass spectroscopic measurements have been developed in an effort to monitor Hb1Ac but they suffer from setbacks, e.g., technical complexity, high cost, long detection time and false positives to varying degrees.<sup>2</sup> Gooding *et al.* turned to the electrochemical detection of Hb1Ac monoclonal antibody using *N*-glycosylated –VHLTP (GPP), an Hb1Ac epitope, with encouraging results.<sup>2-4</sup> In this chapter, a surface-bound ruthenium-based redox label will be first studied electrochemically then evaluated based on the voltammetry responses to the Hb1Ac antibody.

## 4.2 Voltammetry Responses Generated by Redox Label upon Target Binding

A reagentless biosensor is preferable for the general user because of its simplicity, i.e., the user needs only to expose the sensing surface to a sample for the detection of target analytes. Electrochemical biosensors require signal outputs generated by redox-active molecules – if the analyte itself is redox-active, this property can be exploited for this purpose; for redox-inactive analytes, a redox-active species or reaction product has to be present in the sensing system to relay the electrochemical signal upon target binding. In the case where a redox label is bound to a bioreceptor, the binding

event is reported through a change in the electrochemical signal given off by the label, which originates from the changes in the microenvironment around the label. These changes are related to the thermodynamics and kinetics of electron-transfer of the label, which are manifested in its voltammetry response in the form of a potential shift and/or change in the magnitude of the current.<sup>5</sup>

The magnitude of voltammetry responses generally depends on the proximity of the bioreceptor to the redox label and the charge density of the target ions if it is of significance, alongside detection conditions such as supporting electrolytes and solvent.<sup>6</sup> The positioning of redox labels relative to the rest of the assembly on a sensing surface is of importance: the flexibility displayed by redox labels in their covalent binding to bioreceptors has been shown to contribute to electron transfer between sterically incompatible sites<sup>7</sup> while redox labels immobilised on shorter chain thiol SAMs were reported to improve binding efficiency with target analytes and minimise signal.<sup>8</sup>

Ferrocene-based metal-ion receptors are reported to have their redox potentials shifted anodically as a result of the binding of cations making the oxidation of ferrocene more difficult<sup>6</sup> while several protein biosensors have been shown to give a the potential shift and/or decrease in current intensity due to the formation of protein films or immunocomplex close to the redox labels when the target analytes are present.<sup>2,4,9,10</sup> For example, Mahmoud and Kraatz conjugated a peptide recognition sequence to ferrocene, which was in turn anchored onto a gold surface by a thioctic acid linkage with the view that a surface-bound redox probe will be unaffected by diffusive processes due to its close proximity to the electrode.<sup>10</sup> The formal potential of the ferrocene probe was shifted anodically with the increasing binding of protein to the peptide, until a plateau was reached. The plateau suggests that the surface had become saturated with the protein. A slight decrease in the overall signal intensity was noted, which was attributed to the likelihood that the supporting electrolyte has failed to reach the ferrocene label efficiently.

In short, binding-induced structural changes of the bioreceptors can affect the electron transfer properties of the redox labels, which are measurable in the form of

potential shifts and/or change in current intensity to indicate the presence of target analytes.<sup>11</sup>

#### 4.2.1 Surface-Bound Redox Labels

Previously discussed in Chapter 1, Section 1.9, the formation of SAMs on gold electrodes provide better control over molecular orientation, surface reproducibility and durability in the fabrication of sensing surfaces. There are two ways in which surface-bound redox labels can be anchored onto a sensing surface: pre-synthesised redox-active SAMs and immobilisation of the redox label onto a preformed SAM.<sup>12</sup> The challenges associated with pre-synthesising ruthenium-containing SAMs before immobilisation make this method an unfavourable one for this application. Hence, the more straightforward strategy of direct immobilisation of redox labels onto SAMs is adopted. This step-wise approach proceeds by firstly, the functionalisation of coordinating ligand on the redox label; secondly, the covalent binding of redox labels onto SAMs and finally, the covalent binding of bioreceptors onto the redox labels to complete the fabrication of the sensing interface.

The choice of SAM depends largely on the requirement of the sensing systems. SAMs formed by longer chain thiols are more stable due to higher degree of van der Waals interactions, consequently a wider potential window can be obtained.<sup>13</sup> Nonetheless, the redox label, now further away from the transducer, suffers from a lower rates of electron transfer, therefore a reduction in current is observed.<sup>13</sup> In order to strike a balance between electron transfer rate and the stability of SAMs, two different organosulfur compounds, both of six-carbon chain length, 6-mercaptohexanoic acid (MHA) and thioctic acid (TA) were chosen to form SAMs on gold electrodes (Figure 4.1).

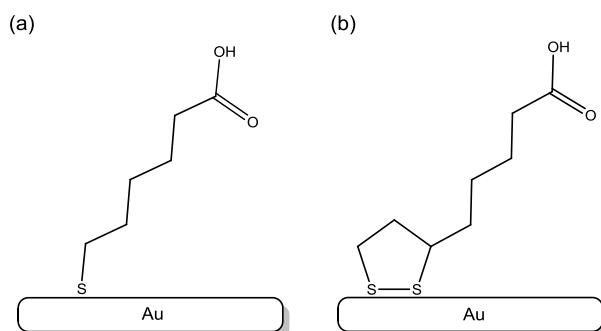


**Figure 4.1** (a) MHA- and (b) TA-modified gold electrodes.

A number of immobilisation techniques such as carbodiimide coupling, “click” chemistry, Diels-Alder reactions and acetylenic coupling are available to immobilise redox species on SAMs.<sup>12,14,15</sup> To facilitate covalent binding to the carboxyl-terminated SAMs, the coordinating ligand on the redox label needs to be functionalised with pendant amine groups. The binding between a carboxyl terminus on a SAM and a primary amine group can then be achieved using carbodiimide coupling.<sup>16,17</sup> In this thesis, the coordinating ligand chosen to be functionalised with the primary amine groups is 2,2'-bipyridyl (bpy) on the ruthenium complex. There are several positions where these groups can be introduced on bpy (Figure 4.2). The 6,6'-position is not advisable because the amines, together with the nitrogen donors on the bpy can form a tetradentate ligand.<sup>18</sup> The 4,4'-position is deemed the most suitable because of the relative ease of substitution at this position and that the substituents at these positions are the least sterically demanding.<sup>19,20</sup> Ligand 4,4'-bis(aminomethyl)-2,2'-bipyridine (bpy-NH<sub>2</sub>) on ruthenium will be used as homobifunctional linker where one of the amine groups will act as an anchor to allow attachment of the redox label onto SAMs and the other for the covalent binding of a bioreceptor.

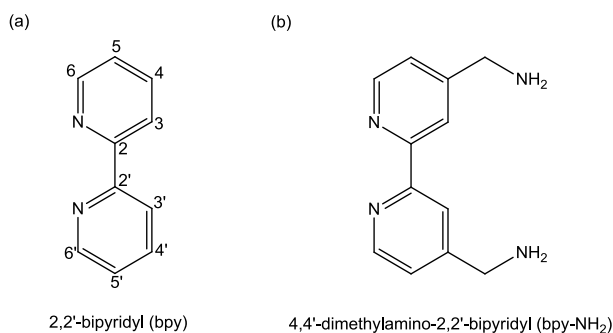


**Figure 4.2** Structures of (a) bpy and (b) bpy-NH<sub>2</sub>.

Of all the ruthenium complexes prepared in Chapter 3, there were two which suit the potential windows (-0.3 V to + 0.5 V *vs* Ag/AgCl) for sensing applications, namely Ru(acac)<sub>2</sub>(bpy) (**8**) and Ru(dbm)<sub>2</sub>(bpy) (**19**) (dbm = dibenzoylmethanato) with  $E_{1/2}$  of -0.035 V and +0.027 V (*vs* Ag/AgCl), respectively. Thus, the bpy ligand on these complexes will be replaced by bpy-NH<sub>2</sub> to prepare them as redox labels.

### 4.3 Objectives

The objectives of this chapter are to firstly synthesise ruthenium-based redox labels with primary amine groups; secondly, the redox label will be anchored onto SAMs by carbodiimide coupling followed by the binding of a pentapeptide, GPP, capable of binding the Hb1Ac antibody, to the redox label and finally, the sensing surface will be introduced to solutions containing Hb1Ac antibodies and the changes in the voltammetry responses will be monitored.

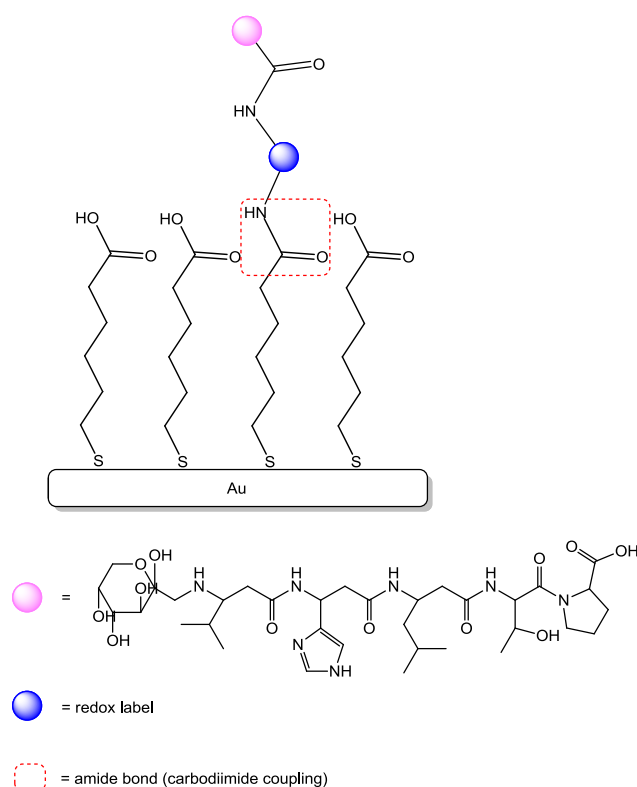


**Figure 4.3** The sensing surface showing an immobilised redox label on MHA and the covalent binding of GPP onto redox label by carbodiimide coupling.

## 4.4 Experimental Section

### 4.4.1 Chemicals

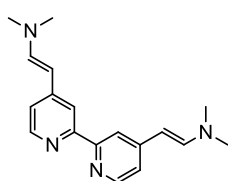
All chemicals and reagents used in this chapter are listed in Chapter 2, Section 2.2.

### 4.4.2 Experimental Techniques

Mass spectrometry, NMR spectrometry, CV, SWV and XPS measurements were conducted as described in Chapter 2, Section 2.3.

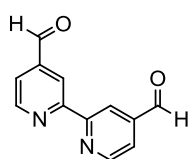
### 4.4.3 Synthesis of Redox Label, Ru(acac)<sub>2</sub>(bpy-NH<sub>2</sub>)

#### Synthesis of ligand precursors



#### 4,4'-bis(*N,N*-dimethylaminovinyl)-2,2'-bipyridine.<sup>21</sup>

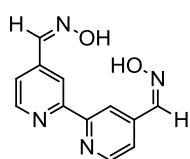
4,4'-dimethyl-2,2'-bipyridine (1.85 g, 10.0 mmol) was dissolved in DMF (15 mL) in a Schlenk flask. Brederick's reagent [*tert*-butoxybis(dimethylamino)methane] (9.70 mL, 47.0 mmol) was added to the mixture *via* a syringe. The reaction mixture was heated at 140 °C for 18 hours. After cooling to room temperature, the resulting dark orange solution was hydrolysed with deionised water (25 mL). The product was extracted by DCM (80, 50, and 30 mL) to give a light yellow solution. The solution was dried over MgSO<sub>4</sub>, filtered and solvent removed *in vacuo* to give the crude as a light yellow solid. The solid was recrystallised from DCM/pentane to give the product as a saffron-yellow powder. Yield: 2.03 g, 70%. <sup>1</sup>H NMR (400 MHz, CDCl<sub>3</sub>): δ 2.88 (s, 12H), 5.09 (d, *J* 13.7 Hz, 2H), 6.95 (dd, *J* 5.3 Hz, 1.8 Hz, 2H), 7.19 (d, *J* 13.7 Hz, 2H), 8.11 (d, *J* 1.7 Hz, 2H), 8.35 (d, *J* 5.3 Hz, 2H). MS (ESI): 295.1920 ([M + H]<sup>+</sup> required 295.1917).



#### 4,4'-diformyl-2,2'-bipyridine.<sup>21,22</sup>

In a Schlenk flask, 4,4'-bis(*N,N*-dimethylaminovinyl)-2,2'-bipyridine (1.08 g, 3.67 mmol) was dissolved in tetrahydrofuran (THF) (80 mL) and an aqueous solution of sodium periodate (6.24 g, 29.2 mmol) was

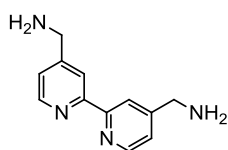
added dropwise to the organic layer. The orange organic layer turned white as more sodium periodate was added. The mixture was stirred at 40 °C for 18 h. After cooling to room temperature, the white solids were filtered off and washed with THF (3 × 30 mL) to give a light yellow organic phase. The organic phase was evaporated and DCM (80 mL) added. The organic layer was washed with saturated NaHCO<sub>3</sub> solution (3 × 30 mL), dried over MgSO<sub>4</sub> and evaporated to give product as an off-white solid. Yield: 0.484 g, 62%. <sup>1</sup>H NMR (400 MHz, CDCl<sub>3</sub>): δ 7.79 (d, *J* 4.9 Hz, 2H), 8.89 (s, 2H), 8.96 (d, *J* 4.9 Hz, 2H), 10.21 (s, 2H). MS (ESI): *m/z* 213.0653 ([M + H]<sup>+</sup> required 213.0659).



4,4'-bis(hydroxyiminomethyl)-2,2'-bipyridine.<sup>23</sup>

4,4'-diformyl-2,2'-bipyridine (0.705 g, 3.32 mmol), hydroxylamine hydrochloride (0.565 g, 8.13 mmol) and pyridine (0.76 g, 9.61 mmol) were added to a Schlenk flask followed by EtOH (40 mL). The reaction was refluxed for 5 hours. After cooling down to room temperature, water (70 mL) was added to the light purple mixture. The mixture was stored at 4 °C overnight. The resulting solid was separated from the solvent by filtration and washed with cold water to give product as a light pink solid after drying at 45 °C for several hours. Yield: 0.70 g, 88%. <sup>1</sup>H NMR (300 MHz, DMSO-*d*<sub>6</sub>): δ 7.64 (d, *J* 5.0 Hz, 2H), 8.31 (s, 2H), 8.51 (s, 2H), 8.71 (d, *J* 4.9 Hz, 2H), 11.85 (s, 2H). MS (ESI): *m/z* 243.0869 ([M + H]<sup>+</sup> required 243.0877).

#### Synthesis of ligand, 4,4'-bis(aminomethyl)-2,2'-bipyridine

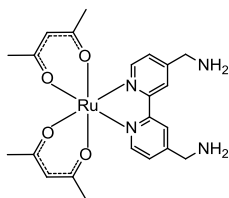


4,4'-bis(aminomethyl)-2,2'-bipyridine (bpy-NH<sub>2</sub>).<sup>23</sup>

4,4'-bis(hydroxyiminomethyl)-2,2'-bipyridine (0.243, 1.00 mmol) and palladium on carbon (0.160 g, 15 mol%) were added to a flask followed by the addition of water (13 mL) and concentrated hydrochloric acid (0.600 mL). The flask was placed in a pressure vessel and purged with hydrogen gas before hydrogenated at 120 psi at 40 °C for 6 h. The catalyst was removed, and filtrate concentrated to *ca.* 4 mL before being basified by 50% NaOH (5 mL) to pH 14. The mixture was extracted with DCM (60 mL × 2, 40 mL × 2, 20 mL × 2). The organic phases were combined, dried over anhydrous K<sub>2</sub>CO<sub>3</sub> and evaporated to give the product as a white solid. Yield: 0.16 g, 74%. <sup>1</sup>H NMR (400 MHz, DMSO-*d*<sub>6</sub>): δ 3.83 (s, 4H),

7.40 (d, *J* 5.0 Hz, 2H), 8.39 (s, 2H), 8.57 (d, *J* 5.0 Hz, 2H). MS (ESI): 215.1288 ( $[M+H]^+$  215.1291).

#### Synthesis of Ru(acac)<sub>2</sub>(bpy-NH<sub>2</sub>) (30)



#### Ru(acac)<sub>2</sub>(bpy-NH<sub>2</sub>), **30**

Complex Ru(acac)<sub>2</sub>(MeCN)<sub>2</sub> (**10**) (0.127 g, 0.333 mmol) and bpy-NH<sub>2</sub> (0.071 g, 0.331 mmol) were added to a Schlenk flask followed by EtOH (15 mL). The mixture was refluxed for 3 h during which the colour changed from orange to dark green in the first half hour of the reaction. The mixture was filtered through a bed of celite, dried under vacuum and recrystallised with DCM/pentane (× 3, 10 mL each) under nitrogen before giving the product as a dark green solid. Yield: ~0.12 g, ~70%. <sup>1</sup>H NMR (400 MHz, DMSO-*d*<sub>6</sub>): δ 1.47 (s, 6H), 2.08 (s, 6H), 3.90 (s, 4H), 5.21 (s, 2H), 7.28 (d, *J* 5.9 Hz, 2H), 8.36 (s, 2H), 8.56 (d, *J* 5.9 Hz, 2H) ppm. <sup>13</sup>C NMR (150.90 MHz, DMSO-*d*<sub>6</sub>): δ 27.10, 27.86, 44.55, 99.23, 120.18, 122.53, 149.26, 151.56, 160.38, 182.69, 184.55 ppm. MS (ESI): *m/z* 515.0922 ( $[M + H]^+$  515.1227)

#### 4.4.4 Construction of Sensing Surface

The surface with redox label bound was prepared in the following fashion: first, cleaned gold electrodes were modified with MHA or TA by immersing the electrodes in 1 mM ethanolic solution of MHA or TA for 4 h. After rinsing with EtOH and Milli-Q water, the carboxylic acid groups on the SAMs were activated by EDC/NHS (2:1, 100 mM:50 mM) in MES buffer (0.1 M, pH 6.8) for 3 h before incubation with redox label **30** (1 mM in EtOH) overnight at 4 °C.

The MHA-modified electrodes with redox label bound were rinsed with Milli-Q water and EtOH, dried under a nitrogen flow before incubating with 2mM GPP in EDC/NHS solution (2:1, 20 mM:10 mM, phosphate buffer) for 4 h at 4 °C to allow covalent attachment of the GPP onto redox label (see Figure 4.3). The gold electrodes were rinsed with Milli-Q water and EtOH and dried under a nitrogen flow. The construction of sensing surface was now complete.

Gold surfaces for XPS analysis were treated following the same procedure.

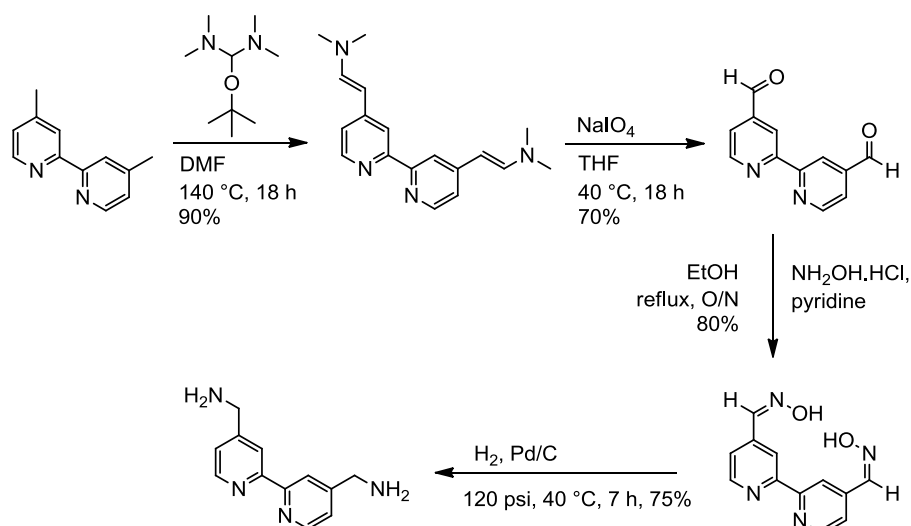
#### 4.4.5 Determination of Hb1Ac antibody

The sensing surface was incubated with Hb1Ac antibody ( $8 \mu\text{g mL}^{-1}$ , PBS) at room temperature for different time periods. The voltammetry responses from the redox label was recorded by square-wave voltammetry (SWV) after incubation at different time periods at 130 Hz, 200 Hz or 210 Hz (step potential = 4 mV; amplitude = 25 mV).

### 4.5 Results and Discussion

#### 4.5.1 Synthesis of $\text{Ru}(\text{acac})_2(\text{bpy-NH}_2)$

Two suitable candidates,  $\text{Ru}(\text{acac})_2(\text{bpy})$  and  $\text{Ru}(\text{dbm})_2(\text{bpy})$  were chosen for the preparation of redox labels with the  $\text{bpy-NH}_2$  ligand. The attempts to prepare  $\text{Ru}(\text{dbm})_2(\text{bpy-NH}_2)$  failed to give the desired product hence efforts were concentrated on the successfully synthesised redox label,  $\text{Ru}(\text{acac})_2(\text{bpy-NH}_2)$  (**30**). To enable carbodiimide coupling of **30** onto the electrode and also bioreceptor onto **30**, the  $\text{bpy-NH}_2$  ligand, a homobifunctional ligand which contains pendant amine groups (Scheme 4.1) was synthesised in four steps. This ligand was used to displace MeCN in  $\text{Ru}(\text{acac})_2(\text{MeCN})_2$  to prepare **30**.



**Scheme 4.1** Synthesis of ligand, 4,4'-bis(aminomethyl)-2,2'-bipyridine (bpy-NH<sub>2</sub>).

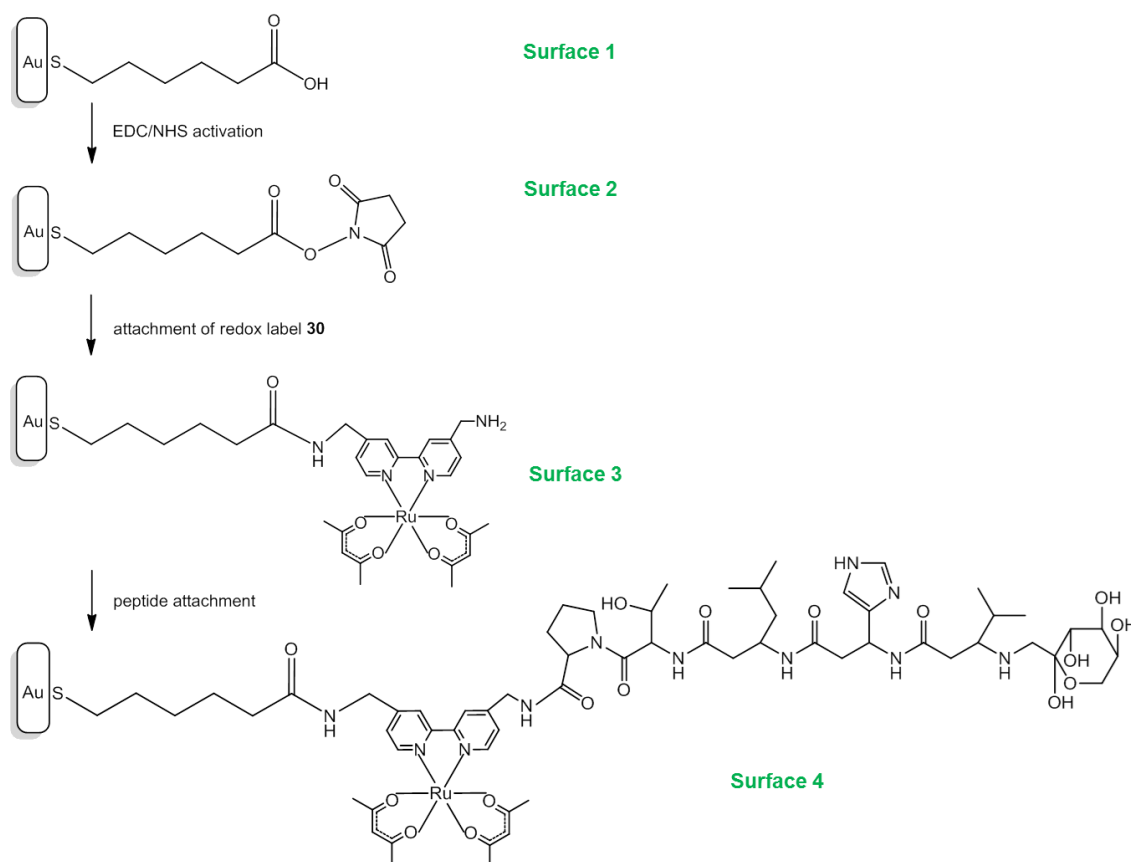
Tris-bpy ruthenium and osmium complexes containing amino groups were previously reported to be stable in air-saturated aqueous or organic solvents.<sup>24</sup> However, the bpy-NH<sub>2</sub> ligand was found to be hygroscopic and had to be stored under inert atmosphere. The resultant redox label **30** was air-sensitive, therefore it was stored in a glove box prior to use. The presence of amine groups on the bpy would cause the  $E_{1/2}$  of the complex to shift cathodically as they are electron-donating.<sup>20,25</sup> Upon comparing the  $E_{1/2}$  of **8** and **30**, it was found that the amine groups had shifted the  $E_{1/2}$  of **30** (-0.455 V vs Fc<sup>0/+</sup>) anodically for 23 mV compared to **8** (-0.478 V vs Fc<sup>0/+</sup>). This anomaly could be due to the methyl carbon spacers between the amino groups and the bpy ring, though the shift is only slight. The  $D_o$  of **30** ( $0.4013 \times 10^{-9} \text{ m}^2 \text{ s}^{-1}$ ), smaller than **8** ( $1.3535 \times 10^{-9} \text{ m}^2 \text{ s}^{-1}$ ), concurs with the presence of bulkier aminomethyl groups on bpy in **30**.

#### 4.5.2 Redox Label, Ru(acac)<sub>2</sub>(bpy-NH<sub>2</sub>) on SAM-modified Gold Surfaces

Two different organosulfur compounds with carboxylic acid termini – MHA and TA, both six carbons in length – were used to form SAMs (Figure 4.1). The difference between the two lies in the head group: MHA is an alkanethiol which will form a thiolate–Au bond whereas TA has a cyclic disulfide base giving it two contact points on the gold electrodes.

The SAMs were formed by simply immersing the gold surfaces in 1 mM ethanolic solution of MHA or TA for a minimum of 4 h followed by the carboxyl activation by coupling reagent/additive 1-(3-dimethylaminopropyl)-3-ethylcarbodiimide hydrochloride (EDC) and *N*-hydroxysuccinimide (NHS) (2:1) in MES buffer (pH 6.8) for 3 h.<sup>26</sup> The activated surfaces now consisted of reactive succinimide ester intermediates susceptible to nucleophilic attack by amines<sup>12</sup> on the redox labels. The electrodes were subsequently kept in 1 mM ethanolic solution of **30** overnight at 4 °C to allow attachment of **30** onto the modified gold surfaces.

One of the amine groups was used to covalently bind the redox labels onto MHA while the other free amine on redox label was used to form an amide bond with a bioreceptor, GPP, a pentapeptide which selectively recognises Hb1Ac monoclonal antibody, a diabetes marker protein.<sup>2</sup> The presence of only one free carboxylic group on GPP ensures site-specific binding of the peptide to the redox label (Scheme 4.2).



**Scheme 4.2** Schematic on the attachment of redox label **30** on MHA-modified gold electrode (Surface 1 – 4).

### 4.5.3 XPS Characterisation of Modified Gold Surfaces

The surface composition of the assembly of the sensing surface followed by XPS after each of the four steps: SAM formation, EDC/NHS activation of SAMs, attachment of redox label **30** onto SAMs and attachment of peptide GPP onto redox label. XPS wide scans for both MHA- and TA-modified gold surfaces with **30** attached are shown in Figure 4.5. Distinctive Au 4f peaks at 83.8 and 87.5 eV were observed for both MHA-modified and TA-modified gold surfaces (Figure 4.4).

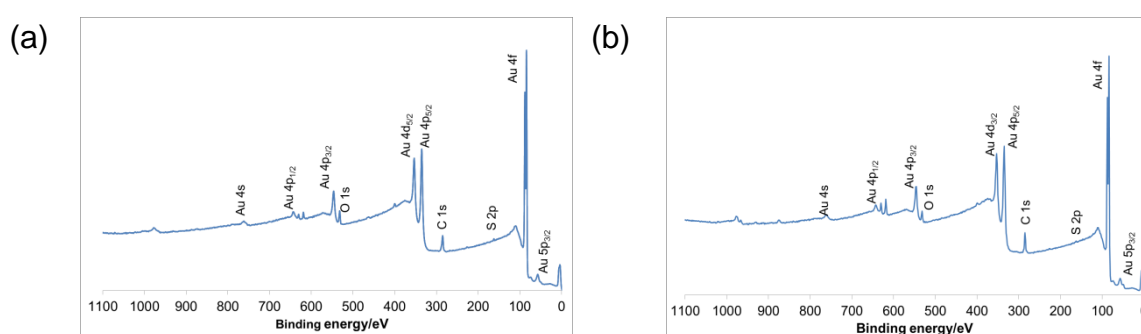


**Figure 4.4** Wide scans for (a) MHA- and (b) TA-modified gold surfaces with redox label **30** attached.

#### I. MHA- and TA-modified Gold Surfaces

First, the MHA- and TA-modified gold surfaces were examined. Confirmation of MHA formation was obtained from the S 2p narrow scan. The set of S 2p peaks at 161.9 eV and 163.1 eV was identified as a spin doublet corresponding to S 2p<sub>3/2</sub> and S 2p<sub>1/2</sub>, respectively, which fits well with the reported values of surface-bound alkanethiols (Figure 4.5a).<sup>27</sup> The TA-modified gold surface also shows a similar peak profile at 162.2 and 163.5 eV confirming that the TA was surface-bound (Figure 4.5b).<sup>28</sup>

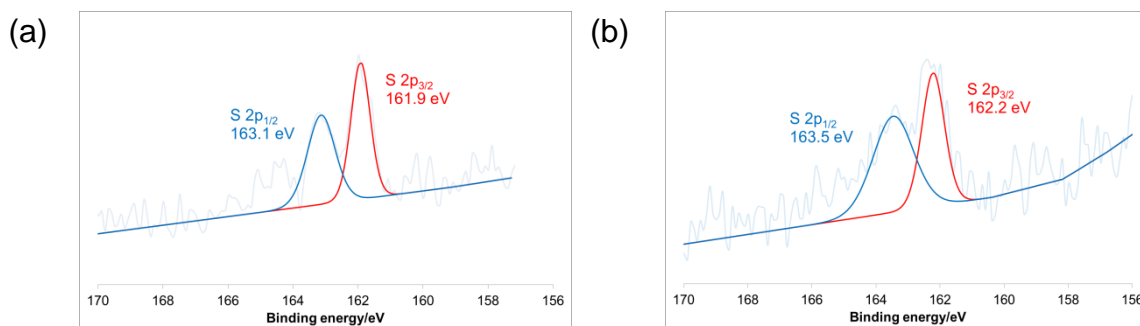


**Figure 4.5** S 2p narrow scans for (a) MHA- and (b) TA-modified gold surfaces.

The following major peaks in C 1s narrow scan are observed on the MHA-modified surface (Figure 4.6a): a peak at 288.7 eV which corresponds to the carboxylic acid tail group and a large peak at 284.9 eV from the methylene carbons on the MHA chain. In addition, a carbon atom adjacent to the electron-withdrawing carboxylic acid terminus shows up at a higher binding energy of 286.0 eV, compared to the rest of the methylene carbons. The atomic percentage (At %) of the carbon component on MHA is determined to be ~1:1:6, which is in good agreement with the number of carbons (1:1:4) present on the chain. C 1s narrow scan of the TA-modified gold surface (Figure 4.6b) reveals a similar peak profile with peaks at 289.1, 286.3 and 284.9 eV. The At % of the three C 1s species is found to be at 1:1:4.5, which is close to the expected value of 1:1:6 for a TA-modified surface.

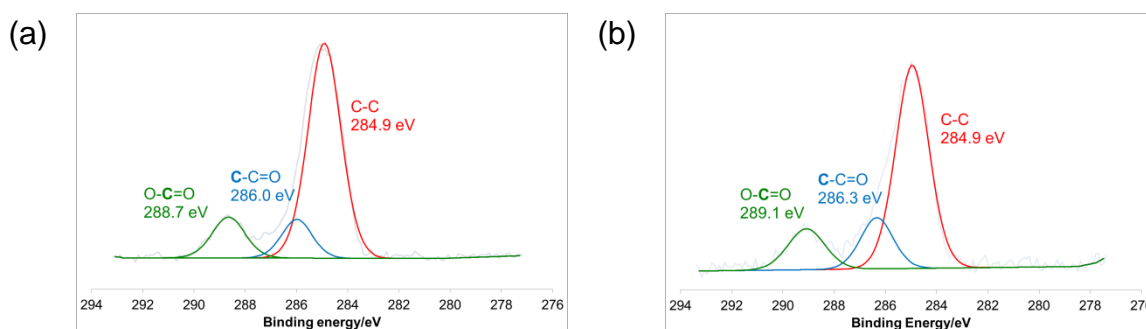


**Figure 4.6** C 1s narrow scans for (a) MHA- and (b) TA-modified gold surfaces.

## II. Activation of MHA- and TA-modified Surfaces

Next, a comparison was made between MHA- and TA-modified gold surfaces which were activated by EDC/NHS and the ones which were not. The key difference between these two is the presence of the succinimide ester on the activated surface.

Figure 4.7a and 4.7c show N 1s peaks in the region of 402 eV which are attributed to the nitrogen on succinimide ester, while the peaks at 400 eV originated from the nitrogen on EDC which did not proceed to react with NHS to form succinimide ester.<sup>29</sup> XP spectra of the surfaces which were not activated (Figure 4.7b and 4.7d) show very little trace of N 1s peak. The peak area ratio of succinimide ester peak and the carboxylic acid terminal group on C 1s narrow scan on the activated MHA surface gives an activation efficiency of 63% compared to 20% on the TA-modified surface.

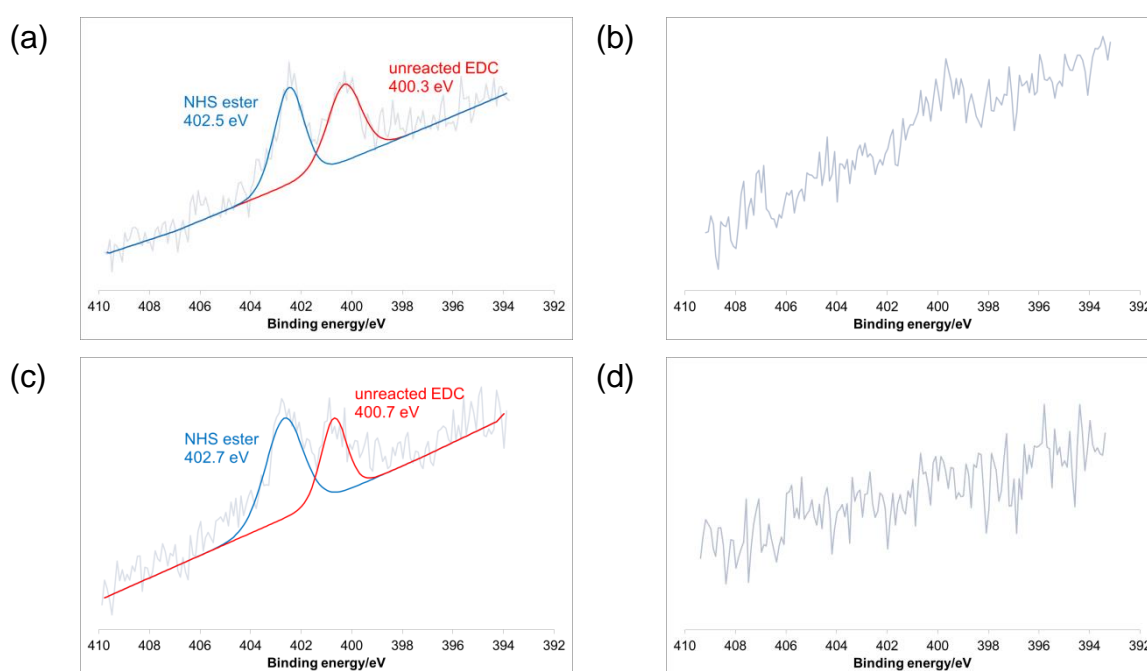


**Figure 4.7** N 1s narrow scans for MHA-modified gold surface: (a) activated and (b) not activated; TA-modified gold surface: (c) activated and (d) not activated.

### III. Attachment of Redox Label onto MHA- and TA-modified Surfaces

As SAM formation and activation by EDC/NHS were shown to be successful, the next step was to attach **30** to the activated surface. The disappearance of the peak belonging to succinimide ester at 402 eV, along with the appearance of amine peaks at 399.5 eV provides evidence that **30** was attached to the activated surfaces (Figure 4.8). As the binding energies for amide and amine nitrogens are very close together, it is difficult to distinguish the binding energies of amine and amide species with certainty. However, a concomitant increase in the At % of N 1s peak before and after attachment

of redox label for both surfaces suggest that the redox label was bound onto the surfaces. For the MHA surface, an increase from 0.96% to 4.8% for MHA-modified surface gave a coupling yield at 125%, which is most likely due to non-specific adsorption of the redox label on MHA surface. In contrast, an increase from 1.16% to 2.83% for TA surface gave the coupling yield at 62.5%. The increase in At % of these surfaces with redox label attached is consistent with the increased amount of amide nitrogen and the nitrogen on the redox label (free amine and nitrogen on bpy). Although this increase in the At % of N 1s cannot be used to quantify the amount of redox labels bound to the surface, the apparent surface coverage of redox labels can be estimated by CV, which will be discussed in Section 4.5.4.

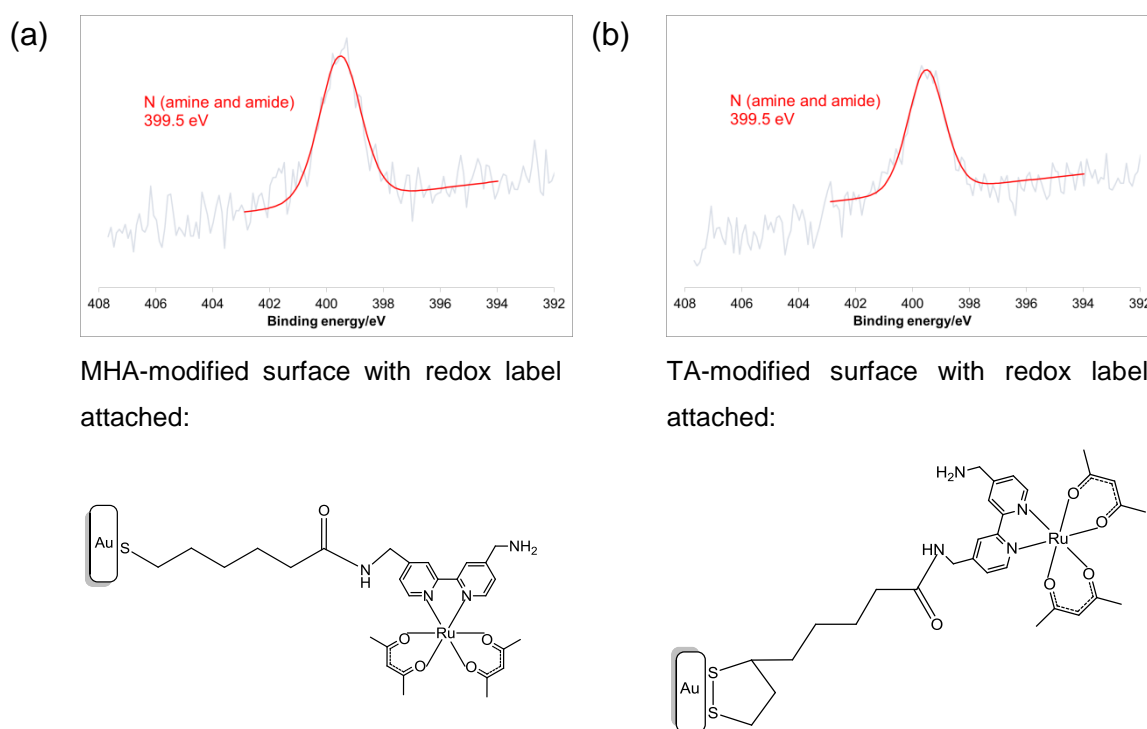


**Figure 4.8** N 1s narrow scan for modified gold surface with **30** attached: (a) MHA-modified; (b) TA-modified.

The binding energy of Ru 3d<sub>3/2</sub> will not be discussed because of the overlapping of the signal with that of C 1s.<sup>30</sup> The peak of Ru 3d<sub>5/2</sub> was therefore examined on both the activated and non-activated surfaces. A peak at 280.4 eV on the activated surface, similar to literature values for Ru<sup>II</sup>(acac)<sub>2</sub> complexes, indicates that Ru<sup>2+</sup> was bound to the surface.<sup>31</sup> Nonetheless, a ruthenium peak was also present on the non-activated surface (Figure 4.9b) to show that some species could physisorb onto the surface.

However, as will be demonstrated in Figure 4.14, the contribution of physisorbed species towards current response is negligible.

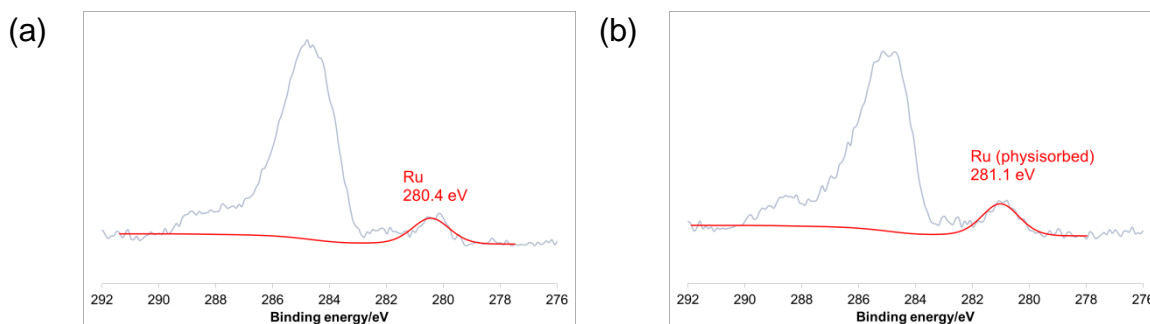


**Figure 4.9** Ru 3d<sub>5/2</sub> narrow scan for MHA-modified gold surface: (a) activated surface incubated with **30**; (b) non-activated surface incubated with **30**.

#### IV. Attachment of Peptide GPP onto MHA-modified Gold Surfaces

The attachment of peptide GPP was only performed on the MHA-modified surfaces for a preliminary study on the performance of the redox label for the detection of Hb1Ac. The C 1s narrow scans in Figure 4.10 track the changes after each modification step, however the At % cannot give an absolute figure in terms of the number of species present of the surface in the last two steps. In Figure 4.10c, where the redox label was attached to the MHA-modified surface, there are slightly more C=O groups from the acac ligand on the redox label, and an amide C=O peak was found at 288.2 eV. However, because the coupling was not quantitative, the calculated ratio of C=O (amide) over C=O (acac) of 1:2.2 was not expected to meet the theoretical ratio of 1:4. In Figure 4.10d, where the peptide was bound to the surface, the ratio of C=O (amide) peak and C=O (acac) is almost 1:1, suggesting that there is an increase of amide C=O groups, which were attributable to the amide bonds in the peptide.

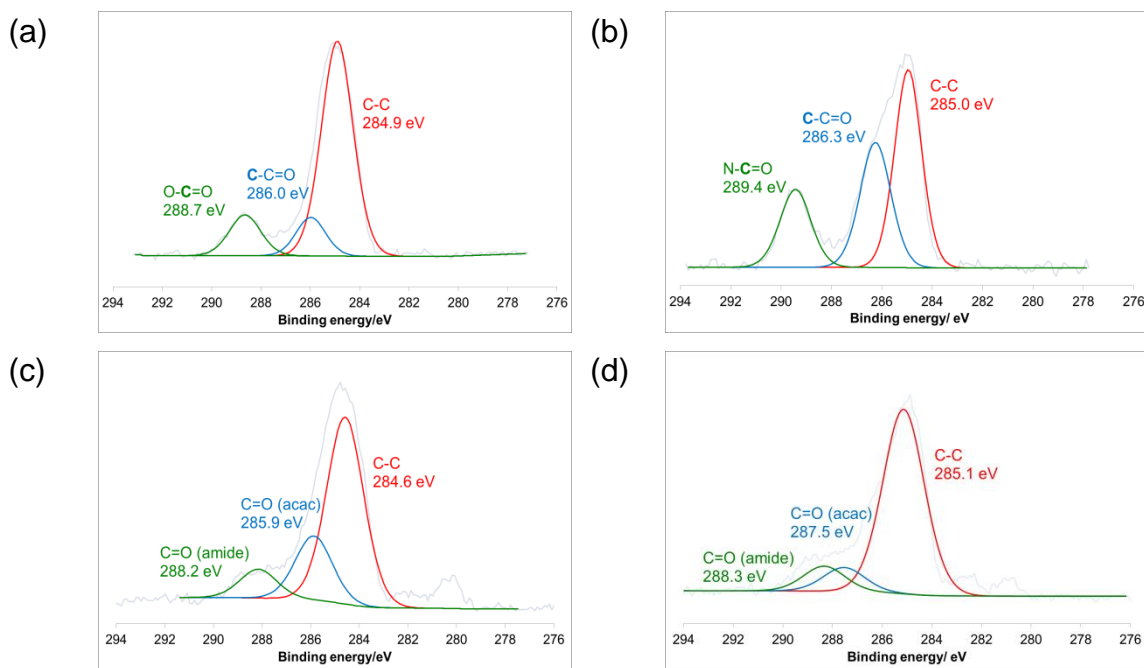


**Figure 4.10** C 1s narrow scan for modified gold surface: (a) MHA; (b) activated MHA; (c) MHA with **30** attached; (d) MHA with **30** and peptide.

The same can be done with N 1s narrow scans of the modified surfaces. To ensure that the peptide was covalently bound onto the surface, a control surface was incubated with 2 mM GPP in phosphate buffer by skipping the EDC/NHS activation step such that no covalent bonds could be formed between the redox label and GPP. The XP spectrum of the control surface (Figure 4.11a) is highly similar to the MHA-modified surface with bound redox label (Figure 4.8a), with no peak at 402 eV to conclude that the peptide did not bind onto the surface. Figure 4.11b shows a small peak at 402.0 eV ascribed to the amide bonds formed by the activated GPP with redox labels.

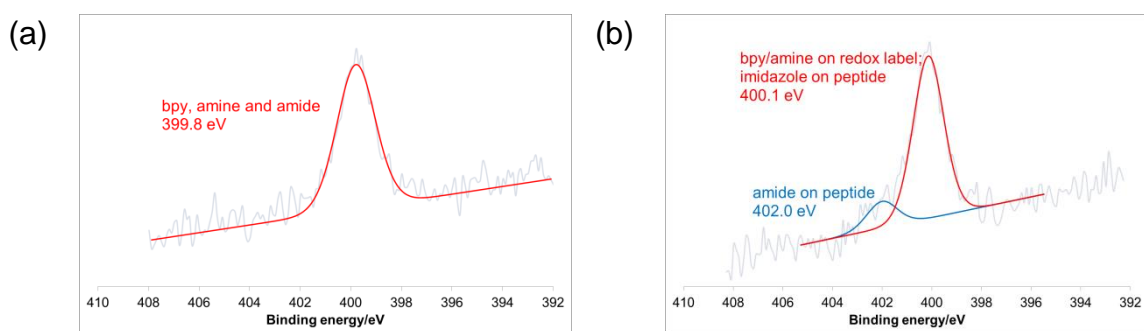
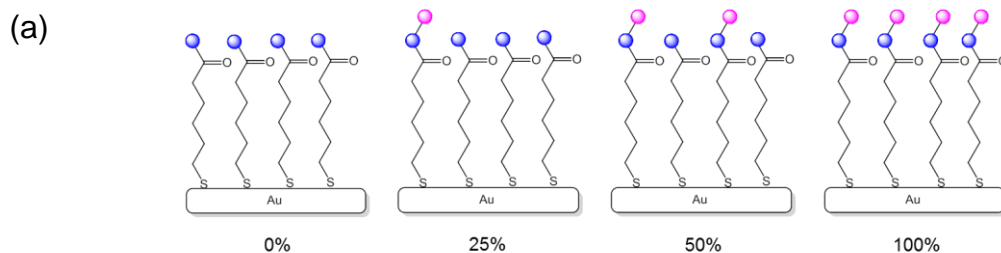


**Figure 4.11** N 1s narrow scan for modified gold surface incubated with: (a) GPP and (b) EDC/NHS activated GPP.

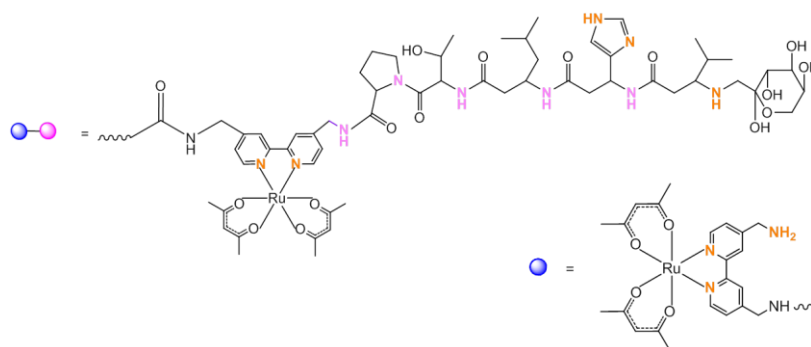
### Estimation of the Coupling Yield of GPP on Redox Label

The coupling yield of the covalent binding of GPP to redox label bound to MHA-modified surface can be estimated by examining the binding energies of the nitrogen atoms as they exist in different environments. First, the redox label contains three nitrogen atoms (two on bpy ring and one on the free amine, coloured orange in Figure 4.12a) occurring at 400 eV when there is no GPP bound onto the label. The amide nitrogen from the amide bond responsible for binding the redox label to the MHA-modified surface is not taken into account because the signal is small (see Figure 4.8a). Second, there are two main nitrogen environments on the GPP backbone – one of amide nitrogens occurring at 402 eV (coloured pink in Figure 4.12a) and the other from the imidazole nitrogens occurring at 400 eV (coloured orange in Figure 4.12a).

The assumption model is based on the coupling efficiency between the peptide and the redox label, in which four different coupling efficiencies at 0%, 25%, 50% and 100% were used. In the scenario where all redox labels are completely bound with peptide, that is at 100% coupling efficiency, there will be five nitrogens occurring at 400 eV and five at 402 eV. The number of nitrogens at the two binding energies, i.e., 400 and 402 eV, is assumed to vary according to the percentage of coupling efficiency between GPP to the redox label (Figure 4.12b, Table 1 and Graph 1). From the At % of 0.73 of N 1s peak at 402.0 eV and 4.45 at 400.1 eV, the minimum coupling yield of GPP to redox label is estimated to be at 16.4% as there were redox labels non-specifically adsorbed on the MHA-modified surface (Figure 4.12b, Table 2).



N.B. % indicates the coupling efficiency between the peptide and the redox label



(b) Table 1. Ratio of nitrogen at 402 eV over 400 eV for the estimation of the % peptide bound on redox label.

coupling efficiency (%)	No. of N at 400 eV	No. of N at 402 eV	Ratio of N No. of N at 402 eV No. of N at 400 eV	% peptide bound to redox label
0	3	0	0	0
25	14	5	0.357	35.7
50	8	5	0.625	62.5
100	5	5	1	100

Graph 1: Plot of % peptide bound vs % coupling efficiency

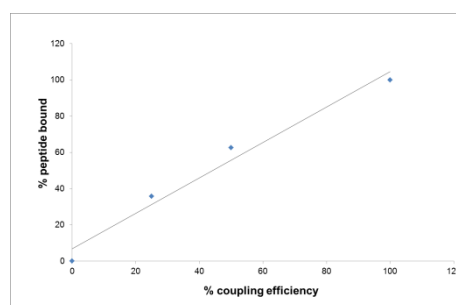


Table 2: Estimation of % peptide bound on redox label

Binding energy (eV)	At % of N	Ratio of N	% peptide bound to redox label
400	4.45	0.164	16.4
402	0.73		

**Figure 4.12** (a) Assumption model of four coupling efficiencies: 0%, 25%, 50% and 100%; (b) Table 1: % peptide bound to redox label based on the number of nitrogens present at different binding energies; Graph 1: A calibration of % peptide bound vs % coupling efficiency and Table 2: Estimation of % peptide bound on redox label.

#### 4.5.4 Electrochemical Studies on Modified Gold Electrodes

The presence of Faradaic peaks, both oxidation and reduction, in the CVs indicates attachment of **30** on MHA- and TA-modified gold electrodes (see Figure 4.13a). The successful attachment is further supported by a linear relationship of peak current *versus* scan rate for both surfaces (Figure 4.13b). Both MHA- and TA-modified electrodes gave similar current response.

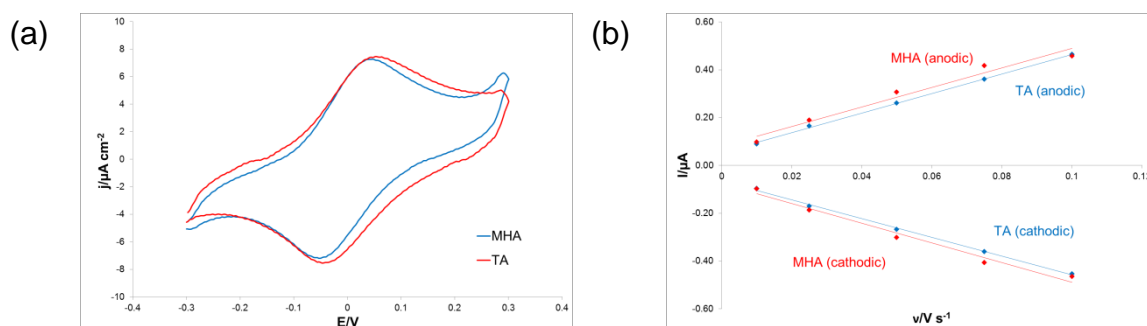


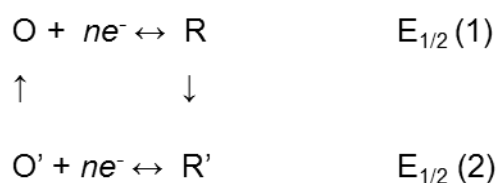
**Figure 4.13** (a) Plot of current density *vs* potential for MHA- and TA-modified gold electrode in phosphate buffer, pH 7,  $\nu = 0.1 \text{ V s}^{-1}$ . (b) Linear plots of current *vs* scan rate for MHA- and TA-modified electrodes.

Comparisons were made between **30** in solution and as surface-bound species on SAMs (see Table 4.1). It is common for a surface-bound redox species to have close redox potentials to that of a solution analogue, which means that both surface-bound and solution redox species experience highly similar solvation environments.<sup>32</sup> The  $E_{1/2(\text{surf})}$  of **30** for both MHA and TA differ less than 20 mV from that of  $E_{1/2(\text{sol})}$ . The  $i_{\text{pa}}/i_{\text{pc}}$  for both surfaces are nearly identical (0.98 for MHA- and 0.92 for TA-modified surface), confirming that the redox process is chemically reversible.

**Table 4.1**  $E_{1/2(\text{solution})}$  and  $E_{1/2(\text{surface-bound})}$  of **30**

Potential/ V ( <i>vs</i> Ag/AgCl; $\nu = 0.1 \text{ V s}^{-1}$ )	in Solution	on MHA	on TA
$E_{\text{pa}}$	0.0240	0.0369	0.0418
$E_{\text{pc}}$	-0.0468	-0.0412	-0.0363
$E_{1/2(\text{sol})}$ or (surf)	-0.0114	-0.00214	0.00275
$\Delta E$	0.0708	0.0781	0.0781
$E_{\text{fwhm}(\text{surf}/\text{anodic})}$	-	0.155	0.182
$E_{1/2(\text{surf})}$ relative to $E_{1/2(\text{sol})}$	-	0.0167	0.0141

In an ideal system, the  $\Delta E$  should be 0 V and the peaks symmetrical with a  $\Delta E_{\text{fwhm}}$  of  $90.6/n$  mV ( $n$  = number of electrons transferred).<sup>14,32</sup> However, non-ideal values of  $\Delta E$  and  $\Delta E_{\text{fwhm}}$  are very common for the stepwise assembly of redox species on SAMs.<sup>12</sup> The deviation from 0 V in  $\Delta E$  is caused by two main factors. Firstly, the solvation of the redox centre or the structure of the SAM may change with the oxidation state of the redox centre, following a “square” scheme of the redox cycle is shown in Scheme 4.3.<sup>32</sup> Examples of this change include the formation of strong ion pairs in the more highly charged oxidation state, and a major change in the hydrophobicity or hydrophilicity of the redox centre as a function of its oxidation state.<sup>32</sup> Secondly, there may be a phase change in the SAM resulting from the change in free energy of one oxidation state to another when the redox species undergoes a redox cycle.<sup>32</sup> The  $\Delta E$  values of 78 mV for both SAMs show that the systems are non-ideal, which implies that redox label **30** exist in a range of microenvironments to cause this distribution of  $E_{1/2}$ .



**Scheme 4.3** “Square” scheme of a redox cycle on SAM.

Like  $\Delta E$ ,  $E_{\text{fwhm}}$  values of 155 mV and 182 mV for MHA and TA respectively, also deviate from the ideal  $E_{\text{fwhm}}$  of  $90.6/n$  mV. There could be a number of factors at play in the broadening of such peaks. First, it is possible that there is a presence of a group of redox species in different microenvironments due to monolayer defects, ion-pairing, or a distribution of monolayer structures corresponding to various solvation shells.<sup>14,32</sup> A SAM with a high surface concentration of redox species may result in strong interaction between the redox species,<sup>32</sup> if the interaction is deemed repulsive, the  $\Delta E_{\text{fwhm}}$  is larger; if attractive, smaller. The apparent surface coverage of redox label on the modified electrodes is calculated from the anodic peak as an average of  $1.12 \times 10^{-10}$  mol cm<sup>-2</sup> and  $1.54 \times 10^{-10}$  mol cm<sup>-2</sup> for MHA- and TA-modified gold electrodes, respectively. Against the maximum theoretical coverage of SAM at  $0.76 \times 10^{-9}$  mol cm<sup>-2</sup>,<sup>27</sup> the surface coverage of the redox label is estimated at between 15% for MHA-modified surface and 20% for TA-modified surface. Hence, it can be assumed that the interactions between the redox labels are only moderate. Second, the peaks can

be broadened due to a change in surface charge, subsequently the surface potential during the Faradaic reaction of the redox species.<sup>32</sup> Third, double-layer effects can affect the shape of CVs quite significantly. The CV waves can be skewed when the surface potential rises quickly as the redox species gets oxidised to cause a deviation from the true redox potentials.<sup>32</sup> However, the skews are less when the absolute surface charges of the redox species are higher, e.g. 2+/3+ vs 0/+ and when electrolyte concentrations are high.<sup>32</sup> Redox label **30** is oxidised from 2+ to 3+ in 0.2 M KCl hence this contribution might not be as significant in the broadening of the peaks.

This approximation of surface coverage calculated before allows for a tentative quantification of the number of redox labels attached on SAMs and therefore the area available for each bioreceptor. Using the surface coverage of MHA-modified surface as an example,  $1.12 \times 10^{-10}$  mol cm<sup>-2</sup> gives the number of molecules at  $6.74 \times 10^{13}$  molecule cm<sup>-2</sup>. After conversion, there is 1.48 nm<sup>2</sup> available for each molecule of redox label. Given that the coupling yield of GPP to redox label at about 16% (Figure 4.12b), the upper limit for the area of each GPP-bound redox label can be estimated at 9.25 nm<sup>2</sup>. The crystallographic dimensions of an IgG antibody were  $A_{\text{front}} = 85.1$  nm<sup>2</sup>,  $A_{\text{side}} = 65.8$  nm<sup>2</sup> and  $A_{\text{top}} = 57.9$  nm<sup>2</sup> and the dimension of the binding domain of an IgG antibody is estimated at 4 nm × 2.5 nm × 2.5 nm.<sup>33</sup> An average carbodiimide coupling yield is around 20 – 30%; hence, this density of GPP is likely to provide adequate space for the binding of Hb1Ac antibody, assuming that the GPP are homogeneously distributed across the surface.

#### 4.5.4.1 Redox Label Physisorbed onto Modified Gold Electrodes

MHA- and TA-modified gold electrodes were incubated with **30** overnight without the EDC/NHS activation step such that **30** could not form covalent bonds with the SAMs. The weak redox peaks indicate that **30** was weakly physisorbed onto both of the modified electrodes, however, their overall contribution to the current response was negligible.

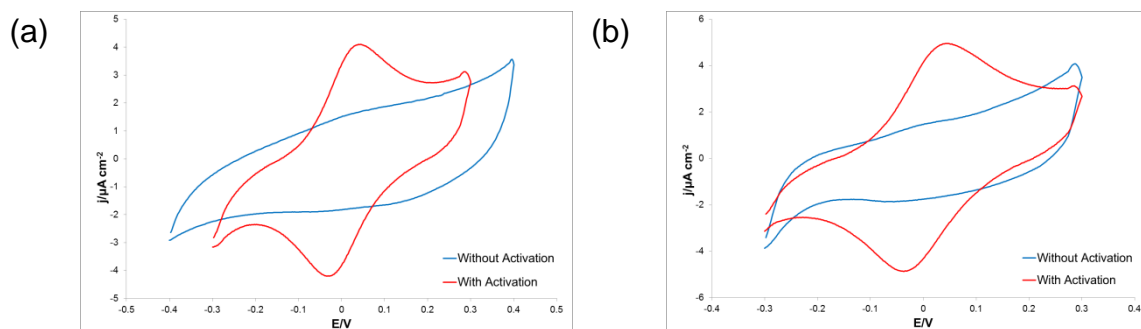


**Figure 4.14** CVs of **30** on (a) MHA- and (b) TA-modified gold electrodes, with and without EDC/NHS activation, in phosphate buffer, pH 7,  $\nu = 0.05 \text{ V s}^{-1}$ .

#### 4.5.4.2 Stability of Redox Label

This section reports on the effect of pH and chloride-containing buffers on the electrochemistry of **30**. Both MHA- and TA-modified electrodes were subject to cycles in phosphate buffers of pHs ranging from 5 – 9. The plot of pH *versus* potential (Figure 4.15) shows that both anodic and cathodic potentials on both MHA- and TA-modified surfaces between one pH and the next, differ in the range of 15 – 22 mV. Neither the potential, nor the current density across the electrodes, varied much with pH through the 5 – 9 range. This shows that the redox label can work reliably in this pH range. Further, Zakerruddin *et al.* reported that the redox potentials of iron, ruthenium and osmium complexes with tris(bpy) ligands bearing amino, dimethylamino or diethylamino groups did not show pH dependence; they reasoned that the complexes were not available for protonation due to conjugation of nitrogen lone-pair electrons with the electrons in bpy rings.<sup>24</sup>

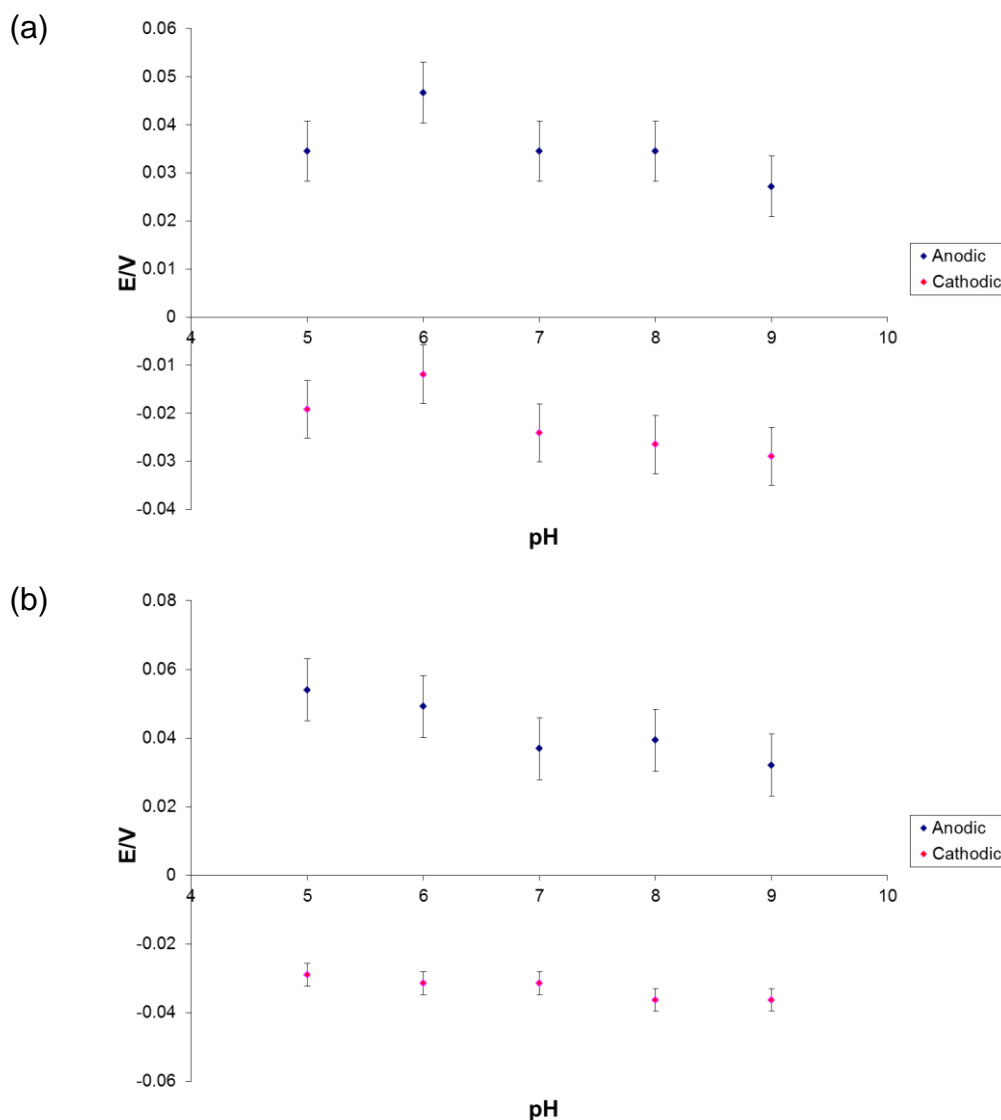


**Figure 4.15** pH vs potential for (a) MHA- and (b) TA-modified gold electrodes in phosphate buffers of pHs 5 – 9,  $v = 0.05 \text{ V s}^{-1}$ .

The question which follows is whether this ruthenium-based redox label is more stable than the ferrocene-based labels in chloride-containing buffers. To investigate the differences in their behaviours, three different electrodes modified with the following surfaces: 6-(ferrocenyl)hexanethiol, MHA- and TA-modified surface with redox label **30** were subjected to >100 scans in phosphate buffer made up of 0.05 M  $\text{KH}_2\text{PO}_4/\text{K}_2\text{HPO}_4$  and 0.2 M KCl.

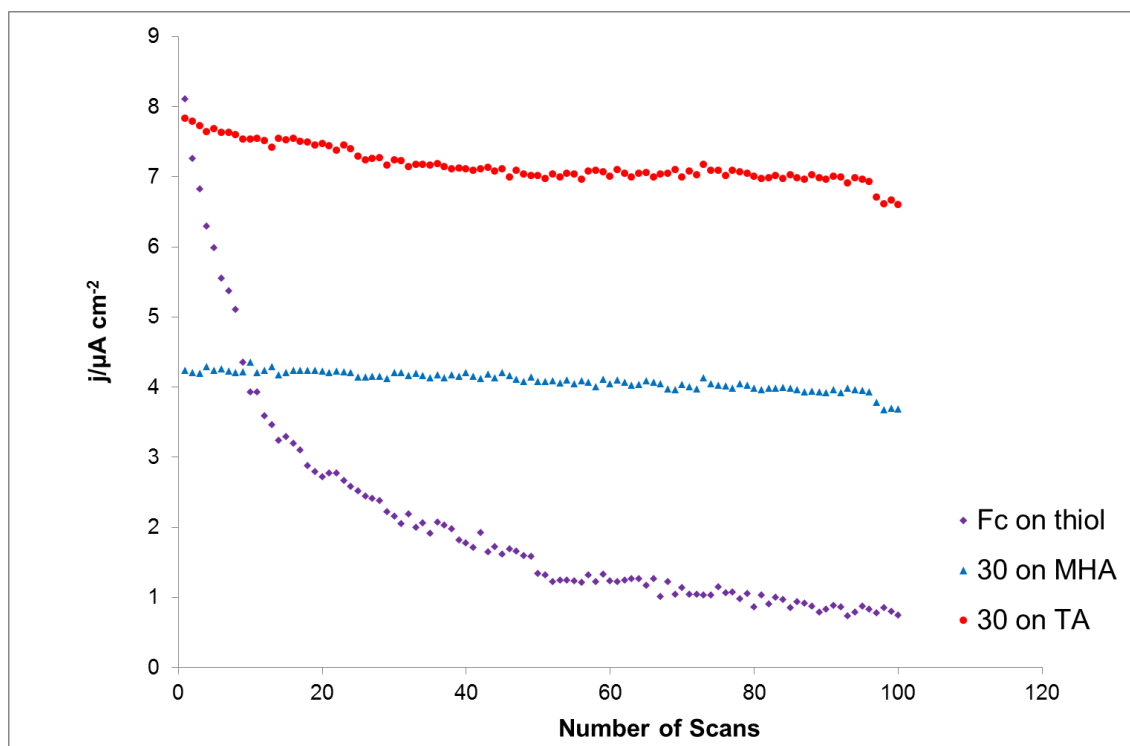


**Figure 4.16** Current decrease of Fc on thiol compared to **30** bound to MHA and TA on gold electrodes.

Figure 4.16 shows that there was a 52% of signal decay suffered by ferrocene-modified surface after the first 10 scans and this loss of signal reached 91% by the 100<sup>th</sup> scan while the signals from surfaces with ruthenium redox label **30** bound were significantly more stable. Compared to MHA-modified surface, the initial drop experienced by the TA-modified surface suggested that perhaps some redox labels were physisorbed on TA. TA has a cyclic disulfide group as its head group which chemisorbs to the gold electrode and in the process gives greater stability for the formed SAM.<sup>13</sup> It has been said that the TA SAM might be less densely packed due to its cyclic ring base, but various disulfide SAMs have been shown to have comparable blocking properties with those of thiols.<sup>32</sup> However, it is highly likely that a small fraction of redox labels which were physisorbed on the surface were removed by the first few scans. In some cases, continuous CV scans are employed to remove physisorbed species from modified surfaces until stable electrochemistry is obtained.<sup>4</sup>

This set of repeated CV scans shows that unlike the ferrocene label, the redox activity of ruthenium label **30** is retained during scanning cycles in buffers containing

chloride salts. Despite its sensitivity to air, this redox label, once bound onto surface is stable to use and far superior than the ferrocene-label in chloride-containing buffers.

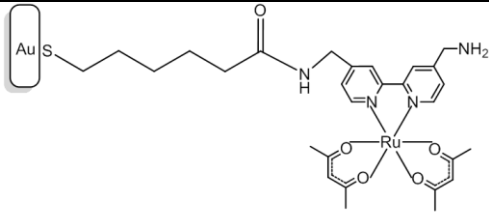
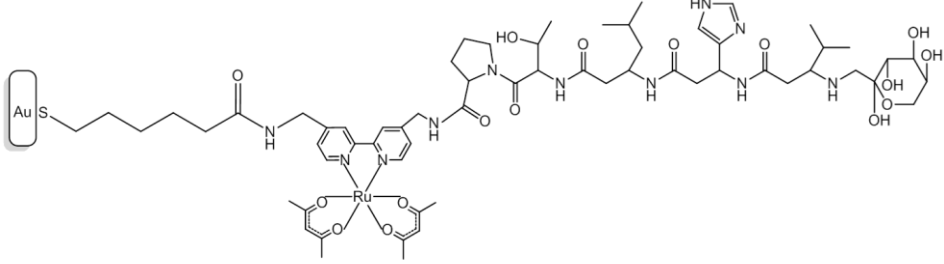
The stability scans in phosphate buffers of different pHs and moderate ionic strength (0.2 M KCl) show that the performance of redox label **30** is not affected by pH and chloride salts. Compare to the ferrocene label which decomposes in chloride-containing buffers during redox cycles, the ruthenium-based redox label **30** synthesised in this chapter fulfils the major criteria for it to function as a redox label in sensing applications: low and pH-independent  $E_{1/2}$ , chemically stable in both oxidised and reduced form and the redox process is both chemically and electrochemically reversible.

#### **4.5.5 Detection of Hb1Ac Antibody**

To evaluate the performance of this redox label in a sensing system, GPP was attached to the redox label on MHA-modified surface to be used for the detection of Hb1Ac antibody.

##### **4.5.5.1 Peptide GPP on Redox Label**

Having confirmed that the redox label was stable on the surface (Figure 4.17, Surface 3), the next step would be to bind the bioreceptor, peptide GPP to the free amine site on the redox label (Figure 4.17, Surface 4). The carbodiimide coupling between the peptide and the redox label was achieved by incubating modified gold electrodes with activated GPP in phosphate buffer for 4 h at 4 °C.

Surface	Potential (vs Ag/AgCl)
 <p style="text-align: center;">Surface 3</p>	$E_{1/2}$ -2 mV  $E_{fwhm}$ 155 mV
 <p style="text-align: center;">Surface 4</p>	$E_{1/2}$ ~ -60 mV  $E_{fwhm}$ $260 \pm 20$ mV

**Figure 4.17** Surface 3 – MHA-bound redox label and Surface 4 – GPP-bound redox label covalently attached on MHA-modified gold surface.

When bound to bioreceptors, significant shifts in redox potentials of the redox labels can result.<sup>34</sup> On Surface 4, the  $E_{1/2}$  of the redox label ranges from -12 mV to -68 mV for the electrodes prepared, with most of them centred around -60 mV, in comparison against the  $E_{1/2}$  of -2 mV from Surface 3. The  $E_{fwhm(\text{anodic})}$  of Surface 4 is in the range of  $260 \pm 20$  mV, which deviates further from the calculated  $E_{fwhm}$  of 155 mV of Surface 3 to suggest that the redox labels now exist in more microenvironments due to the presence of peptides bound to the labels. The slight shift of the  $E_{1/2}$  between surfaces is possibly a result of interelectrode variations. As formation of immunocomplex has been shown to cause a current suppression, the voltammetry response from the detection of Hb1Ac will be monitored by changes in current intensity.<sup>4</sup>

#### 4.5.5.2 Detection of Hb1Ac Antibody by Square-Wave Voltammetry

The experiments on the detection of Hb1Ac antibodies were performed using SWV because of its ability to discriminate against capacitive current from Faradaic current, and the increase in sensitivity when an electron exchange is involved.<sup>35</sup> The

modified gold electrodes with GPP bound were incubated with Hb1Ac antibodies in PBS at a concentration of  $8 \mu\text{g mL}^{-1}$ .

The effect of PBS on the current was investigated. The recorded SWV showed that the current stabilised after the surface was placed in PBS for 5 min (Figure 4.18a). Furthermore, a SWV taken after immersing Surface 4 with Hb1Ac antibody solution for 5 h did not show any noticeable decrease after 10 scans (Figure 4.18b). Together, these show that the responses of the surface were equilibrated after 5 min in PBS and that they are stable.

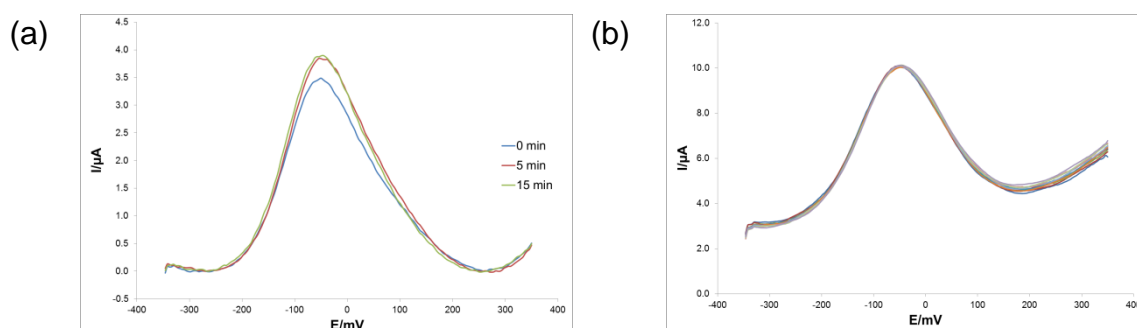


**Figure 4.18** (a) A SWV showing that the signal of Surface 4 was equilibrated after 15 min in PBS, recorded at 200 Hz. (b) Repeated scans ( $\times 10$ ) after Surface 4 was incubated in Hb1Ac antibody solution for 5 h, recorded at 210 Hz.

Once the responses of the surface were established to be stable, various SWV were recorded at different incubation times in order to investigate the extent of current suppression imposed by the binding of Hb1Ac on GPP. First, a SWV was recorded before incubation with Hb1Ac antibody solution, shown as 0 h in Figure 4.19. After incubation of various time periods (3 h and 5 h), the sensing surface was soaked in PBS for a few times to remove unbound antibodies before more SWV were recorded. A decrease in current is observed going from incubation time at 3 h and 5 h, which is due to the binding of more antibodies to the peptides. Alongside the decrease in current, a cathodic shift from  $-0.018 \text{ V}$  to  $-0.058 \text{ V}$  (*vs* Ag/AgCl) was observed.

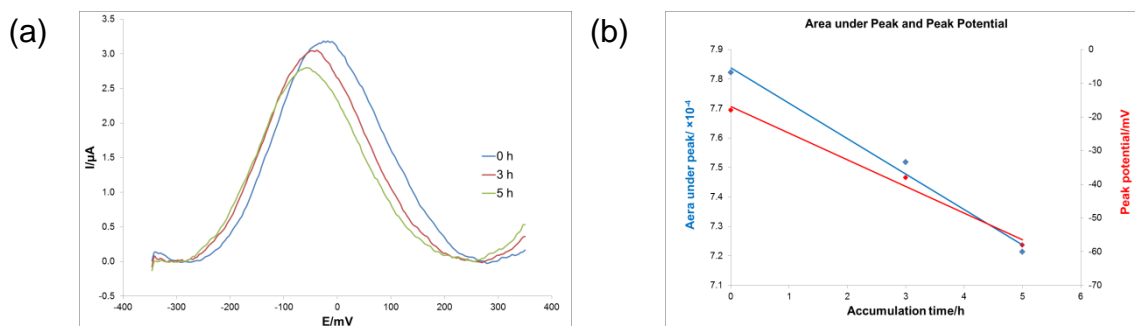


**Figure 4.19** (a) SWV of Surface 4 when exposed to Hb1Ac antibodies in PBS at varying incubation time, recorded at 130 Hz. (b) Area under peak and peak potential of Surface 4 after exposing to Hb1Ac antibodies at varying incubation time.

In this system, a current attenuation is obtained upon antibody binding. The reason for this is the antibody-epitope combinations which restrict the access of counter ions to the redox labels.<sup>2</sup> On these surfaces, only a minor suppression of  $12 \pm 4\%$  in current was observed compared to the  $67 \pm 4\%$  obtained using ferrocene label immobilised on a molecular wire for Hb1Ac detection.<sup>2</sup> The construct of the sensing surface with molecular wires permitted the ferrocene labels to rise above its antifouling/diluent layer, in the process preventing steric interactions between target antibodies and the binding peptides. Meade's group reported similar results whereupon the surfaces with higher concentration of diluents *vs* redox clusters result in larger changes in the electron transfer properties of the clusters shown as higher cathodic shift upon protein binding.<sup>36</sup> Thus, this relatively small current attenuation can be possibly ascribed to the steric effects which hinder the binding of Hb1Ac to the GPP peptide on the redox labels. With optimisation of the ratio of diluent: redox label concentrations the steric effect could, in the future, be lessened to enhance the sensitivity of the detection.

## 4.6 Summary

A ruthenium-based redox label,  $\text{Ru}(\text{acac})_2(\text{bpy-NH}_2)$ , was synthesised and characterised before being anchored onto both MHA- and TA-modified gold surfaces. The surfaces constructed step-wise were characterised by XPS and electrochemistry to supply evidence that the redox label was surface-bound. Comparisons were made between ferrocene label and ruthenium label in chloride-containing phosphate buffer showing that the ruthenium label was far more stable than the ferrocene label. A

pentapeptide, GPP was covalently bound to the redox label anchored on MHA-modified gold electrode for the detection of Hb1Ac antibody. The  $E_{1/2}$  of the redox label was shifted cathodically after the binding of peptide. When incubated with Hb1Ac antibody solution the current generated by the redox label was shown to decrease with increasing incubation time to indicate that more antibodies were binding to the peptide as time passed. This chapter demonstrates that a ruthenium-based complex has the potential to replace ferrocene label in sensing systems if surface design was optimised to enhance the sensitivity of the surface.

#### 4.7 References

- (1) Wang, J. *Chem. Rev.* **2008**, *108*, 814.
- (2) Liu, G.; Khor, S. M.; Iyengar, S. G.; Gooding, J. J. *Analyst* **2012**, *137*, 829.
- (3) Liu, G.; Iyengar, S. G.; Gooding, J. J. *Electroanal.* **2012**, *24*, 1509.
- (4) Liu, G.; Iyengar, S. G.; Gooding, J. J. *Electroanal.* **2013**, *25*, 881.
- (5) Yan, J.; Tender, L. M.; Hampton, P. D.; López, G. P. *J. Phys. Chem. B* **2001**, *105*, 8905.
- (6) Tucker, J. H. R. In *Supramolecular Chemistry: From Molecules to Nanomaterials.*; John Wiley & Sons, Ltd.: 2012.
- (7) Mehrvar, M.; Abdi, M. *Analyt. Sci.* **2004**, *20*, 1113.
- (8) Labib, M.; Shipman, P. O.; Martié, S.; Kraatz, H.-B. *Analyst* **2011**, *136*, 708.
- (9) Kerman, K.; Mahmoud, K. A.; Kraatz, H.-B. *Chem. Commun.* **2007**, 3829.
- (10) Mahmoud, K. A.; Kraatz, H.-B. *Chem. Eur. J.* **2007**, *13*, 5585.
- (11) White, R. J.; Plaxco, K. W. *Anal. Chem.* **2010**, *82*, 73.
- (12) Gooding, J. J.; Ciampi, S. *Chem. Soc. Rev.* **2011**, *40*, 2704.
- (13) Chow, E.; Hibbert, D. B.; Gooding, J. J. *Anal. Chim. Acta* **2005**, *543*, 167.
- (14) Eckermann, A. L.; Feld, D. J.; Shaw, J. A.; Meade, T. J. *Coord. Chem. Rev.* **2010**, *254*, 1769.
- (15) Samanta, D.; Sarkar, A. *Chem. Soc. Rev.* **2011**, *40*, 2567.
- (16) Sam, S.; Touahir, L.; Salvador Andresa, J.; Allongue, P.; Chazelviel, J.-N.; Gouget-Laemmel, A. C.; Henry de Villeneuve, C.; Moraillon, A.; Ozanam, F.; Gabouze, N.; Djebbar, S. *Langmuir* **2010**, *26*, 809.
- (17) Staros, J. V.; Wright, R. W.; Swingle, D. M. *Anal. Biochem.* **1986**, *156*, 220.
- (18) Wang, Z.; Riebenspies, J.; Motekaitis, R. J.; Martell, A. E. *J. Chem. Soc. Dalton Trans.* **1995**, *1995*, 1511
- (19) Newkome, G. R.; Parti, A. K.; Holder, E.; Schubert, U. S. *Eur. J. Org. Chem.* **2004**, 235.
- (20) Kavanagh, P.; Leech, D. *Tetrahedron Lett.* **2004**, *45*, 121.
- (21) Maury, O.; Guegan, J.-P.; Renouard, T.; Hilton, A.; Dupau, P.; Sandon, N.; Toupet, L.; Le Bozec, H. *New J. Chem.* **2001**, *25*, 1553.
- (22) Dupau, P.; Renouard, T.; Le Bozec, H. *Tetrahedron Lett.* **1996**, *37*, 7503.
- (23) Beer, P. D.; Szemes, F.; Passaniti, P.; Maestri, M. *Inorg. Chem.* **2004**, *43*, 3965.
- (24) Zakeeruddin, S. M.; Fraser, D. M.; Nazeeruddin, M. K.; Grätzel, M. *J. Electroanal. Chem.* **1992**, *337*, 253.

- 
- (25) Ahrens, M. J.; Bertin, P. A.; Gaustad, A. G.; Georganopoulou, D.; Wunder, M.; Blackburn, G. F.; Gray, H. B.; Meade, T. J. *Dalton Trans.* **2011**, *40*, 1732.
- (26) Chow, E.; Wong, E. L. S.; Böcking, T.; Nguyen, Q. T.; Hibbert, D. B.; Gooding, J. J. *Sens. Act. B* **2005**, *111-112*, 540.
- (27) Chidsey, C. E. D.; Loiacono, D. N. *Langmuir* **1990**, *6*, 682.
- (28) Willey, T. M.; Vance, A. L.; Bostedt, C.; van Buuren, T.; Meulenberg, R. W.; Terminello, L. J.; Fadley, C. S. *Langmuir* **2004**, *20*, 4939.
- (29) Jiang, L.; Glidle, A.; Griffith, A.; McNeil, C. J.; Cooper, J. M. *Bioelectrochem. Bioenerg.* **1997**, *42*, 15.
- (30) Hashimoto, T.; Endo, A.; Nagao, N.; Satô, G. P.; Natarajan, K.; Shimizu, K. *Inorg. Chem.* **1998**, *37*, 5211.
- (31) Varughese, B.; Chellamma, S.; Lieberman, M. *Langmuir* **2002**, *18*, 7964.
- (32) Finklea, H. O. In *Electrochemistry. A Series of Advances*; Bard, A. J., Rubinstein, I., Eds.; Marcel Dekker: New York, 1996; Vol. 19, p 109.
- (33) Khor, S. M.; Liu, G.; Fairman, C.; Iyengar, S. G.; Gooding, J. J. *Biosens. Bioelectron.* **2011**, *26*, 2038.
- (34) Vrábel, M.; Hocek, M.; Havran, L.; Fojta, M.; Votruba, I.; Klepetář, B.; Pohl, R.; Rulíšek, L.; Zendlová, L.; Hobza, P.; Shih, I.; Mabery, E.; Mackman, R. *Eur. J. Inorg. Chem.* **2007**, 1752.
- (35) O'Dea, J. J.; Osteryoung, J.; Osteryoung, R. A. *Anal. Chem.* **1981**, *53*, 695.
- (36) Dixon, I. M.; Lebon, E.; Sutra, P.; Igau, A. *Chem. Soc. Rev.* **2009**, *38*, 1621.

## *Chapter 5*

### ***Concluding Remarks and Future Work***

## 5.1 Summary

Interfacial design of sensing surfaces is key to the performance of electrochemical biosensors. The ultimate aim is to create a biorecognition interface which can give accurate results and is simple to use. A reagentless biosensor essentially requires the user to only introduce a sample to the sensing surface for the qualification and quantification of target analytes, which is highly desirable.<sup>1</sup> One of the design aspects is the surface-bound redox labels for the detection of redox-inactive biomolecules, the reason being target binding is addressed solely by the changes in electron transfer properties of these labels. Properly designed redox labels improve sensitivity and detection limit of the sensing surfaces, leading to better performance of these surfaces.

An important shortcoming of ferrocene-based labels, the most popular transition-metal based redox labels, is that the oxidised ferricenium ions are unstable in the presence of chloride salts, which are prevalent in biological samples.<sup>2</sup> In some cases, the addition of a high concentration of perchlorate salt is necessary to prevent their degradation.<sup>3</sup> This change in ionic strength may affect target binding and sometimes does not prevent signal decay.<sup>4</sup> Hence, alternative transition-metal redox labels may alleviate the stability issues suffered by ferrocene-based labels. In this thesis, ruthenium-based complexes were chosen as the candidates for transition-metal based redox labels.

Chapter 3 reported the synthesis of two series of ruthenium complexes,  $[\text{Ru}(\text{bpy})_2(\beta\text{-diketonato})](\text{PF}_6)$  and  $\text{Ru}(\beta\text{-diketonato})_2(\text{bpy})$ , where the modulation of half-wave potentials ( $E_{1/2}$ ) was achieved by varying the ligand substituents on the  $\beta$ -diketonate ligands. Correlations were first made between donor properties of the substituents and the  $E_{1/2}$  of the complexes, showing that  $E_{1/2}$  could be fine-tuned by appropriate placement and selection of the substituents on the  $\beta$ -diketonate ligands. More correlations were made between the  $E_{1/2}$  and Hammett constant, ligand electrochemical parameter and UV-Vis absorbance. The first two tools are useful in deciding how best to achieve modulation of the  $E_{1/2}$  by substituent variations. Two

potential candidates to function as redox labels were identified, as they fell within the desired -0.3V to + 0.5 V (*vs* Ag/AgCl) range.

Following this, Chapter 4 reported the synthesis and electrochemical characterisation of the redox label Ru(acac)<sub>2</sub>(bpy-NH<sub>2</sub>), with bpy-NH<sub>2</sub> ligand providing an attachment point to both the electrode surface and bioreceptor. Next, the redox label was covalently bound to gold electrodes modified with SAMs of 6-mercaptopentanoic acid (MHA) and thioctic acid (TA), the surfaces of which were characterised by XPS and studied electrochemically. The redox label bound to MHA and TA was shown to be far more stable than the ferrocene label in chloride-containing buffer after repetitive cycling. The binding of the pentapeptide, *N*-glycosylated VHLTP, onto the redox label bound to MHA-modified electrode allowed the detection of Hb1Ac, an antibody which is a diabetes marker protein, by the formation of an antibody-epitope combination which suppressed the current produced by Ru(acac)<sub>2</sub>(bpy-NH<sub>2</sub>).

Summing up, a ruthenium-based redox label, Ru(acac)<sub>2</sub>(bpy-NH<sub>2</sub>), was synthesised and shown to bind to SAMs and a bioreceptor. Preliminary studies showed that the current of the redox label was suppressed upon target binding as a consequence of immersion of the label in a protein environment,<sup>5</sup> thus demonstrating that this redox label has the potential to be used in sensing applications.

## 5.2 Future Perspective

Optimisation of sensing surfaces is needed in order for the surfaces to perform ideally. In this thesis,  $\Delta E$  and  $E_{fwhm}$  of the ruthenium redox labels bound onto modified surface deviate from the ideal values of 0 mV and 90.6 mV/ $n$  ( $n$  = number of electron transferred) respectively. One approach is to presynthesise redox labels with pendant thiol groups<sup>6-8</sup> and directly bind these species onto the electrodes; however, the more straightforward step-wise anchoring of redox labels on sensing surfaces offers the advantage of simple removal of excess reactants and byproducts by washing.<sup>9,10</sup> A common strategy is to lower the surface coverage of redox labels by a combination of non-electroactive/anti-fouling diluent and redox-active monolayer (mixed layer) to give a narrower and more symmetrical peak (Figure 5.1).<sup>11</sup> The ratio and chain length of

diluent:redox label adlayer will also lessen steric effects between the target analytes, as the bioreceptors are more spaced out, thus giving more access to binding sites.<sup>12</sup>

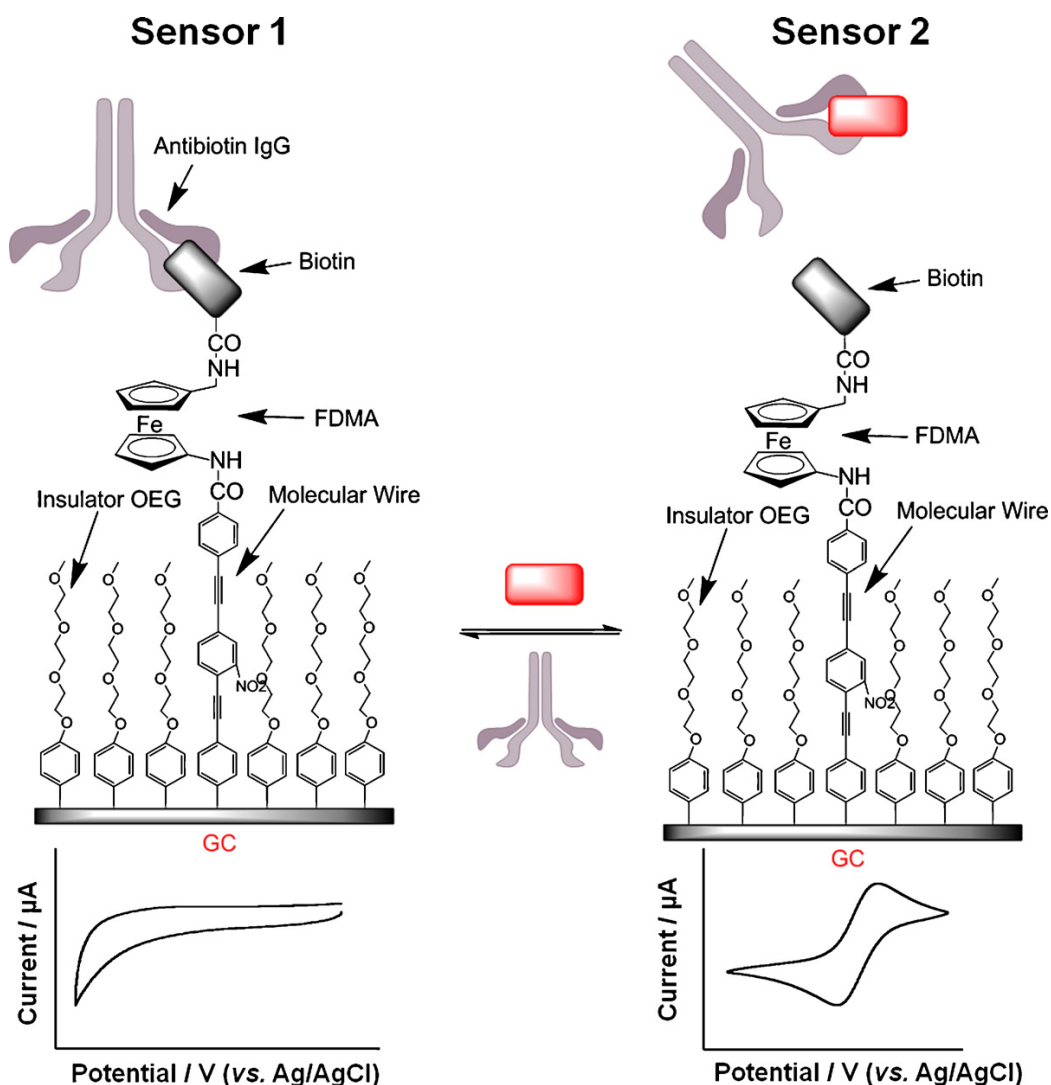


**Figure 5.1** An example of a sensing surface constructed with a mixed layer of a diluent, insulator oligoethyleneglycol (OEG), and a redox-active adlayer, ferrocene (FDMA) on molecular wire, for the detection of biotin in a displacement assay.<sup>13</sup>

It is readily apparent that the choice of ligands dictates how well a redox label performs electrochemically. The scope of ruthenium complexes can be further expanded by incorporating ligands with different substituents to prepare redox labels, ideally with a larger separation of  $E_{1/2}$  between them because, as shown in Chapter 4, the  $E_{1/2}$  of the redox label was shifted after binding to surface and/or bioreceptor. The chelating ligands should feature structural flexibility, such as pincer ligands (preferably without ionisable protons)<sup>14-16</sup> and polypyridine ligands<sup>15,17,18</sup> which not only confer better

stability to the redox labels,<sup>16</sup> they also provide “synthetic handles”<sup>19</sup> to allow functionalisation of linkers for the covalent binding to the surface and bioreceptor. Importantly, the binding should occur at monovalent sites to ensure there is no cross-linking of bioreceptors on surfaces.<sup>20</sup> This makes possible a multi-analyte array<sup>21</sup> by employing redox labels of different  $E_{1/2}$  for the detection of different target analytes. If the redox labels are equipped with suitable attachment points, different types of bioreceptors belonging to the same group can be introduced to the surfaces of spatially separated redox labels on a branched electrode platform to enable differentiation of closely-related targets, such as tumour markers (Figure 5.2).<sup>22</sup>

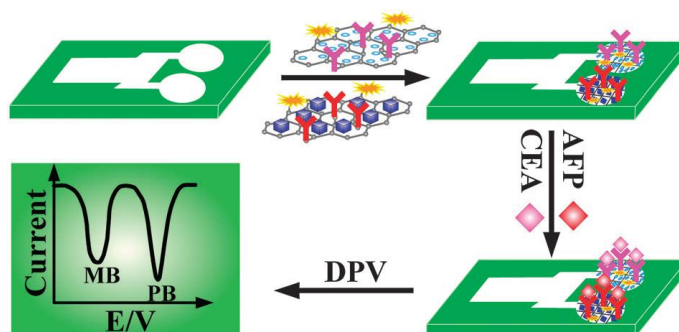


**Figure 5.2** An example of a branched electrode approach to detecting tumour markers, carcino-embryonic antigen (CEA) by anti-CEA conjugated to methylene blue (MB) and  $\alpha$ -fetoprotein (AFP) by anti-AFP conjugated to Prussian blue (PB) by differential pulse voltammetry (DPV); MB and PB are organic redox labels, the currents of which were reduced upon binding of CEA and AFP.<sup>22</sup>

One can borrow ideas from multilayered or nanoarrayed assemblies of metal complexes for the building of molecular devices<sup>6</sup> and apply them to a variety of different surfaces, including gold nanoparticles,<sup>23,24</sup> or on diazonium salt-modified surfaces with expanded potential windows in which the redox labels can operate.<sup>25</sup> For example, a multipod anchoring group (Figure 5.3) can be used to attach redox labels and will also control the number of available bioreceptors because of the molecular spacing they create; moreover, they are more stable than the monopod anchoring groups.<sup>6</sup> If possible, one can utilise a branched SAM<sup>26</sup> with different reactive groups so as to have one end linked to the redox label and another to the bioreceptor; another similar construct is to have the redox label bound to a monolayer and the bioreceptor introduced to the monolayer next to the redox label for them to be close in space. The

change experienced by the bioreceptor upon target binding will be relayed to the redox label due to their close proximity and the changes in the immediate environment of the redox label will be transduced by the electrode. Furthermore, improvement to immunobiosensors using a multimetallic redox cluster which contains multiple bioreceptors was reported, the main contributing factor to the improved performance being the amplification of signals from multiple redox centres upon target binding.<sup>27</sup>

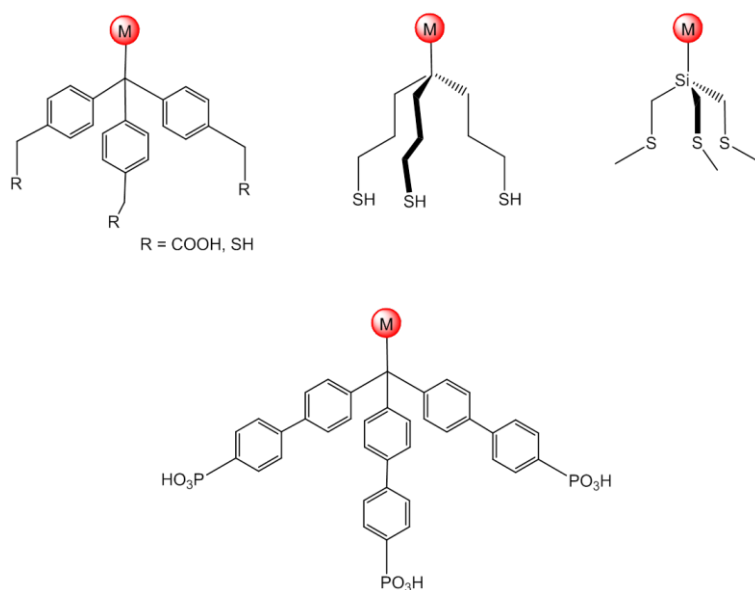


**Figure 5.3** Partial structures of multipod anchoring groups suitable on gold and indium tin oxide surfaces;<sup>6</sup> M represents a redox label.

### 5.3 Conclusion

This thesis reported on the development of ruthenium complexes as redox labels for use in biosensors with the following criteria: low and pH-independent  $E_{1/2}$ , tuneable potentials by structural changes on ligands, chemically stable in both oxidised and reduced form and the electron-transfer are kinetically reversible. The choice of ligands surrounding the metal centre is the most important factor in the design of redox labels for their biosensing applications. As the technology in the assembly of sensing surfaces progresses,<sup>28</sup> the forms a redox label can take can be expected to expand in order to suit the applications. The ligands used in this thesis centred on bpy and  $\beta$ -diketonate derivatives to create heteroleptic complexes, resulting in complexes possessing a variety of  $E_{1/2}$  values. Alternative ligands based on nitrogen, phosphorus and carbonyl<sup>29</sup> or

pincer ligands can be considered so long as the resultant redox labels are stable to use in biosensing systems.

#### 5.4 References

- (1) Jhaveri, S. D.; Mauro, J. M.; Goldston, H. M.; Schauer, C. L.; Tender, L. M.; Trammell, S. A. *Chem. Commun.* **2003**, 338.
- (2) Prins, R.; Korwagen, A. R.; Kortbeek, A. G. T. G. *J. Organometal. Chem.* **1972**, *39*, 335.
- (3) Rowe, G. K.; Creager, S. E. *Langmuir* **1991**, *7*, 2307.
- (4) Kang, D.; Zuo, X.; Yang, R.; Xia, F.; Plaxco, K. W.; White, R. J. *Anal. Chem.* **2009**, *81*, 9109.
- (5) Liu, G.; Paddon-Row, M. N.; Gooding, J. J. *Chem. Commun.* **2008**, 3870.
- (6) Haga, M.; Kobayashi, T.; Terada, K. *Coord. Chem. Rev.* **2007**, *251*, 2688.
- (7) Smalley, J. F.; Finklea, H. O.; Chidsey, C. E. D.; Linford, M. R.; Craeger, S. E.; Ferraris, J. P.; Chalfant, K.; Zawodzinsk, T.; Feldberg, S. W.; Newton, M. D. *J. Am. Chem. Soc.* **2003**, *125*, 2004.
- (8) Cormode, D. P.; Evans, A. J.; Davis, J. J.; Beer, P. D. *Dalton Trans.* **2010**, *39*, 6532.
- (9) Zanarini, S.; Rampazzo, E.; Bich, D.; Canteri, R.; Della Ciana, L.; Marcaccio, M.; Marzocchi, E.; Montalti, M.; Panciatichi, C.; Pederzoli, C.; Paolucci, F.; Prodi, L.; Vanzetti, L. *J. Phys. Chem. C* **2008**, *112*, 2949.
- (10) Luo, J.; Isied, S. S. *Langmuir* **1998**, *14*, 3602.
- (11) Finklea, H. O. In *Electrochemistry. A Series of Advances*; Bard, A. J., Rubinstein, I., Eds.; Marcel Dekker: New York, 1996; Vol. 19, p 109.
- (12) Eckermann, A. L.; Feld, D. J.; Shaw, J. A.; Meade, T. J. *Coord. Chem. Rev.* **2010**, *254*, 1769.
- (13) Khor, S. M.; Liu, G.; Fairman, C.; Iyengar, S. G.; Gooding, J. J. *Biosens. Bioelectron.* **2011**, *26*, 2038.
- (14) Araujo, C. M.; Doherty, M. D.; Konezny, S. J.; Luca, O. R.; Usyatinsky, A.; Grade, H.; Lobkovsky, E.; Soloveichik, G. L.; Crabtree, R. H.; Batista, V. S. *Dalton Trans.* **2012**, *41*, 3562.
- (15) Dixon, I. M.; Lebon, E.; Sutra, P.; Igau, A. *Chem. Soc. Rev.* **2009**, *38*, 1621.
- (16) Slattery, S. J.; Bare, W. D.; Jameson, D. L.; Goldsby, K. A. *J. Chem. Soc. Dalton Trans.* **1999**, 1999, 1347.
- (17) Marcaccio, M.; Paolucci, F.; Fontanesi, C.; Fioravanti, G.; Zanarini, S. *Inorg. Chim. Acta* **2007**, *360*, 1154.
- (18) Anderson, P. A.; Deacon, G. A.; Haarman, K. H.; Keene, F. R.; Meyer, T. J.; Rietsma, D. A.; Skelton, B. W.; Strouse, G. F.; Thomas, N. C.; Treadway, J. A.; White, A. H. *Inorg. Chem.* **1995**, *34*, 6145.
- (19) Ahrens, M. J.; Bertin, P. A.; Gaustad, A. G.; Georganopoulou, D.; Wunder, M.; Blackburn, G. F.; Gray, H. B.; Meade, T. J. *Dalton Trans.* **2011**, *40*, 1732.
- (20) Liu, G.; Khor, S. M.; Iyengar, S. G.; Gooding, J. J. *Analyst* **2012**, *137*, 829.
- (21) Ebrahimi, D.; Chow, E.; Gooding, J. J.; Hibbert, D. B. *Analyst* **2008**, *133*, 1090.
- (22) Kong, F.; Xu, B.; Du, Y.; Xu, J.; Chen, H. *Chem. Commun.* **2013**, *49*, 1052.
- (23) Dong, T.-Y.; Huang, C.; Chen, C.-P.; Lin, M.-C. *J. Organometal. Chem.* **2007**, *692*, 5147.
- (24) Liu, G.; Iyengar, S. G.; Gooding, J. J. *Electroanal.* **2013**, *25*, 881.
- (25) Liu, G.; Böcking, T.; Gooding, J. J. *J. Electroanal. Chem.* **2007**, *600*, 335.

- (26) Ulman, A. *Chem. Rev.* **1996**, 96, 1533.
- (27) Feld, D. J.; Hsu, H.-T.; Eckermann, A. L.; Meade, T. J. *Langmuir* **2012**, 28, 939.
- (28) Senaratne, W.; Andruzzi, L.; Ober, C. K. *Biomacromolecules* **2005**, 6, 2427.
- (29) Whittlesey, M. K. In *Comprehensive Organometallic Chemistry III: Group 8*; 1st ed.; Crabtree, R. H., Mingos, D. M. P., Bruce, M. I., Eds.; Elsevier Science: 2006; Vol. 6, p 353.